

**UWB Based High Precision  
Localisation Technology for the Low  
Cost Autonomous UAV Inspection in  
GPS-Denied and Extremely Confined  
Environments**

**Beiya Yang**

Department of the Design, Manufacturing and Engineering Management  
University of Strathclyde, Glasgow

A thesis presented in partial fulfilment of the requirements for  
the degree of Doctor of Philosophy

June 6, 2023

# Declaration

This thesis is the result of the author's original research. It has been composed by the author and has not been previously submitted for examination which has led to the award of a degree.

The copyright of this thesis belongs to the author under the terms of the United Kingdom Copyright Acts as qualified by University of Strathclyde Regulation 3.50. Due acknowledgement must always be made of the use of any material contained in, or derived from, this thesis.

Signed: Beiya Yang

Date:

# Acknowledgements

First and foremost, I would like to express my gratitude to my supervisor Dr. Erfu Yang. His immense knowledge and rich experiences in the relevant research area has provided the critical guidance for my research and inspired me to find the research challenges and questions. He is not only the supervisor who leads my research, but also the mentor for my life.

I would also like to thank Mr. Leijian Yu, Dr. Cong Niu and Mr. Andrew Loeliger who provide me the kindly support on the development of the testing platform and their helpful suggestions.

My thanks also go to my second supervisor Prof. Xiu-tian Yan for his advice and useful discussions. I would also like to thank him for helping me on the experiment of my research, especially in this difficult time.

Last but not least, I would like to express my eternal gratitude to all my family and friends for their companionship and support during the pandemic period. Especially for my parents Liuyin Yang and Chune Gong, and my wife Ting Hu who always hold my back in this difficult time. Without all of you, I could not get where I am today. Much appreciate for all the support and help from you.

# Abstract

Owing to the specific characteristics of unmanned aerial vehicles (UAVs), the demands and applications increase dramatically for them being deployed in extremely confined or closed space for surveying, inspection or detection to substitute human. However, global positioning system (GPS) may lose effectiveness or become unavailable due to the potential signal block or interference in such environments. Under such circumstances, an imperative requirement on new positioning technology for UAV has emerged. With the rapid development of radio frequency (RF) based localisation technologies, especially for the ultra-wideband (UWB) based localisation technology, leveraging small wireless sensor nodes for low cost, low latency, low energy consumption and accurate localisation on UAV has received significant attention. However, the research challenges and issues such as the unreasonable values within the UWB measurements, the geometry configurations of the anchor nodes in the extremely confined environments, the requirement of the prior information, the performance influence from the unpredictable propagation condition and the geomagnetic disturbances for inertial measurement unit (IMU) still exists which limit the applications on UAV.

To avoid these aforementioned research challenges and issues, the researches in this thesis are carried out from different perspectives. Firstly, the maximum

likelihood estimation (MLE) based algorithm plus with the anchor distribution strategy is proposed focused on the development of the pure UWB based localisation system. With the proposed algorithm and strategy, the most suitable geometry configurations of the anchor node can be found to achieve the accurate and robust UAV positioning in focused environments. However, considering the unreasonable values within the UWB measurements still have the huge impact on the localisation performance for the pure UWB based localisation approach, according to the simulation and experiment, the investigation on the sensor fusion based approaches which integrated the IMU and UWB is carried out.

To overcome the performance degradation and oscillation leads by the unreasonable values, the extended Kalman filter (EKF) based algorithm can be seen as the ideal candidate, owing to the implementation simplicity and acceptable accuracy. Yet, the unknown prior information about the noise covariance matrices still has the great impact on the localisation performance, especially for the applications in the extremely confined environment. To mitigate the effects, in this thesis, a high precision UAV positioning system which integrates the IMU and UWB with the adaptive extended Kalman filter (AEKF) is proposed. Compared with the traditional EKF based approach, the estimated and recorded information from previous processes is exploited to adaptively estimate and further control the estimation of the noise covariance matrices for performance improvement. Nevertheless, the proposed AEKF algorithm and system still suffer from the performance influence caused by the geomagnetic disturbances for the additional IMU. To remedy this for further performance improvement, in this thesis, the tightly coupled adaptive extended Kalman filter (TC-AEKF) based algorithm is proposed. With the additional angular rate in the state prediction process and

the adaptively estimated noise covariance matrices, the proposed algorithm can significantly improve the localisation performance in the focused environments, according to the simulations and experiments.

Even the proposed AEKF and TC-AEKF based algorithm can attain the high accuracy and precision localisation performance of the UAV in focused environments, however, there is still limitation for the proposed algorithm. Due to the principal of the proposed algorithms, the additional linearisation process is required in the correction process. Currently, the first order Taylor expansion is utilised for the linearisation of the observation matrix. This may directly lead to the performance degradation and oscillation, owing to the neglected high order terms. To mitigate the effect, in this thesis, an adaptive square root cubature Kalman filter (ASRCKF) based sensor fusion algorithm is proposed. With the integration of the IMU and UWB, the utilisation of the cubature rule, the adaptively estimated noise covariance matrices and the added estimation weighting factors, the performance degradation and oscillation led by the unreasonable value within the ranging information, the linearisation of the observation matrix and the unknown and hard-to-adjust noise covariance matrices can all be resolved. Finally, from the numerical simulations, experiments and autonomous inspection flight test, it can be proved that the proposed algorithm and system can attain 0.081m median error, 0.172m 95<sup>th</sup> percentile error and 0.045m average standard deviation (STD), which is feasible for the autonomous inspection in the focused environments.

# Contents

<b>Acknowledgements</b>	<b>ii</b>
<b>Abstract</b>	<b>iii</b>
<b>List of Figures</b>	<b>xii</b>
<b>List of Tables</b>	<b>xvii</b>
<b>List of Acronyms</b>	<b>xx</b>
<b>Publications</b>	<b>xxii</b>
<b>1 Introduction</b>	<b>1</b>
1.1 Research background and motivation . . . . .	1
1.2 Aim and objectives . . . . .	7
1.3 Research methodology . . . . .	9
1.4 Thesis organisation . . . . .	11

<b>2</b>	<b>Literature Review</b>	<b>14</b>
2.1	Introduction . . . . .	14
2.2	RF based UAV localisation technologies . . . . .	15
2.2.1	Wi-Fi based localisation technology . . . . .	16
2.2.2	Bluetooth based localisation technology . . . . .	18
2.2.3	Zigbee based localisation technology . . . . .	20
2.2.4	RFID based localisation technology . . . . .	21
2.2.5	UWB based localisation technology . . . . .	23
2.2.6	Summary and discussion on the RF based UAV localisation technologies . . . . .	27
2.3	Classical localisation mechanisms . . . . .	27
2.3.1	RSS based localisation mechanism . . . . .	29
2.3.2	AOA based localisation mechanism . . . . .	31
2.3.3	TOF/TOA based localisation mechanism . . . . .	33
2.3.4	TDOA based localisation mechanism . . . . .	35
2.3.5	Fingerprint based localisation mechanism . . . . .	38
2.3.6	Summary and discussion on the classical localisation mech- anisms . . . . .	40
2.4	UAV platforms . . . . .	40

## Contents

2.5	Evaluation framework for UAV positioning with RF based technologies in GPS-denied environments . . . . .	43
2.5.1	Localisation accuracy (LA) . . . . .	44
2.5.2	Localisation latency/ Update rate (L/U) . . . . .	44
2.5.3	Stability in different environment (SDE) . . . . .	45
2.5.4	Auxiliary equipment requirements (AER) . . . . .	45
2.5.5	Weight/Size (W/S) . . . . .	46
2.5.6	Localisation coverage (LCR) . . . . .	46
2.5.7	Energy consumption (EC) . . . . .	47
2.5.8	System cost (SC) . . . . .	47
2.5.9	Demand level discussion under different application scenarios	47
2.5.10	Evaluation and analysis on the existing RF based UAV localisation systems . . . . .	50
2.6	Current challenges on UAV positioning with RF based localisation technologies . . . . .	54
2.6.1	Unreasonable value . . . . .	55
2.6.2	Anchor self-positioning and relative localisation of UAV . .	55
2.6.3	NLOS error . . . . .	56
2.6.4	Node synchronisation . . . . .	60

Contents

2.6.5	Signal block or interference between localisation server or ground station and UAV . . . . .	62
2.6.6	Energy consumption . . . . .	63
2.6.7	Summary and discussion on the current challenges of the RF based UAV localisation technologies . . . . .	64
2.7	Summary . . . . .	64
<b>3</b>	<b>UWB based UAV positioning technology</b>	<b>67</b>
3.1	Introduction . . . . .	67
3.2	MLE based UAV positioning algorithm . . . . .	68
3.3	Anchor distribution strategy . . . . .	74
3.4	Performance evaluation in the simulation environment . . . . .	75
3.5	System implementation and experiment setup . . . . .	83
3.6	Performance evaluation in the experiment environment . . . . .	84
3.7	Summary . . . . .	92
<b>4</b>	<b>UWB and IMU based EKF sensor fusion UAV positioning technology</b>	<b>94</b>
4.1	Introduction . . . . .	94
4.2	Coordinate system transformation . . . . .	97
4.3	EKF based sensor fusion with the integration of IMU and UWB . . . . .	100

## Contents

4.3.1	State prediction . . . . .	100
4.3.2	Observation correction . . . . .	103
4.3.3	Position estimation . . . . .	105
4.4	Adaptive EKF based sensor fusion . . . . .	105
4.4.1	Estimation of the noise covariance matrices . . . . .	107
4.4.2	Estimation of weighting factors . . . . .	108
4.5	Tightly coupled adaptive EKF based sensor fusion . . . . .	111
4.5.1	State prediction . . . . .	111
4.5.2	Observation correction . . . . .	115
4.5.3	Estimation of the noise covariance matrices . . . . .	117
4.5.4	Estimation of weighting factors . . . . .	118
4.6	Performance evaluation in the simulation environment . . . . .	122
4.6.1	Simulation configuration . . . . .	122
4.6.2	Simulation for the AEKF based sensor fusion approach . . . . .	122
4.6.3	Simulation for the TC-AEKF based sensor fusion approach . . . . .	130
4.7	Performance evaluation in the experiment environment . . . . .	134
4.7.1	System implementation and experiment setup . . . . .	134
4.7.2	Performance evaluation for the AEKF based approach in the experiment environment . . . . .	136

Contents

4.7.3	Performance evaluation for the TC-AEKF based approach in the experiment environment . . . . .	143
4.7.4	Autonomous inspection flight test with the TC-AEKF al- gorithm . . . . .	146
4.8	Summary . . . . .	147
<b>5</b>	<b>UWB and IMU based SRCKF sensor fusion UAV positioning technology</b>	<b>149</b>
5.1	Introduction . . . . .	149
5.2	SRCKF based sensor fusion with the integration of IMU and UWB	150
5.2.1	State prediction . . . . .	151
5.2.2	Observation correction . . . . .	152
5.3	Adaptive SRCKF based sensor fusion . . . . .	154
5.3.1	Estimation of the noise covariance matrices . . . . .	154
5.3.2	Additional weighting factors . . . . .	157
5.4	Performance evaluation in the simulation environment . . . . .	160
5.5	Performance evaluation in the experiment environment . . . . .	165
5.5.1	Experiment setup . . . . .	165
5.5.2	Performance evaluation for the SRCKF and ASRCKF based approach . . . . .	165

Contents

5.5.3	Autonomous inspection flight test . . . . .	170
5.6	Summary . . . . .	171
<b>6</b>	<b>Conclusion and future work</b>	<b>173</b>
6.1	Conclusions of the research . . . . .	173
6.2	Contributions to knowledge . . . . .	175
6.3	Recommendation of future work . . . . .	178
<b>A</b>	<b>TC-AEKF based autonomous inspection</b>	<b>181</b>
<b>B</b>	<b>ASRCKF based autonomous inspection</b>	<b>182</b>
	<b>Bibliography</b>	<b>182</b>

# List of Figures

1.1	UAV applications in GPS-denied and extremely confined environments . . . . .	2
1.2	The overview for the research methodology . . . . .	10
2.1	RF based localisation technologies . . . . .	15
2.2	RSS based localisation mechanism . . . . .	29
2.3	AOA based localisation mechanism . . . . .	32
2.4	TOF/TOA based localisation mechanism . . . . .	34
2.5	TWR/TW-TOF based localisation approach . . . . .	35
2.6	DS-TWR based localisation approach . . . . .	36
2.7	TDOA based localisation mechanism . . . . .	37
3.1	Structure for the MLE based positioning algorithm. . . . .	73
3.2	Geometry configurations of anchor nodes. . . . .	76
3.3	GDOP under configuration A of anchor nodes. . . . .	77

## List of Figures

3.4	GDOP under configuration B of anchor nodes. . . . .	78
3.5	GDOP under configuration C of anchor nodes. . . . .	78
3.6	GDOP under configuration D of anchor nodes. . . . .	79
3.7	RMSE under configuration A of anchor nodes. . . . .	80
3.8	RMSE under configuration B of anchor nodes. . . . .	80
3.9	RMSE under configuration C of anchor nodes. . . . .	81
3.10	RMSE under configuration D of anchor nodes. . . . .	81
3.11	Localisation structure for the pure UWB based UAV localisation system. . . . .	84
3.12	Laboratory experiment environment for the pure UWB based localisation system and the DJI Tello EDU. . . . .	85
3.13	Operational process for the pure UWB based system. . . . .	85
3.14	RMSE under different geometry configurations of anchor nodes. . . . .	87
3.15	STD of RMSE under different geometry configurations of anchor nodes. . . . .	88
3.16	eCDF for representative test points under different geometry configurations of anchor nodes. . . . .	89
3.17	Localisation results for the flight tests with the MLE based UWB localisation system. . . . .	91
4.1	Transformation of the coordinate system. . . . .	98

## List of Figures

4.2	Structure for the EKF based algorithm. . . . .	101
4.3	Structure for the AEKF based algorithm. . . . .	106
4.4	Structure for the TC-AEKF based algorithm. . . . .	112
4.5	Simulation environment. . . . .	123
4.6	Simulation 1 flight results for the AEKF with constant noise model. (a) 3D trajectories. (b) X direction trajectories. (c) Y direction trajectories. (d) Z direction trajectories. (e) X direction RMSE (m). (f) Y direction RMSE (m). (g) Z direction RMSE (m). (h) eCDF. . . . .	125
4.7	Simulation 2 flight results for the AEKF with changing noise model. (a) 3D trajectories. (b) X direction trajectories. (c) Y direction trajectories. (d) Z direction trajectories. (e) X direction RMSE (m). (f) Y direction RMSE (m). (g) Z direction RMSE (m). (h) eCDF. . . . .	127
4.8	Simulation results for the TC-AEKF with changing noise model. (a) 3D trajectories. (b) X direction trajectories. (c) Y direction trajectories. (d) Z direction trajectories. (e) X direction RMSE (m). (f) Y direction RMSE (m). (g) Z direction RMSE (m). (h) eCDF. . . . .	132
4.9	System structure. . . . .	135
4.10	Experiment environment for the EKF, AEKF (LC-AEKF) and TC-AEKF based sensor fusion algorithms. . . . .	137

List of Figures

4.11	Experiment 1 flight test results for the AEKF. (a) 3D trajectories. (b) X direction trajectories. (c) Y direction trajectories. (d) Z direction trajectories. (e) X direction RMSE (m). (f) Y direction RMSE (m). (g) Z direction RMSE (m). (h) eCDF. . . . .	138
4.12	Experiment 2 flight test results for the AEKF. (a) 3D trajectories. (b) X direction trajectories. (c) Y direction trajectories. (d) Z direction trajectories. (e) X direction RMSE (m). (f) Y direction RMSE (m). (g) Z direction RMSE (m). (h) eCDF. . . . .	141
4.13	Experiment results for the TC-AEKF. (a) 3D trajectories. (b) X direction trajectories. (c) Y direction trajectories. (d) Z direction trajectories. (e) X direction RMSE (m). (f) Y direction RMSE (m). (g) Z direction RMSE (m). (h) eCDF. . . . .	145
4.14	Flight trajectory for the TC-AEKF based autonomous inspection. (a) Trajectory in X(m) direction in the autonomous inspection flight test. (b) Trajectory in Y(m) direction in the autonomous inspection flight test. (c) Trajectory in Z(m) direction in the autonomous inspection flight test. . . . .	147
5.1	Structure for the SRCKF based algorithm. . . . .	150
5.2	Structure for the ASRCKF based algorithm. . . . .	155

List of Figures

5.3	Simulation flight results for the SRCKF and ASRCKF with changing noise model. (a) 3D trajectories. (b) X direction trajectories. (c) Y direction trajectories. (d) Z direction trajectories. (e) X direction RMSE (m). (f) Y direction RMSE (m). (g) Z direction RMSE (m). (h) eCDF. . . . .	162
5.4	Laboratory experiment environment. . . . .	166
5.5	The UAV positioning system components. . . . .	167
5.6	Experiment localisation results for the SRCKF based approaches. (a) 3D trajectories. (b) X direction trajectories. (c) Y direction trajectories. (d) Z direction trajectories. (e) X direction RMSE (m). (f) Y direction RMSE (m). (g) Z direction RMSE (m). (h) eCDF. . . . .	168
5.7	Flight trajectory for the ASRCKF based autonomous inspection. (a) Trajectory in X(m) direction in the autonomous inspection flight test. (b) Trajectory in Y(m) direction in the autonomous inspection flight test. (c) Trajectory in Z(m) direction in the autonomous inspection flight test. . . . .	170

# List of Tables

1.1	Comparison for conventional technologies on UAV positioning . . .	6
2.1	Comparison for the existing RF based UAV localisation technologies with different radio communication protocols . . . . .	28
2.2	Comparison for the existing RF based UAV localisation technologies with the classical localisation mechanisms . . . . .	41
2.3	Analysis of current RF based UAV localisation systems under the proposed evaluation framework . . . . .	51
2.4	Discussion on current challenges for UAV positioning with RF based localisation technologies . . . . .	65
3.1	Coordinates of anchor nodes under different geometry configurations	77
3.2	Localisation error for representative test points . . . . .	90
4.1	Detailed localisation results for the AEKF based sensor fusion approach with constant noise model in simulation 1 . . . . .	124

List of Tables

4.2	Detailed localisation results for the AEKF based sensor fusion approach with changing noise model in simulation 2 . . . . .	128
4.3	The probability for filtering divergence . . . . .	129
4.4	Detailed simulation results for the TC-AEKF based sensor fusion approach with changing noise model . . . . .	133
4.5	Size, weight and price for each component. . . . .	135
4.6	Detailed localisation results for the AEKF based sensor fusion approach in flight test 1 . . . . .	139
4.7	Detailed localisation results for the AEKF based sensor fusion approach in flight test 2 . . . . .	142
4.8	Detailed experiment results for the TC-AEKF based sensor fusion approach . . . . .	144
5.1	Coordinates of the anchor nodes. . . . .	161
5.2	Detailed simulation results for the SRCKF and ASRCKF based sensor fusion approaches with changing noise model . . . . .	163
5.3	Detailed experiment localisation results for the SRCKF based approaches . . . . .	169

# List of Acronyms

<b>6-DOF</b>	6 Degrees of Freedom
<b>AEKF</b>	Adaptive Extended Kalman Filter
<b>AOA</b>	Angle of Arrival
<b>ASRCKF</b>	Adaptive Square Root Cubature Kalman Filter
<b>AWGN</b>	Additive White Gaussian Noise
<b>eCDF</b>	Empirical Cumulative Distribution Function
<b>CRLB</b>	Cramér–Rao Lower Bound
<b>DS-TWR</b>	Double-sided Two-way Ranging
<b>EKF</b>	Extended Kalman Filter
<b>GDOP</b>	Geometric Dilution of Precision
<b>GNSS</b>	Global Navigation Satellite System
<b>GPS</b>	Global Positioning System
<b>IMU</b>	Inertial Measurement Unit
<b>INS</b>	Inertial Navigation System
<b>KPIs</b>	Key Performance Indicators
<b>LC-AEKF</b>	Loosely Coupled Adaptive Extended Kalman Filter
<b>LiDAR</b>	Light Detection and Ranging
<b>MAVs</b>	Micro Air Vehicles

Chapter 0. List of Acronyms

**MLE** Maximum Likelihood Estimation

**NED** North-east-down

**NLOS** Non-line-of-sight

**RF** Radio Frequency

**RFID** Radio Frequency Identification

**RMSE** Root Mean Squared Error

**SDS-TWR** Symmetric Double-sided Two-way Ranging

**SRCKF** Square Root Cubature Kalman Filter

**STD** Standard Deviation

**TC-AEKF** Tightly Coupled Adaptive Extended Kalman Filter

**TDOA** Time Difference of Arrival

**TOA** Time of Arrival

**TOD** Time of Departure

**TOF** Time of Flight

**TWR** Two-way Ranging

**TW-TOF** Two-way Time of Flight

**UAVs** Unmanned Aerial Vehicles

**UWB** Ultra-wideband

**VO** Visual Odometry

# Publications

## Articles:

[1] **B. Yang** and E. Yang. “A survey on radio frequency based precise localisation technology for UAV in GPS-denied environment,” in *Journal of Intelligent & Robotic Systems*, vol. 103, no. 3, pp. 1-30, 2021.

[2] **B. Yang**, E. Yang, L. Yu and A. Loeliger, “High-Precision UWB-Based Localisation for UAV in Extremely Confined Environments,” in *IEEE Sensors Journal*, vol. 22, no. 1, pp. 1020-1029, Jan.1, 2022, doi: 10.1109/JSEN.2021.3130724.

[3] **B. Yang**, E. Yang, L. Yu and C. Niu, “Adaptive Extended Kalman Filter-Based Fusion Approach for High-Precision UAV Positioning in Extremely Confined Environments,” in *IEEE/ASME Transactions on Mechatronics*, vol. 28, no. 1, pp. 543-554, Feb. 2023, doi: 10.1109/TMECH.2022.3203875.

[4] **B. Yang**, E. Yang, L. Yu and C. Niu, “Ultrasonic and IMU Based High Precision UAV Localisation for the Low Cost Autonomous Inspection in Oil and Gas Pressure Vessels,” in *IEEE Transactions on Industrial Informatics*, 2023, doi: 10.1109/TII.2023.3240874.

[5] **B. Yang**, E. Yang, L. Yu and C. Niu, “Sensor Fusion Based UAV Lo-

calisation System for Low Cost Autonomous Inspection in Extremely Confined Environments,” in IEEE Transactions on Automation Science and Engineering. (Under the first round review)

[6] **B. Yang**, E. Yang, L. Yu and C. Niu, “Adaptive Square Root Cubature Kalman Filter Based Low Cost UAV Positioning System for Autonomous Inspection in Extremely Confined Environments,” in IEEE Transactions on Systems, Man, and Cybernetics: Systems. (Under the first round review)

[7] L. Yu, E. Yang, and **B. Yang**, “AFE-ORB-SLAM: robust monocular VS-LAM based on adaptive FAST threshold and image enhancement for complex lighting environments.” in Journal of Intelligent & Robotic Systems, vol. 105, no. 2, pp. 1-14, 2022.

[8] L. Yu, E. Yang, **B. Yang**, Z. Fei and C. Niu, “A Robust Learned Feature-based Visual Odometry System for UAV Pose Estimation in Challenging Indoor Environments.” in IEEE Transactions on Instrumentation and Measurement, 2023, doi: 10.1109/TIM.2023.3279458

## Conference proceedings:

[1] **B. Yang**, E. Yang and L. Yu, “Vision and UWB-based anchor self-localisation system for UAV in GPS-denied environment,” in Journal of Physics: Conference Series, vol. 1922, no. 1, p. 012001. IOP Publishing, 2021.

[2] L. Yu, E. Yang, **B. Yang**, A. Loeliger and Z. Fei, “Stereo Vision-based Autonomous Navigation for Oil and Gas Pressure Vessel Inspection Using a Low-cost UAV,” 2021 IEEE International Conference on Real-time Computing and Robotics (RCAR), 2021, pp. 1052-1057, doi: 10.1109/RCAR52367.2021.9517584.

Chapter 0. Publications

[3] Z. Fei, E. Yang, **B. Yang**, and L. Yu, “Image enhancement and corrosion detection for UAV visual inspection of pressure vessels,” in *Intelligent Life System Modelling, Image Processing and Analysis*, 2021, pp. 145-154, Springer, Singapore.

# Chapter 1

## Introduction

### 1.1 Research background and motivation

With the rapid development of unmanned aerial vehicles (UAVs) technology, their applications are no longer limited to open environments. Exploiting UAVs to substitute human for surveying, inspection, inventory management and emergency rescue in closed, confined, inaccessible or potentially dangerous space has already become a much-sought research direction [1–6]. However, all these applications summarised in Fig. 1.1, are homogeneously within the environments where the operational space is confined and the global positioning system (GPS) is insufficient or unavailable to provide precise position information needed for UAV, due to the satellite signal lost or interference, which is also denoted as the GPS-denied environment. The commercial off-the-shelf (COTS) product named Elios 2 [7] has already been released by Flyability and widely utilised on inspection in extremely confined environments. To overcome the satellite signal block, problem, instead of the precise UAV positioning, a protective frame was

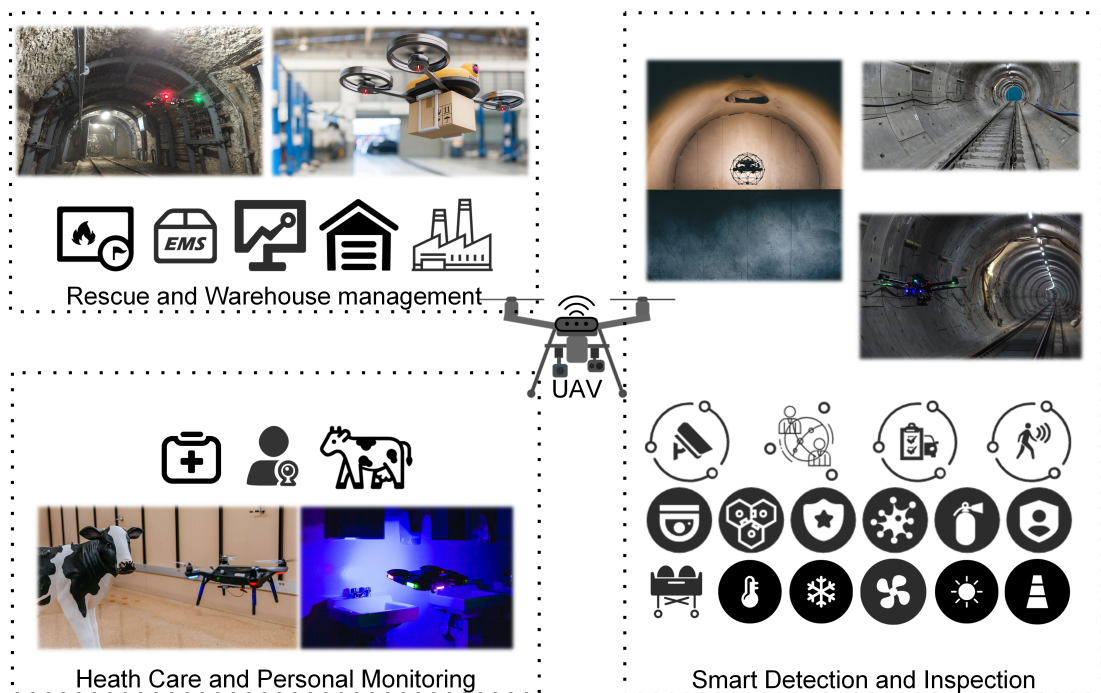


Figure 1.1: UAV applications in GPS-denied and extremely confined environments

mounted on Elios 2 for collision avoidance. However, without the precise position information, the flight of UAV can only rely on the manual control of the well-trained professionals. Besides, the high system cost and instability of UAV in such environments may extremely limit the application scenarios of the system. Under such circumstances, the demand for new positioning technology to achieve the precise localisation of UAV in that operational environment becomes impressively.

Currently, different localisation technologies have been developed for UAV positioning, such as vision, inertial navigation system (INS), infrared, light detection and ranging (LiDAR), ultrasonic and radio frequency (RF) based localisation technologies, where Table 1.1 provides a comparison for all these technologies. Among these, vision based localisation technologies consisting of visual odometry

(VO) and motion capture systems (Vicon, OptiTrack) are known as ones with the highest accuracy which often serve as the ground-truth for performance evaluation. At present, the vision based approaches especially for VO are the most widely utilised technologies on UAV positioning. Due to the highest accuracy and low prior information requirement, the UAV positioning with vision based technologies is suitable for the rescue or exploration missions in unknown environment. Moreover, with the captured image information, the collision avoidance, mapping and smart path planning are able to be implemented which is critical for UAV navigation. Currently, different vision based positioning systems have already been designed for the inspection in extremely confined environments. In [8], a smart UAV inspection system was designed for the application inside an industrial boiler. The precise UAV positioning was achieved through the integration of inertial measurement unit (IMU) or INS and vision based approach. Different from the approach in [8], authors in [9] and [10] from the same research group proposed a deep learning based direction identification approach for micro aerial vehicle (MAV) inspection inside a mining tunnel. Instead of the precise localisation, the images captured by the on-board camera were exploited for heading direction identification to prevent collision. In their approaches, the MAV were considered as a free-flying object, only the heading direction was provided. For the focused application, known as the extremely confined space, with only the heading direction information, the MAV or UAV may crash. Even the precise UAV positioning can be achieve for the inspection in extremely confined environments as aforementioned, however, the low-visibility condition and error accumulation for VO, tedious procedure for the deployment and extremely expensive system cost of motion capture systems will still restrict their applications on UAV in the

focused environments. On the other hand, the INS is the other widely used localisation technology for UAV due to the existing of built-in IMU in flight controller. IMU is known as the sensor which is consist of the three-axis accelerometer, the three-axis gyroscope and magnetometer [11]. It can provide the attitude information (Euler angle and orientation) and motion characteristics (acceleration and angular rate) of the UAV [12]. For the IMU, the position information of the UAV can be directly estimated through the acceleration information with no requirements of any auxiliary components [13]. Due to the implementation simplicity, no auxiliary components requirements, low cost, no impact from the changing environment and high accuracy in a short time period characteristics, the INS or IMU based systems have already been widely utilised on pedestrian positioning [14]. Yet, the error accumulation and external magnetic field effects will lead to the accuracy degradation. Thus, the INS based approaches are often served as part of the sensor fusion method for UAV positioning to smoothen the localisation result [15, 16]. Apart from vision based technologies and INS, there are still some other localisation technologies being applied on UAV in recent years. For instance, the ultrasonic localisation system developed by Marvelmind has been applied and tested by lots of researchers [17–20]. It is able to provide up to 2cm accuracy for UAV positioning. With the on-board battery, the ultrasonic sensor nodes also have no influence on the UAV operation time. Nevertheless, considering the inherent nature of acoustic waves, system performance will drop sharply in cluttered environment, the localisation coverage is limited and the auxiliary nodes are required for localisation [21]. Furthermore, the infrared and LiDAR based localisation technologies are also able to provide the centimetre-level accuracy in GPS-denied environments which have already attracted lots of

attention on UAV positioning [22]. However, for the infrared technologies, the communication range are limited within 2m to preserve the accuracy. For the LiDAR technologies, apart from the positioning, the precise feature map of the environment can also be established with no extra equipment required, which is significant for the UAV navigation in unknown and GPS-denied environment. Currently, lots of research has already been done in this area to achieve the UAV inspection with the LiDAR system. Authors in [23] achieved the precise UAV positioning in dark areas of large historical monuments with the easy-to-obtain 3D point cloud and 2D LiDAR. However, how to generate the precise point cloud in the difficult access space will be a problem. Ozaslan et al. [24,25] designed a MAV based autonomous navigation and mapping system for the autonomous inspection of penstocks and tunnels leveraging the integration of LiDAR, IMU and vision. Yet, the high energy consumption of the LiDAR system will have the huge impact on the operation time of MAV, and the system cost needs to be considered. Mansouri et al. [26] proposed another autonomous navigation approach for MAV in dark underground mine environment with the utilisation of the optical flow and 2D LiDAR. Instead of localisation, they were more focused on the direction identification. Nevertheless, the completely dark environment still has the influence on the localisation performance of optical flow, and the energy consumption of the 2D LiDAR still needs to be taken into account. Furthermore, due to the weight of the LiDAR system, a relatively large UAV like DJI F550 is required to carry all the components. According to all of these, the high system cost, extremely high energy consumption, size and weight of the LiDAR system will restrict its UAV positioning applications in the focused environments.

Towards this end, a new localisation technology and approach which is able to

Table 1.1: Comparison for conventional technologies on UAV positioning

	Accuracy	Localisation Coverage	System Cost	Deployment Difficulty	Weaknesses
Visual Odometry	Up to centimetre	N/A	Low	Low	Suffer from low-visibility condition, error accumulation
Motion Capture System	Millimetre accuracy	Around 6-30m for each camera	Extremely high	High	Extremely high system cost, hard to deploy
INS (IMU)	Up to decimetre	N/A	Low	Low	Error accumulation, external magnetic field effects
Ultrasonic	Up to centimetre	Up to 10m	Low	Medium	Vulnerable to non-line-of-sight (NLOS) path and environment variation, require auxiliary nodes, no orientation information
Infrared	Up to millimetre	Up to 2m	High	Medium	Small coverage, vulnerable to NLOS path, high system cost, no orientation information
LiDAR	Up to millimetre	N/A	High	Low	High system cost, vulnerable to NLOS path, high energy consumption
RF	Up to centimetre	Up to 300m	Low	Medium	Require auxiliary nodes, high communication cost, vulnerable to NLOS path, no orientation information
Sensor fusion based on RF and other technologies	Up to centimetre	Up to 300m	Medium	Medium	System performance may be restricted by the limitation of one localisation technology, the additional components may lead to the increase of the system cost and energy consumption

achieve the high accuracy, high precision, low latency, low energy consumption, robustness to different operational environment positioning of UAV is required for the focused applications in extremely confined and GPS-denied environments.

## 1.2 Aim and objectives

Owing to the rapid development and existing characteristics of the RF based localisation technologies, especially for the ultra-wideband (UWB) based localisation technology, with the ultra-wideband and impulse radio, the high accuracy (up to centimetre-level accuracy), high precision, low cost, low latency and low energy consumption positioning performance can be achieved. Moreover, the RF based localisation technologies will never suffer from the low-visibility condition and error accumulation due to the inherent nature of the electromagnetic wave. These all make these localisation technologies become the ideal candidates for the focused UAV applications in extremely confined and GPS-denied environments.

Nevertheless, in contrast to other localisation technologies, the RF based localisation technologies still have their limitations in the focused applications. Firstly, the distribution strategy of the fixed anchor nodes (auxiliary nodes with known positions) has the great influence on the localisation performance. Secondly, the unreasonable value within the measured information may cause the huge positioning performance oscillation. Thirdly, the RF based localisation systems cannot provide the orientation information for UAV positioning.

Thus, in order to solve the existing issues to achieve the high accuracy, high precision, low latency, low energy consumption and reliable UAV positioning

in the focused environments, in this thesis, the investigation on the RF based localisation technologies, especially for the UWB based localisation technology has been carried out. The UWB based localisation technology is selected here is under the consideration of the existing characteristics of it, including the high precision, high accuracy, low energy consumption and robustness to different operational environments.

According to the in-depth discussion and comprehensive overview for the existing scientific issues and current situation for the RF based UAV localisation technologies, a UWB based low cost, low energy consumption, low computational complexity, high accuracy (at least decimetre-level accuracy) and high precision UAV localisation system will be designed, to achieve the stable and precise control of the UAV for the autonomous inspection in GPS-denied and extremely confined environments. The object of the system can be divided into several parts.

- Comprehensive overview for the state-of-the-art RF based UAV localisation technologies and the existing RF based UAV positioning systems to identify the research challenges in this area.
- Achieve the high accuracy and precision localisation of UAV in GPS-denied environments through the investigation on the UWB based localisation technology.
- Design the anchor distribution strategy help to find the suitable geometry configuration of anchor nodes to improve the localisation performance and keep the system could be applied in the focused extremely confined environments.

- Significantly improve the localisation performance of the pure UWB based localisation technology to achieve the reliable UAV positioning through the sensor fusion based approach with the integration of the UWB and IMU.
- Integrate all the proposed algorithms or strategies into the system to achieve the stable and accurate positioning of UAV with low cost, low energy consumption, low computational complexity and low latency feature in GPS-denied and extremely confined environments.

### 1.3 Research methodology

According to the discussion on the aim and objectives of this thesis, the process about how to carry out the researches to achieve these objectives which known as the research methodology of this thesis will be described and analysed in this section.

In order to find the research challenges and provide the critical analysis for the state-of-the-art solutions to achieve the high precision UAV positioning in GPS-denied and extremely confined environments with the RF based localisation technologies, the comprehensive overview has been done firstly.

Followed by the generalised and summarised research challenges and the issues for the existing solutions, the researches in this thesis have been divided into two parts. The first one is the investigation on the pure UWB based localisation technology, which is to remedy the limitations for other localisation technologies such as the vision, ultrasonic, infrared and LiDAR in the focused environments. Within this, two different approaches have been investigated including the max-

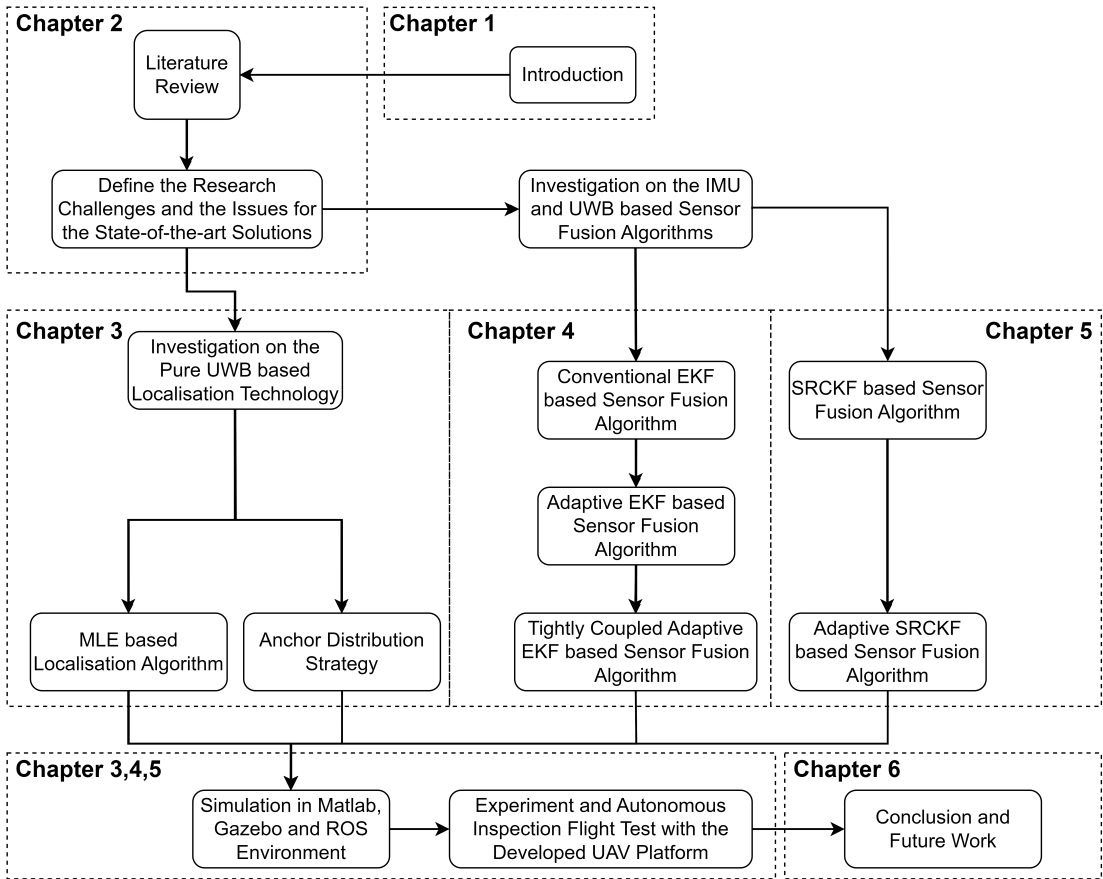


Figure 1.2: The overview for the research methodology

imum likelihood estimation (MLE) based localisation algorithm and the anchor distribution strategy for the precise UAV positioning with the pure UWB based localisation system from different perspectives.

On the other hand, for the purpose of overcoming the performance oscillation and increase the positioning update rate of the pure UWB based system to improve the stability of the UAV in the focused environments. In the second part of the research, the investigation on the IMU and UWB based sensor fusion algorithms have been conducted. Firstly, the introduction for the conventional extended Kalman filter (EKF) based sensor fusion approach has been made help to find the research questions. Afterwards, to deal with the summarised research

questions including the requirement of the prior information for the noise model and the performance degradation caused by the drift from the IMU, the adaptive extended Kalman filter (AEKF) based algorithm and the tightly coupled adaptive extended Kalman filter (TC-AEKF) based algorithm are proposed. However, the leading research question, which known as the linearisation of the transfer matrix, comes from the EKF, AEKF and TC-AEKF based algorithms still limit their positioning performance. To overcome this and further improve the positioning performance, the adaptive square root cubature Kalman filter (ASRCKF) based algorithm is proposed. With the ability for approximation the prediction and observation process, and the ability for adaptive estimation of the noise model, an accurate, precise and reliable UAV positioning can be achieved.

Considering the safety reason for implementing and testing the proposed algorithms on the UAV platform in actual environment. The simulation platform in Matlab, ROS and Gazebo environment has been developed firstly to verify the effectiveness and performance of the proposed algorithms. Finally, the UAV platform has been designed and implemented to evaluate the performance of the proposed algorithms and validate the engineering practicality of the UAV based inspection system. The overview for the research methodology of this thesis is depicted in Fig. 1.2.

## **1.4 Thesis organisation**

This thesis is composed of six chapters including the introduction chapter. The organisation of the following chapters are outlined as follows:

## Chapter 1. Introduction

Chapter 2 is dedicated the literature review. From different perspectives, the comprehensive overview for the existing RF based UAV localisation technologies, the classical localisation mechanisms with these technologies and the existing RF based UAV positioning systems is given help to find the research challenges in this area and the limitations for the existing systems. Followed by, the overview for different types of the UAV platforms has been provided help to find the suitable one for the focused applications. Moreover, according to the overview, the evaluation framework for the RF based UAV positioning system is established in this chapter which can be served as the criterion to validate the performance of the system. Finally, the comprehensive analysis and discussion on the current challenges in this area are made to elicit the potential research issues in this area to serve as the guidance for the following researches.

The main content of the Chapter 3 can be divided into three parts. Firstly, the introduction for the MLE based UAV positioning algorithm is provided which is to achieve the localisation of the UAV in GPS-denied and extremely confined environments with the UWB based localisation system. Followed by, the description for the designed anchor distribution strategy is given help to find the best geometry configuration of the fixed anchor nodes in different operational environment. Finally, the simulation and experiment in the laboratory environment are carried out to comprehensively validate the effectiveness of the positioning algorithm and the distribution strategy.

In order to limit the performance influence leads by the unreasonable value within the measurements from the UWB sensor nodes, Chapter 4 is mainly focused on the investigation on the UWB and IMU based EKF sensor fusion al-

gorithms. The description and discussion for the EKF, AEKF and TC-AEKF sensor fusion algorithms is provided to solve the existing questions including the unreasonable value within the measurements from the UWB sensor nodes, unknown prior information about the noise model and the drift within the IMU measurements. To comprehensively evaluate the performance of these proposed algorithms, the simulation in Gazebo environment and the experiment in laboratory environments are conducted. The analysis for the final simulation and experiment results are also provided in this chapter.

Considering the performance oscillation caused by the linearisation of the transfer matrix within the EKF based sensor fusion algorithm and the unknown prior information about the noise model, in Chapter 5, the investigation on the square root cubature Kalman filter (SRCKF) and ASRCKF based sensor fusion algorithm is made. The simulation in Gazebo environment and the experiment in laboratory environments are carried out in this chapter to validate the effectiveness of the proposed algorithms. Furthermore, for the purpose of proving the engineering practicability of the proposed algorithm and the designed UAV system, the autonomous inspection flight tests are also conducted in this chapter.

Finally, Chapter 6 concludes the thesis with the discussion of all the proposed algorithms, strategies and the systems in relation to the aim and objectives. Afterwards, the major contributions for this thesis have been summarised, the limitations which relevant to the future work of my research is made.

## Chapter 2

# Literature Review

### 2.1 Introduction

According to the discussion for the existing UAV positioning technologies, the RF based technologies can be the ideal candidate for the focused application scenarios. Therefore, in this chapter, the comprehensive overview for the RF based localisation technologies with different radio communication protocols, the classical localisation mechanisms and the state-of-the-art RF based UAV positioning systems will be carried out to help to identify the research challenges and existing solutions for each in the relevant area, and to establish the evaluation framework for the performance validation of the RF based UAV positioning system. Furthermore, the suitable UAV platform is also the essential part for the focused applications in the extremely confined environments. Therefore, the overview for the existing UAV platforms have also been provided in this chapter help to find the suitable one for the focused applications.

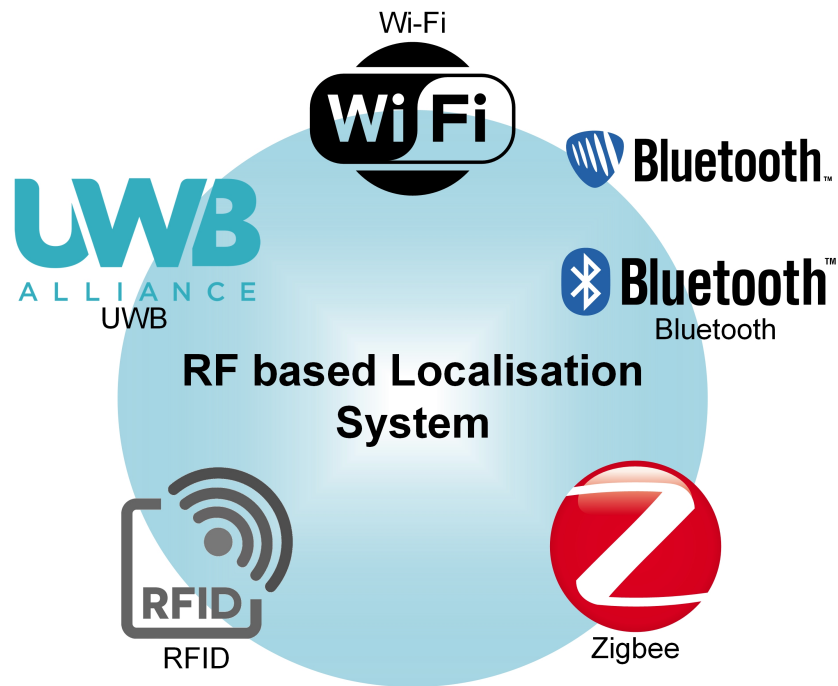


Figure 2.1: RF based localisation technologies

## 2.2 RF based UAV localisation technologies

In this section, an overview of the existing RF based UAV localisation technologies with different radio communication protocols are elaborated. Subsequently, an in-depth discussion and analysis for the suitability and challenges of each technology on precise UAV localisation are presented. Moreover, several state-of-the-art RF based localisation technologies which successfully achieve decimetre-level localisation accuracy are also reviewed, owing to the potential applications on UAV localisation in the future. RF based localisation technologies including Wi-Fi, Bluetooth, Zigbee, radio frequency identification (RFID), UWB and the sensor fusion based localisation technologies shown in Fig. 2.1 are discussed in detail in the following subsections.

### 2.2.1 Wi-Fi based localisation technology

Wi-Fi, belonging to the IEEE 802.11 standard family, is known as one of the most commonly used wireless network technologies in the last several decades. Due to the universality, Wi-Fi turns into one of the simplest implementation localisation technology, and several researches have already been done on UAV positioning.

In [27], a Wi-Fi based precise UAV position estimation and collision avoidance system was implemented through the consideration of the coloured measurement noise model and the localisation with the EKF. Differently, another Wi-Fi based UAV navigation system was designed in [28], with the linear Kalman filter (KF) to lower the computational complexity of the EKF for energy consumption reduction. On the other hand, different from the localisation with the single technology, a cooperative UAV localisation approach was proposed in [29]. With the combination between the global navigation satellite system (GNSS), UWB, IMU and Wi-Fi, a decimetre-level localisation accuracy was achieved. However, the accuracy was reduced to 3m when only the Wi-Fi module exists. Considering the meter-level accuracy, only outdoor application is suitable for the aforementioned systems. To further improve the accuracy, the algorithm proposed in [30] leveraged multidimensional scaling (MDS) and weighted centroid localisation (WCL) achieved decimetre-level localisation accuracy. However, many more access points (anchor nodes) are required to preserve the accuracy and the evaluation has only been done in simulation. Importantly, the influence of NLOS error caused by the unpredictable people or object was not taken into account for all the aforementioned systems.

As discussed, the UAV positioning with the Wi-Fi based localisation system

is still restricted owing to the unacceptable accuracy and unreliable performance. However, the development of the Wi-Fi technology and the introduction of the additional equipment like the massive antenna array still preserve the opportunity for decimetre-level accuracy and reliable localisation performance with the Wi-Fi based system. Currently, the most popular works in this area are the Chronos [31] and SpotFi [32]. They all achieved decimetre-level accuracy with the Wi-Fi based system but under different methods. In [31], frequency hopping was exploited for the emulation of wideband radio to enhance the bandwidth of the Wi-Fi signal. Time resolution is inversely related to the radio bandwidth, that is the reason why precise time based measurement can be obtained. Meanwhile, orthogonal frequency division multiplex (OFDM) and inverse non-uniform discrete Fourier transform (inverse-NDFT) were applied to eliminate the packet detection delay and identify direct path to keep system performance in the NLOS environment. Finally, a median accuracy of 65cm in the line-of-sight (LOS) and 98cm in the NLOS environment were attained with the off-the-shelf commercial Wi-Fi modules. Moreover, the system performance was tested on a commercial drone (AscTec Quadrotor) where the root mean squared error (RMSE) of the relative distance was 4.2cm. However, in strong NLOS environments it will lose effectiveness, due to the dominant peak of channel impulse response (CIR) not necessarily characterising the direct path. In addition, energy consumption of the system keeps high owing to the sweep of multi-frequencies. Unlike [31] and [32] introduced the angle of arrival (AOA) for precise localisation. A super-resolution algorithm was presented for the precise AOA computation and combination of the AOA and time of flight (TOF) was utilised for direct path identification to overcome the influence of the NLOS path in the cluttered environment. Finally,

the median error of 0.4m and 1.6m were achieved in LOS and strong NLOS scenarios. However, with the additional antenna array, the operation time and application scenarios will be restricted. In order to reduce the communication cost and exclude the additional components, Li et al. [33] designed a time difference of arrival (TDOA) based localisation approach with commercial 80MHz Wi-Fi system achieved 0.23m and 1.5m accuracy for outdoor and indoor applications which is much more suitable for the UAV localisation. However, a localisation server and additional synchronisation algorithm are needed for the precise localisation. Moreover, many more sniffer nodes (anchor nodes) are required to be deployed to preserve the accuracy in the NLOS environment.

On the other hand, lots of fingerprint based approaches emerge in recent years, which are able to achieve the decimetre-level accuracy with the Wi-Fi based system [34–40]. However, with the inherent rule of fingerprint, it is not suitable for the UAV localisation in the dynamic or unknown environment.

### **2.2.2 Bluetooth based localisation technology**

Bluetooth, a family member of the IEEE 802.15 standard, also known as one of the extensively utilised communication technologies in our daily life, which works on the same frequency band compared with Wi-Fi. But Bluetooth shows low cost, lower energy consumption and small size features, especially with the emerging technology Bluetooth low energy (BLE) developed by Bluetooth special interest group (SIG) [41]. With the aforementioned characteristics, scientific researches and applications on the precise localisation technology based on Bluetooth or BLE are growing dramatically in recent years. However, due to the limited bandwidth,

low cost and low energy consumption features, it is unrealistic to implement time based or angle based localisation mechanisms on Bluetooth based localisation systems. Therefore, received signal strength (RSS) turns into the most commonly used localisation mechanism for Bluetooth and BLE.

Currently, several Bluetooth based localisation systems have already been designed for UAV positioning in GPS-denied environments. In [42], a UAV patrol system was designed for UAV navigation in the GPS unstable area through RSS measurements from Bluetooth beacon. In both [43] and [44], relative localisation for UAV swarm was achieved with Bluetooth beacons. To improve the accuracy, authors in [43] and [44] all fused the other measurements such as odometry, altitude, velocity and displacement information from additional components with RSS from BLE and Bluetooth beacons achieved precise localisation and collision avoidance of UAV. Apart from the applications on UAV, [45] and [46] both presented the Bluetooth based localisation system for robot navigation in GPS-denied environments. The authors in [45] mainly focused on the RSS calibration, leveraging the 10th order finite impulse response (FIR) filter for the measurement noise mitigation which finally achieved a nominal error of 10cm on distance measurement. Whereas, the authors in [46] more focused on the distance obtaining and position estimation methods to improve the performance. A novel method for distance estimation and trilateration approach was proposed which achieved the final error of  $0.427 \pm 0.229m$ .

In addition, some commercial BLE based localisation systems which can achieve the decimetre-level accuracy are also reviewed here, due to the potential for UAV positioning. iBeacon [47] proposed by Apple Inc in 2013 is the typical representa-

tive. In [48], the localisation performance of iBeacon was evaluated with different placement patterns. Where the average accuracy below 1m was obtained, but only in the open environment. For the accuracy improvement, a joint Kalman filter and particle filter (KFPPF) algorithm was presented and implemented with iBeacons in [49] which successfully achieved the median localisation error of 0.7m and 0.947m in 2D and 3D environment and showed robustness in the NLOS environment. However, the accuracy was obtained with seven iBeacons, as only three iBeacons exist, the accuracy decreased by half. Besides, with the high computational complexity, the localisation latency and system reliability will also be influenced. Therefore, further research is still required for UAV applications. Rule out of iBeacon, other commercial systems which utilise BLE for precise localisation, like high accuracy indoor positioning (HAIP) [50] developed by Nokia and Gimbal proximity beacon [51] presented by Qualcomm all keep the possibility for UAV localisation in GPS-denied environments. However, further research is still required especially for the problem of small localisation coverage and vulnerable to NLOS path.

### **2.2.3 Zigbee based localisation technology**

Zigbee is the communication protocol that standardises the higher layers of the protocol stack under the IEEE 802.15.4 standard. It defines the characteristics of the physical and MAC layers for low-rate wireless personal area networks (LR-WPAN) [52]. Zigbee shows low data rate, low energy consumption and low cost features which is targeted towards monitoring, automation and remote-control applications [53]. Compared with Bluetooth, Zigbee shows lower data rate, lower

energy consumption, longer coverage range and accommodate up to 65000 communication nodes for one sub-network. However, Zigbee still vulnerable to the influence of NLOS path and low data rate may cause high localisation latency which runs counter to the requirements on UAV. Thus, only one scientific paper utilising Zigbee based system for UAV localisation has been carried out currently, according to the investigation. In [54], a UAV localisation system was proposed which combined Zigbee with INS achieved the absolute accuracy of 20cm on an automated quadrotor APM 2.0. However, the influence of NLOS path was not considered, system performance was only tested in open area. Meanwhile, the localisation latency was not mentioned, only a sampling rate for localisation at 1s was set in simulation platform.

#### **2.2.4 RFID based localisation technology**

RFID is designed as a wireless communication mean which utilises RF electromagnetic fields for identification and tracking. On the basis of response mode, RFID tag nodes (nodes to be located) can be divided into three categories [55]:

- **Passive tag.** Receive signal passively and answer back using the power from the emitted signal by the RFID reader. There is no requirement of internal power source, smallest size and lowest cost within all the types of RFID tag nodes. However, communication range is limited (roughly one to five meters).
- **Semi-passive tag.** It receives signal passively, but utilises the on-board battery to generate the transmitting power. Additional function such as real-time tracking or environment detection can be provided. However, commu-

nication range still remains short and new problems such as extra weight, larger size, higher cost, shorter life and temperature sensitivity are brought in [56].

- Active tag. It is able to transmit signal actively with the on-board battery. It mainly utilises in real time location service (RTLS). It has the ability to broadcast signal periodically for data communication and localisation. However, its weight, size, cost and energy consumption also need to be considered.

Meanwhile, the aforementioned nodes are all sensitive to harsh environments and contribute to radio noise which may seriously degenerate localisation performance.

Considering the unique characteristics of the passive RFID node, scientific researches on UAV localisation with this technology have emerged in recent years. Within them, two different systems designed by Zhang et al. in [57] and [58] are the typical representative. In [57], a RFID based 6 degrees of freedom (6-DOF) enhanced localisation system for UAV called RFUAV was designed. Thanks to the small size and no power supply features of the passive RFID, position and orientation information could be garnered through communication between the RFID readers and passive RFID tag nodes ( $\geq 3$ ) deployed on UAV in the system. Finally, the mean error of 0.04m and  $2.5^\circ$  were obtained with low localisation latency through commercial off-the-shelf RFID equipment. On the other hand, instead of localising UAV itself, the other UAV navigation system was also designed by the same research group [58], where the navigation was achieved with the localisation of the UAV hand-held controller. In this system, the passive RFID

nodes were deployed on UAV controller. With the same computation method, the 6-DOF pose of the UAV controller could be calculated. Finally, the control commands will be generated from the controller's pose and sent to UAV for navigation in indoor environment. Even the high accuracy and low latency localisation can be achieved as aforementioned. Owing to the inherent characteristics of RFID, the systems are still vulnerable to the NLOS path, and the localisation coverage range is limited by the communication range of RFID readers. Therefore, the aforementioned systems are only suitable for short range and free space UAV positioning or navigation. Differently, Choi et al. [59] and Longhi et al. [60] both designed the passive ultra-high frequency (UHF) RFID based UAV positioning system with RFID reader deployed on UAV. In the localisation process, the communication between RFID reader on UAV and reference RFID nodes embedded on the floor and plant vases was exploited to measure RSS information for UAV positioning. Finally, the authors in [60] declared that a decimetre-level accuracy could be garnered. However, the performance of these two approaches is still vulnerable to the NLOS path and the localisation coverage is still restricted.

### **2.2.5 UWB based localisation technology**

The UWB is known as a sequence of impulse radio utilising ultra-wideband. It offers the enormous development opportunities in radar, safety and position applications [61]. Different from the narrowband signal, with the ultra-wideband and impulse radio, it is possible to transmit the signal with extremely short duration time (0.20ns-1.5ns) where a high temporal resolution can be achieved, also showing the robustness to multipath fading [62]. Moreover, a short duration time

means a low transmit power. Therefore, the low energy consumption will be another key feature for the UWB, in contrast to other UAV localisation technologies. But compared with other radio communication protocols, the energy consumption of UWB still keeps high. Considering the visible characteristics of UWB, it becomes a reliable and feasible localisation technology which has drawn lots of attention for UAV positioning in the past few years [6, 63–81]. Among them, the group from Nanyang Technological University is the most in-depth research group in this area. Up to now, they have already published 9 papers on UAV localisation with UWB within 4 years [63, 65, 71–76, 80].

According to the method for localisation, the review will be given in three parts. The first part will be auxiliary localisation where localisation is achieved with known position and fixed anchor nodes. The system proposed in [6, 63–70] all utilised the communication between tag node deployed on UAV and fixed anchor nodes for UAV localisation. Among them, in [63–65], the conventional two-way time of flight (TW-TOF) approach was exploited to calculate the time delay between tag node and anchor nodes. Meanwhile, velocity and displacement information gathered by IMU was also taken into account which fused with the aforementioned information by EKF to improve the localisation accuracy and keep the reliability. Moreover, authors in [63] also proposed a calibration and outlier detection method through the linear regression and calculation of Mahalanobis distance [82] which was utilised for UWB information calibration and unreasonable data detection. Unlikely, the authors in [65] mainly focused on anchor self-localisation which leveraged the nonlinear regression (NLR) achieved anchor self-localisation and position calibration. Finally, the decimetre-level accuracy was garnered for all these three systems, especially for [63], the average

position error in X-Y plane of 0.071m and the maximum error of 0.2m within  $7 \times 7m$  the GPS-denied area were obtained. To further improve the accuracy, authors in [66–68] all focused on the accuracy improvement through the mitigation of the clock drift. Where the hybrid approach based on MDS, loosely coupled EKF (LC-EKF) and double-sided two-way ranging (DS-TWR) was proposed in [66]. Symmetric double-sided two-way ranging (SDS-TWR) was exploited in [67] and [68] for clock drift mitigation. Differently, You et al. [69] applied unscented Kalman filter (UKF) to avoid neglecting the high-order terms of the nonlinear observation equation for performance improvement. On the other hand, UWB based UAV localisation systems with TDOA localisation mechanism were designed in [6] and [70]. In order to reduce the communication cost compared with TW-TOF, DS-TWR and SDS-TWR, in their systems, UAV position can be calculated directly through the broadcast signal from tag node on UAV. Detailed information about the localisation principle for each localisation mechanism will be given in Section 2.3.

To remedy the requirement of fixed anchor nodes, the approaches which leverage the communication between multi-UAVs for relative localisation emerge in recent years. In [71, 72], a relative localisation approach was designed for the relative localisation and formation control of multi-UAVs. In their system, the accurate distance and displacement information measured by UAV in different position through UWB and IMU were applied for the UAV relative initial position estimation. Afterwards, the relative position between UAVs could be calculated through EKF, where the estimated initial position was utilised as the initial input of EKF. According to their simulation and experiment results, the system was capable of the meter level relative localisation and formation control. However, an

appropriate trajectory for UAV needs to be defined to preserve the performance, including the nonlinear path and piecewise linear path. Length and shape of the trajectory all have huge impact on the different extent of localisation performance. Further development has been done in [73–75] from the same research group. In the new system, the requirement of appropriate trajectory was no longer needed. Instead, they exploited UWB and IMU to measure the distance and velocity information for UAV itself, also leveraged information exchange between dynamic UAVs to obtain the precise relative position for UAV swarm through graph theory based approach. The algorithm could finally achieve the decimetre-level accuracy according to their experiment results. On the other hand, another cooperative localisation approach was presented by the same group [76]. They proposed two different methods called covariance intersection (CI) and linear consensus (LC) based filter achieved the cooperative localisation by information exchange and states estimation with only one landmark. Cao et al. [77] also designed a UWB based relative localisation system which equipped all the anchor nodes on leader UAV to localise the follower equipped with tag node for the formation control of UAV swarm. Likewise, the authors in [78] designed the same UWB based localisation system which deployed four anchor nodes on ground station (vehicle of a military convoy) to navigate UAV.

Finally, in order to improve the localisation accuracy and coverage, sensor fusion methods which combined UWB with different types of vision based localisation approaches have been presented. In [79], RGB-D sensing was combined for mapping and localisation of UAV to implement long-term autonomous operation. In [80], an integrated UWB-vision system was put forward to achieve the autonomous landing for UAV on the moving target. Where UWB, IMU,

Optical-flow and vision were all integrated help for approaching and landing on the moving target. Tiemann et al. [81] also designed a UWB-vision approach which integrated UWB with the monocular simultaneous localisation and mapping (SLAM) [83, 84] to improve system performance and increase localisation coverage.

### **2.2.6 Summary and discussion on the RF based UAV localisation technologies**

A summary and discussion for pros and cons of the existing RF based UAV localisation technologies with different radio communication protocols are given in Table 2.1. Among them, UWB based systems attract lots of attention on precise UAV positioning which has already published over 20 papers in the last five years, owing to the characteristics of high accuracy, low latency and robust to harsh environment. Moreover, considering the superiority of UWB, sensor fusion approaches which combine UWB with vision, IMU or other localisation technologies emerge in recent years are also valuable for further research in this area.

## **2.3 Classical localisation mechanisms**

In this section, a detailed review for the classical localisation mechanisms including RSS, AOA, TOF, time of arrival (TOA), TDOA and Fingerprint etc. with RF based UAV localisation technologies are presented. Meanwhile, the capability, suitability and challenges for each on UAV positioning are also summarised

Table 2.1: Comparison for the existing RF based UAV localisation technologies with different radio communication protocols

	Frequency Band	Data Rate	Accuracy	Advantage	Disadvantage	Existing Literature
Wi-Fi	2.4GHz, 5GHz	144Mbps 250Mbps	Meter-level	Implementation simplicity, large coverage, high transmission rate	High energy consumption, meter-level accuracy, vulnerable to NLOS path	[27–30]
Bluetooth	2.4GHz	1Mbps, 24Mbps for BLE	Around decimetre-level	Implementation simplicity, low energy consumption	Small coverage, low transmission rate, vulnerable to NLOS path	[42–44]
Zigbee	2.4GHz	250kbps	Meter-level	Extremely low energy consumption, low system cost	Low transmission rate, high latency, vulnerable to NLOS path	[54]
RFID	LF(120 150kHz), HF(13.56MHz), UHF(433MHz, 865 868MHz, 902 928MHz), mi- crowave(2450 5800MHz, 3.1 10GHz), mm- wave(24.125GHz)	Depend on the frequency band	Up to centimetre-level	Extremely low energy consumption, implementation simplicity, low system cost, high accuracy with specific approach	Small coverage (1m-5m), vulnerable to NLOS path	[57–60]
UWB	3.1 10.6GHz	Up to 1 Gbps	Up to centimetre-level	High accuracy, extremely high transmission rate, low latency, immune to interference, robustness to NLOS path	High energy consumption and system cost compared with other radio communication protocols	[6, 63–81]

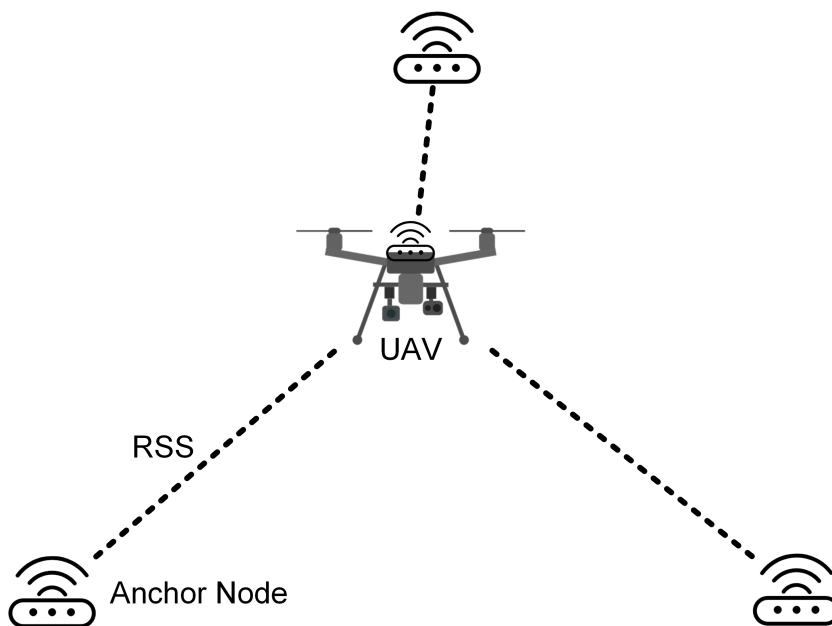


Figure 2.2: RSS based localisation mechanism

by the end of this section.

### 2.3.1 RSS based localisation mechanism

The RSS is known as the field intensity of a signal measured at the receiver [85]. With the measured RSS, it is simple to quantitatively derive the signal attenuation and calculate the transmission distance followed by an appropriate signal propagation model. Subsequently, position information can be estimated with trilateration or multilateration by the transmission distance. The propagation model given by [86] is shown in (2.1), and Fig. 2.2 gives the schematic diagram of the RSS based localisation mechanism.

$$P_{w2} = P_{w1} + 10 \log K_{antgain} - 10 \kappa \log \frac{d_{21}}{d_0} + \epsilon \quad (2.1)$$

Where  $d_{21}$  represents the calculative distance between receiver and transmitter,  $P_{w2}$  and  $P_{w1}$  are assumed as the signal power at each of them,  $K_{antgain}$  is a constant determined by antenna gain and reference distance  $d_0$ ,  $\kappa$  represents the path loss factor,  $\epsilon$  is the measurement noise for RSS which is commonly known as additive white Gaussian noise (AWGN) with zero mean and variance of  $\sigma_\epsilon^2$ .

As recording RSS is the basic function for almost all the communication devices in nowadays. RSS based localisation mechanism becomes the simplest implementable mechanism among RF localisation technologies. However, in actual applications, especially in GPS-denied environments, wireless signal is much more vulnerable to external environmental disturbance, such as occlusion, multipath effect etc. Meanwhile, signal attenuation changes continually with environment variation or media change. Hence, RSS based localisation mechanism is not suitable for UAV localisation in harsh or dynamic environment. However, thanks to cost saving and implementation simplicity features, RSS based localisation mechanism still draws lots of attention in open environment.

As aforementioned in Section 2.2, RSS based localisation mechanism has already been widely used on UAV localisation. In [27], a UAV position estimation and collision avoidance system were designed which analysed coloured noise in RSS measurement to improve system accuracy. Masiero et al. [28] exploited RSS from nodes communication with linear KF for localisation which successful reduced the computational complexity and improved the operation time of UAV. Zhou et al. [42] utilised RSS measured by Bluetooth beacons achieved UAV navigation in GPS unstable environment. Yu et al. [54] exploited RSS measurements collected by Zigbee nodes as the input of EKF achieved decimetre localisation

accuracy. Cheng et al. [87] designed a NLOS detection strategy for mini-UAV localisation system which analysed RSS measurement model to identify propagation condition for NLOS detection to improve localisation accuracy. Tovkach et al. [88] proposed an RSS based localisation approach for UAV with unknown transmit power. Soria et al. [43] and Coppola et al. [44] all designed the relative localisation approaches, applied relative distance from RSS with additional odometry and altitude measurements achieved relative localisation of UAV swarm.

### 2.3.2 AOA based localisation mechanism

The AOA, denoted here as the angle of arrival, also known as the direction of arrival (DOA), is the localisation mechanism which exploits the angle information recorded at multiple receivers for positioning. As shown in Fig. 2.3, with the AOA information from antenna array and the prior location information of anchor nodes, UAV position can be estimated through the triangulation. Clearly, with the AOA based localisation mechanism, the minimum number of anchor nodes for localisation can be reduced which can expand the application scenario of UAV. Moreover, the traditional RF based localisation system only provides position information. However, it is possible for the AOA based localisation mechanism to provide the 6-DOF state information which have great significance for UAV positioning. Owing to the existing characteristics, several scientific researches have been conducted for UAV localisation with the AOA based localisation mechanism.

Pavlenko et al. [89] proposed a 16-element sparse dome array for UAV localisation based on AOA localisation mechanism where  $1\sigma$ -values of less than  $2^\circ$  was achieved. For further research, they also developed another localisation system

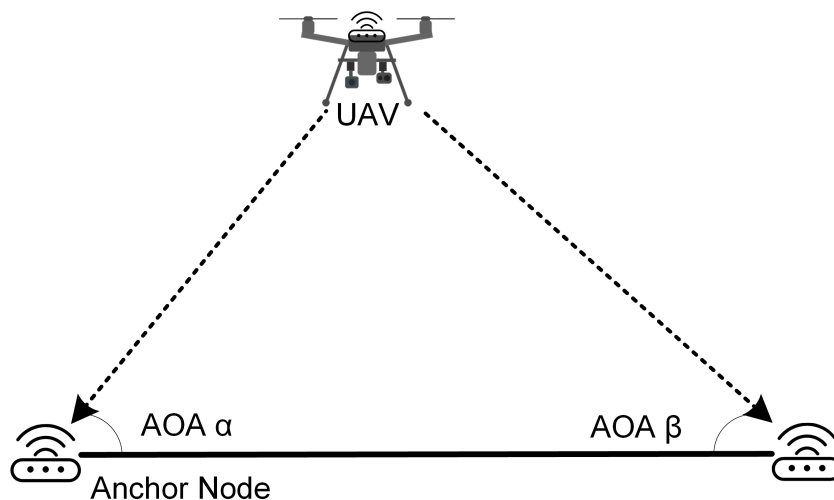


Figure 2.3: AOA based localisation mechanism

for UAV via radar based wireless local positioning system (WLPS) [90]. The experimental results show that the RMSE of the 3D positioning equals to 36cm with one anchor node involved, and improved to 31cm with four anchor nodes involved. However, as discussed in their paper, weight of radar unit with the integrated dome array is about 1.78kg, therefore, the operation time of UAV will be influenced greatly. Different from UAV positioning, Nguyen et al. [91] designed an RF based localisation system focused on the detection and tracking of UAV and its controller with AOA measurements. However, only average error of  $12.2^\circ$  and 12.71m were achieved.

On the other hand, several recent proposed AOA based high accuracy localisation systems have also been reviewed, considering their potential application to UAV positioning. Spotfi [32] is known as the typical representative which realised decimetre-level localisation accuracy in harsh environment with the precise AOA information. Zhang et al. [92] designed a 3D localisation system which achieved the median localisation error of 0.78m in indoor environment through

AOA based localisation mechanism with commercial off-the-shelf infrastructures. Soltanaghaei et al. [93] proposed a novel localisation approach that realised accurate localisation through multipath of AOA with only one anchor node.

Although, much more advantages of the AOA based approaches can be obtained, there are still many factors that may influence the localisation performance, especially in GPS-denied environments. Owing to the inherent features of the triangulation, even a small measurement error can cause a huge impact on the localisation accuracy with the increasing of transmission distance which will restrict the flight range of UAV. Besides, the system cost, energy consumption and payload of UAV will be increased, considering the additional complex hardware. Most importantly, in dense multipath environment, the AOA estimates are biased in general. So, further research is still needed for the AOA based localisation mechanism on UAV positioning in GPS-denied environments.

### **2.3.3 TOF/TOA based localisation mechanism**

Both the TOF and TOA are the classical time based localisation mechanisms for the RF based localisation systems. They all exploit the time delay between the transmitter and receiver for range estimation as shown in Fig. 2.4. With the range information, the UAV positioning can be realised through the trilateration or multilateration. Compared with the RSS and AOA, the TOF/TOA is able to provide the high accuracy performance with no additional equipment required, which is significant for UAV positioning in GPS-denied environments. However, clearly from Fig. 2.4, the strict clock synchronisation between all the sensor nodes in the network is required.

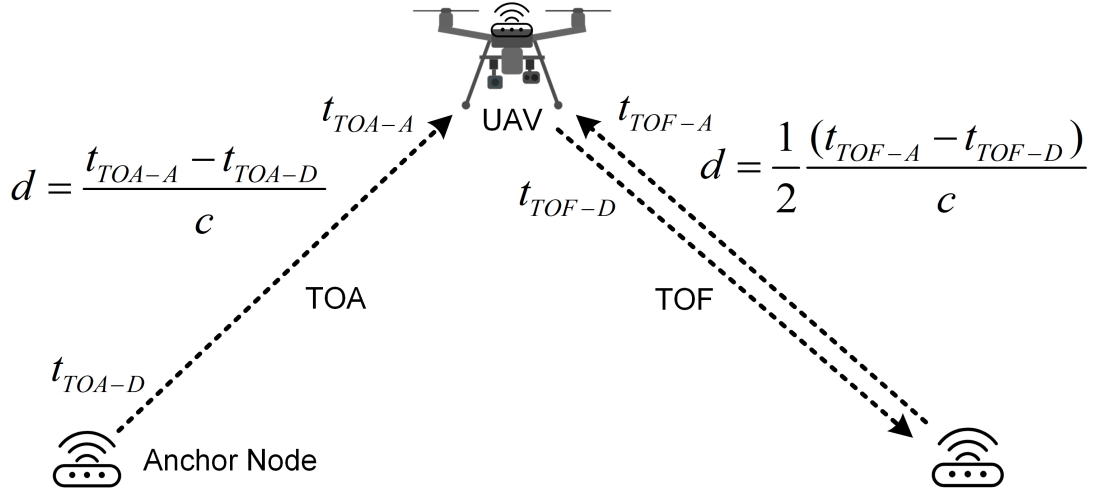


Figure 2.4: TOF/TOA based localisation mechanism

To eliminate the impact of clock difference, several different approaches have been proposed [94, 95]. The conventional approach is known as two-way ranging (TWR) or TW-TOF. As shown in Fig. 2.5, with the existence of time of departure (TOD) and TOA from the transmitter and the measured response delay on receiver, it is able to subtract clock difference theoretically. Owing to the implementation simplicity and high localisation accuracy (up to centimetre-level accuracy), TWR has already been widely used on UAV positioning in GPS-denied environments [63–65, 69, 71–76, 78]. However, clock drift caused by unpredictable response delay and low performance crystal oscillator on sensor nodes, will lead to a precision degradation. In addition, with the increasing communication cost, localisation latency and energy consumption cannot be overlooked.

To settle the matter, DS-TWR is proposed. As shown in Fig. 2.6, the influence of clock drift is mitigated through the average time delay from two-round trip. In [66, 77], DS-TWR has already been applied and tested for the precise localisation and formation control of UAV. In addition, for further improvement, SDS-TWR

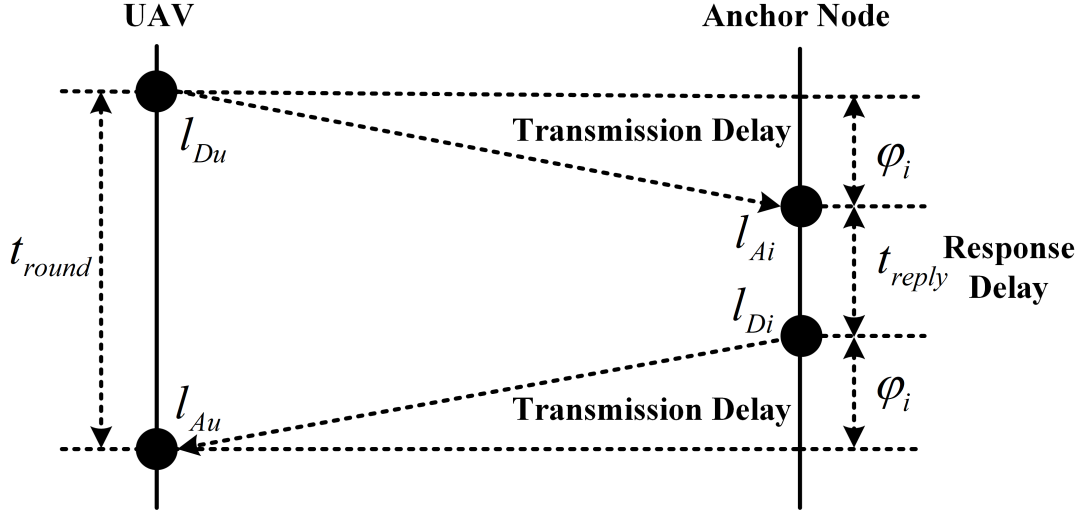


Figure 2.5: TWR/TW-TOF based localisation approach

is designed with the similar principle. Compared with the DS-TWR, the interval delays are equal on the both participating nodes. Performance of SDS-TWR on UAV localisation has been evaluated in [67, 68], even much more precise result can be garnered, but keeping the same clock frequency on both sides is still difficult to implement. Meanwhile, high accuracy is at the expense of additional communication cost, where position update rate will be significantly restricted which may influence the stability of UAV.

### 2.3.4 TDOA based localisation mechanism

Another classical time based localisation mechanism widely used on the RF based systems is the TDOA. Different from the TOF/TOA, the TDOA based localisation mechanism utilises the distance difference between each receiver for positioning. Specifically, it leverages the recordings of the TOAs from the broadcast signals by the transmitter to calculate the TDOAs for the localisation through the hyperbolic theorem. As shown in Fig. 2.7, suppose the distance information

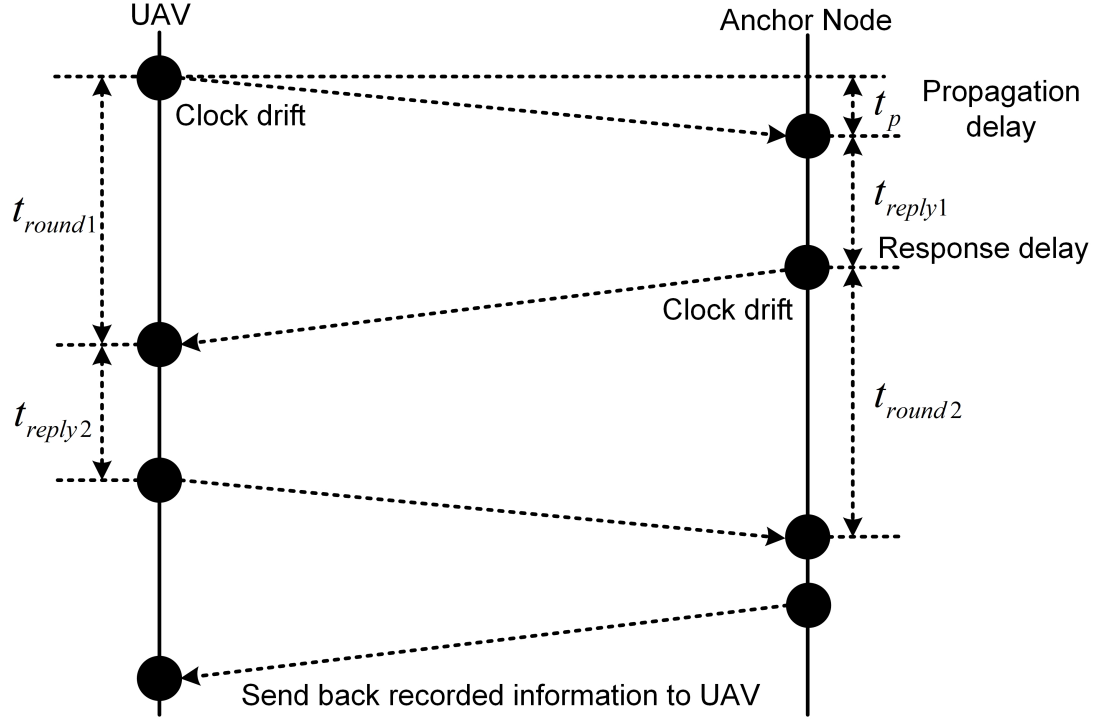


Figure 2.6: DS-TWR based localisation approach

between four anchor nodes and UAV are  $d_i (i = 1, 2, 3, 4)$ . Thus, the distance difference can be calculated and represented as  $d_{ij}$ . With the known position information  $\mathbf{p}_i$  for each anchor node and the record TOAs  $t_i$ , position information  $\mathbf{p}$  of UAV can be estimated through the localisation equation below:

$$\begin{cases} \|\mathbf{p}_1 - \mathbf{p}\| - \|\mathbf{p}_2 - \mathbf{p}\| = c(t_1 - t_2) \\ \|\mathbf{p}_1 - \mathbf{p}\| - \|\mathbf{p}_3 - \mathbf{p}\| = c(t_1 - t_3) \\ \|\mathbf{p}_1 - \mathbf{p}\| - \|\mathbf{p}_4 - \mathbf{p}\| = c(t_1 - t_4) \end{cases} \quad (2.2)$$

Since only the time difference from each sensor node is enough for precise positioning, the localisation latency and energy consumption of the TDOA based localisation mechanism can be reduced greatly compared with the TOA and

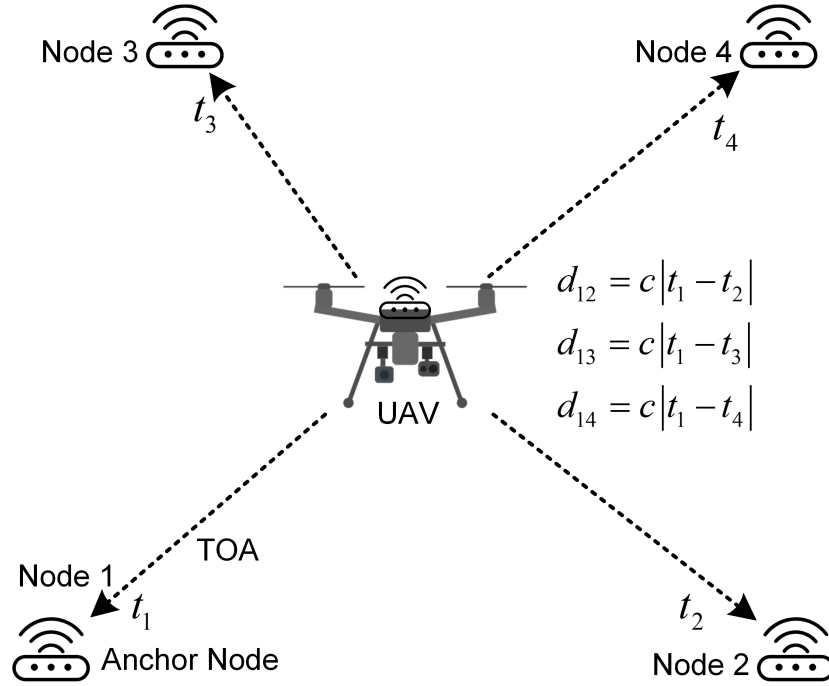


Figure 2.7: TDOA based localisation mechanism

TOF, which can effectively improve the stability and operation time of the UAV in GPS-denied environments. Considering the existing characteristics, different localisation systems have already been designed for UAV positioning with the TDOA based localisation mechanism. Tiemann et al. [6, 96, 97] carried out a series of scientific researches on TDOA based localisation mechanism to achieve precise localisation for multi-UAVs and mobile robots. Likewise, the authors in [98] designed a localisation system which successfully implemented the stable control of UAV in GPS-denied environments with measured TDOA and EKF. Sinha et al. [99] and de Sousa et al. [100] both did related researches for UAV localisation through TDOA. But, not mainly focused on the UAV localisation in GPS-denied environments. Sinha et al. [99] intended to analyse the impact of 3D Antenna Radiation Patterns through TDOA based localisation for UAV. The authors in [100] mainly concerned the precise localisation of UAV in urban

area with a full of NLOS path. They exploited ray-tracing fingerprint build from TDOA to identify the main obstacle reflected signal as virtual anchor to achieve the precise localisation for UAV in NLOS scenario.

Despite precise and low latency localisation is able to achieve through the TDOA based localisation mechanism, there are still several factors that may restrict the performance. Obviously, since TOAs are measured by different anchor nodes, precise synchronisation is required between all these receivers. Similar to other time based approaches, TDOA is also vulnerable to the time-delay caused by the NLOS path and measurement noise. In addition, considering applications on UAV, the localisation process is conducted by receiver or localisation server for the TDOA based localisation mechanism. Therefore, an extra step is required to send back the estimate position to UAV, which may cause the position loss or low update rate due to the potential signal block or interference.

### **2.3.5 Fingerprint based localisation mechanism**

Considering that the RSS based localisation mechanism requires prior information, deviates dramatically with the existence of the NLOS path and external interference, is vulnerable to environment variations and measurement noises. Another method which extracts the features from fingerprint dataset built with RSS or other radio information from the surrounding nodes for positioning is designed. The localisation process of the fingerprint based localisation mechanism is composed of offline and online phases. In the offline phase, the RSS and other radio information from the different location will be recorded to establish the fingerprint database. Then, in the online phase, the measured information from

UAV will be compared with the fingerprint database for localisation.

Owing to the implementation simplicity, acceptable accuracy and ability to construct radio map help for collision detection, fingerprint attracts certain attention on UAV applications. But most of the proposed approaches are focused on the node detection through UAV with the existence of GPS in unknown environment, only few of research pays attention to localise UAV itself. In [101], an indoor localisation system called a high-speed quadrotor localisation (HiQuad-Loc) system was designed, which successfully kept the stability of UAV in indoor environment with RSS fingerprinting. In their system, a 4-D RSS interpolation scheme was proposed which added RSS sample space to mitigate site survey overhead for reducing the requirement of training data volume. Finally, the system successfully reduced the localisation latency, restrained the effect of high-speed movement, reduced the number of RSS sampling and improved the localisation accuracy. In addition, another fingerprint based UAV localisation system proposed in [102] still focused on the offline process. Where tensor completion was exploited to achieve the time reduction of data collection and training process in the offline phase.

As discussed, the characteristics of the fingerprint, including implementation simplicity, high accuracy (decimetre-level) and ability to construct radio map all make it suitable for UAV localisation. However, owing to the demand for large volume of data and vulnerable to dynamic environments, there will be an upsurge of corresponding computational overhead and instability of localisation. Consequently, fingerprint based localisation mechanism is not suitable for UAV localisation in dynamic and unknown environment.

### **2.3.6 Summary and discussion on the classical localisation mechanisms**

A summary and discussion for the pros and cons of the classical localisation mechanisms with RF based localisation technologies on UAV positioning is given in Table 2.2. Among them, time based localisation mechanisms including TOF/TOA and TDOA attract lots of attention due to the high localisation accuracy. Besides, according to the investigation, there are also lots of researches on RSS based localisation mechanisms considering the cost efficient and implementation simplicity features. But mainly focused on the applications in open environment.

## **2.4 UAV platforms**

Generally, the UAV is known as the aircraft which can be control by the ground station or automatically controlled by itself without a pilot exist on board. Currently, the UAV has already been widely utilised for military and civilian usage such as border protection, logistic management, rescue, surveillance and smart inspection, etc [103]. According to the composition structure of the existing UAV platform, it can be divided into two categories, including the fixed wing UAV and rotatory wing UAV.

The fixed wing UAV is similar to an aeroplane design with fixed wings. It utilises attached engines on the fixed wing to generate the forward thrust for taking off and flying. Due to its flight principle, it can only fly in a particular direction with high speed, rather than hovering or remaining in one place. Therefore, the fixed wing UAV has attracted lots of attention in military and

Table 2.2: Comparison for the existing RF based UAV localisation technologies with the classical localisation mechanisms

	Advantage	Disadvantage	Existing Literature
RSS	Implementation simplicity, cost efficient	Low accuracy, vulnerable to NLOS path and environment variation	[27, 28, 42–44, 54, 87, 88]
AOA	High accuracy with specific algorithm, able to provide orientation information, immune to location ambiguity	Vulnerable to measurement noise and NLOS path, require additional equipment, high energy consumption, high system cost	[89–91]
TOF/TOA	High accuracy with specific algorithm, low computational complexity	Synchronisation between all sensor nodes required, high communication cost, low update rate, vulnerable to response delay, vulnerable to NLOS path	[63–69, 71–78]
TDOA	High accuracy, low communication cost, low latency	Synchronisation between anchor nodes required, vulnerable to NLOS path, high computational complexity	[6, 98–100]
Fingerprint	Implementation simplicity, high accuracy, ability to construct radio map help for collision detection	Large volume data required, vulnerable to dynamic environment, high computational complexity	[101, 102]

defense applications and it is not suitable for the stationary applications such as the detailed inspection in the indoor or extremely confined environments [104].

Rotatory wing UAV is the one which utilised the attached rotors for position and attitude control. It is commonly known as the helicopter, tricopter, quadcopter and hexacopter [105]. By altering the rotation rate of the rotors on the UAV, the vertical take off and landing (VTOL) and hovering can be achieved for the rotatory wing UAV, which makes it possible for the stationary applications [106]. However, the payload and speed of the UAV is greatly limited when compared with the fixed wing UAV. But considering the focused application is the autonomous inspection in the extremely confined environments, the rotatory wing UAV becomes the ideal candidate.

As aforementioned, according to the number of rotors on the UAV, the rotatory wing UAV can still be classified into helicopter, tricopter, quadcopter and hexacopter, etc. The control of the helicopter is achieved through the cooperation of one rotor on the head and the other rotor at the tail. The mechanical linkages between these rotors is required in order to achieve the stable control. Compared with the helicopter, for the multicopter (tricopter, quadcopter and hexacopter, etc), this mechanical linkages is not required as the position and attitude control of the multicopter can be achieved through different throttle on each rotor [107]. Meanwhile, the utilisation of the multi-rotors also allows a smaller size for each rotor compared with the helicopter, which minimises the potential crash rate for it, especially in the focused extremely confined environments. On the other hand, when doing the comparison within the multicopter, the tricopter can effectively reduce the system cost and the probability of failure, as less rotors are utilised.

However, this is at the expense of the payload and implementation difficulty. For the hexacopter, six rotors are used, which offers more power supply, stability, payload and the reliability. As in the worst case, even one of the rotor fail, the remain rotors can still keep a safe landing. However, the size and cost of the hexacopter are all increased when compared with tricopter and quadcopter. Quadcopter is known as the most widely utilised multicopter with lots of commercial UAV platforms have already been designed and implemented by DJI, Parrot, Yuneec, Kespry, Skydio, Insitu and Flyability [108]. In comparison with the tricopter, quadcopter can offer greater maneuverability, hovering ability and acceptable payload. In contrast with the hexacopter, the system cost, implementation difficulty and UAV size are all reduced. Considering all of these, and the requirements of the focused application and the operational environments, the smaller size quadcopter becomes to the best candidate.

## **2.5 Evaluation framework for UAV positioning with RF based technologies in GPS-denied environments**

To the best knowledge, the evaluation framework considering both the RF based localisation technologies and UAV positioning in GPS-denied environments is currently missing from the literature. However, quantifying system performance and in-depth analysis for the key factors of the system are important and can be the guidance for subsequent research. Therefore, in this section, the elaboration and analysis for the key performance indicators (KPIs) of the RF based localisation technologies on UAV positioning in GPS-denied environments will be given. The evaluation framework will be established according to the analysed KPIs to serve

as the guidance for the performance evaluation in this area.

### **2.5.1 Localisation accuracy (LA)**

Localisation accuracy is commonly known as the disparity between the estimated position information and the ground-truth. Apparently, it is the conventional and essential index for all the location based applications or systems. In a general sense, a higher accuracy represents a greater performance. However, under different applications, the acceptable accuracy will be varying. For instance, for precision machining, even millimetre-level localisation accuracy is insufficient. But meter-level is enough for rescue mission in mining industry. Thus, considering the operational environment where GPS is unavailable such as oil pressure vessel, warehouse or mine cave, and in order to keep the stability and avoid the collision of UAV, the decimetre-level accuracy is desired. In some extreme cases, such as the place full of obstacles or confined space, the centimetre-level accuracy is also demanded.

### **2.5.2 Localisation latency/ Update rate (L/U)**

Real-time or low latency localisation means the system can calculate reliable localisation results without any noticeable delay. It is often known as one of the indexes to evaluate the localisation performance. Generally, the traditional indoor localisation systems are not sensitive to the localisation latency less than second-level. However, for UAV positioning, the localisation latency will significantly affect the position update rate of UAV. Considering that UAV is always in motion even when hovering, a lower update rate or higher localisation latency will cause

a greater gap between each posture adjustment command, where unstable flight may happen. Thus, the update rate is always one of the most concerned indicators to measure the performance of commercial UAV positioning system. In the design of high-performance localisation algorithm for UAV application, the localisation latency also needs to be considered which can be denoted as the low computational complexity for the algorithm.

### **2.5.3 Stability in different environment (SDE)**

Compared with the outdoor environment, the applications in GPS-denied environments are more complicated and vulnerable to multipath fading and the NLOS path caused by the unpredictable objects or people. These will lead to the precipitous decline or violent oscillation of the localisation accuracy. In addition, the unreasonable value is more easily to occur which may derive a non-smooth result. This precision degradation and oscillation may cause the unstable flight of UAV or increase the crash down probability. Therefore, the environmental adaptability will be the particular index for UAV applications in GPS-denied environments.

### **2.5.4 Auxiliary equipment requirements (AER)**

Traditional RF based localisation systems often require the existence of anchor nodes with known location. As above mentioned, the conventional trilateration and multilateration localisation algorithms demand at least three anchor nodes to locate the target. However, considering the applications for UAV in GPS-denied environments, the difficulty to deploy anchor nodes or measure the precise location of these nodes will become the problem to be remedied. Therefore, the

demand level for the auxiliary equipment will be another key index to measure the performance of a RF based UAV localisation system.

### **2.5.5 Weight/Size (W/S)**

Different from other applications, the payload of UAV is extremely restricted. The loading condition of UAV also have the close connection with the operation time of it. The AOA based localisation mechanism has proven to achieve decimetre-level accuracy and provide the 6-DOF position information [32,90]. However, the size and weight of the additional antenna array will restrict the applications on UAV. Thus, the weight and size of the localisation components becomes another particular index for UAV positioning.

### **2.5.6 Localisation coverage (LCR)**

The localisation coverage for the RF based system is commonly treated as the communication range of sensor nodes which has a huge impact on the operating range of UAV. It is varying under different wireless communication protocols. Besides, higher localisation coverage is also achievable with additional anchor nodes. However, the application scenario will be restricted, due to the demand for the prior location of anchor nodes. Therefore, the balance between localisation coverage and auxiliary equipment requirements need to be considered when designing the RF based localisation system for UAV.

### **2.5.7 Energy consumption (EC)**

Energy consumption is always one of the primary indexes when evaluating the performance of a RF based localisation system. For traditional applications, considering the charging difficulty of tag nodes, low energy consumption often means the system is capable to keep the tag nodes alive for months or years with ordinary batteries, which makes BLE, Zigbee and passive RFID received lots of attention. However, for UAV positioning, there is no need to consider the circumstances that difficult to charge sensor nodes or keep them alive for months. Keeping sensor nodes alive during the operation process and having no impact or little impact on the operation time of UAV is enough.

### **2.5.8 System cost (SC)**

Low cost system which can easily penetrate the consumer market and be widely adopted is always the development direction for robotic technologies in modern society. In addition, considering the UAV applications in GPS-denied environments, it is much more vulnerable to the unpredictable damage like crash down or control failure. Therefore, it is necessary to consider the system cost for designing the RF based UAV localisation system in GPS-denied environments.

### **2.5.9 Demand level discussion under different application scenarios**

To further analyse the key factors for UAV positioning, the discussion for the demand level of each has been made according to the application scenarios. Considering it is difficult to define or provide a very specific value suitable for all

the applications, only a demand level for general applications is provided. The application scenarios of UAV in GPS-denied environments are divided into six areas, including indoor or extremely confined space inspections (the focused applications for this thesis), mining, bridge inspections, search and rescue, critical infrastructure and surveying disaster sites [109]. The demand level for each indicator under these application scenarios have been analysed and summarised as follow.

- Indoor or extremely confined space inspections: Considering the application for indoor or extremely confined space inspections such as the corrosion detection for oil pressure vessel or water tanks, UAV needs to fly close to the wall for a detailed inspection. Thus, the KPIs including LA and L/U will be particularly important in case of any collision and prevent the unexpected drift in the flight area. Furthermore, the flight environment under this application scenario is relatively fixed during the operation process of UAV. Therefore, the demand level for AER and LCR will remain low.
- Mining: Similar to the applications for smart inspection, in case of any potentially harmful for the components and miner in the narrow space inside a mine, the LA and L/U will be particularly important. But differently, the miner or equipment inside the mine will make the environment become cluttered, which means a higher accuracy to the centimetre-level is desired in some extreme cases, and the SDE becomes significant for the applications under this circumstance.
- Bridge inspections: Another popular application for UAV in GPS-denied environments is bridge inspections. The inspector often utilises UAV to

fly underneath bridges to inspect the corrosion, paint loss and rust which is hard to detect with the traditional methods. Clearly, the same as the previous applications, the flight area of UAV under the bridges is sorely limited. The flight environment is relatively fixed during the whole process. Thus, the LA and L/U are still the most important factors. The demand level for the SDE, AER and LCR will all remain low.

- Search and rescue: Different from all the aforementioned applications, the search and rescue mission will pay more attention to search and fast locate the salient entities within an unknown and relatively spacious environment [110]. Thus, the SDE, AER and LCR will become significant, and the oscillation for the LA within the meter-level and low update rate are all acceptable.
- Critical infrastructure: In the consideration of the security risks of GPS, in some restricted area such as military bases or power plants, soldiers or engineers often utilise UAV without GPS for monitoring. The application scenarios in these areas can be supposed as a fixed, open and large environment. Therefore, the LCR for the localisation system is turned to be the most concerned factor.
- Surveying disaster sites: The same as the applications for search and rescue, the most challenging part for surveying disaster sites will be the unknown environment and unpredictable obstructions, which makes the SDE, AER and LCR become significant.

### 2.5.10 Evaluation and analysis on the existing RF based UAV localisation systems

Finally, a comprehensive evaluation and analysis for the aforementioned RF based UAV localisation systems with different radio communication protocols under different localisation mechanisms is given in Table 2.3, utilising the established evaluation framework. Where, L represents low, M is assumed as medium, H means high, N/A indicates not applicable or never mentioned in the paper. Here need to indicate that L/U for [27, 71, 72, 78] are the distance measurement update rate, the localisation latency or position update rate is not mentioned in these papers.

To the best knowledge, no system exists which can satisfy all the indicators in the framework. However, each of them has their own advantages under different circumstance. Considering the meter-level accuracy, implementation simplicity, low system cost and large communication range of Wi-Fi based system with the RSS based localisation mechanism, it is much more suitable for the applications in outdoor environment to substitute or compensate the GPS for localisation. Where the authors in [27] and [28] are all utilised the Wi-Fi based UAV positioning system with the RSS based localisation mechanism for the outdoor applications such as search and rescue, exploration and remote sensing. Differently, for the Bluetooth based system with the RSS based localisation mechanism, the communication range is restricted around 10m to keep the performance, but the weight and size of the sensor nodes, the system cost and energy consumption are significantly reduced in contrast to the Wi-Fi based system. Thus, this type of system is more effective for the applications on MAVs or micro-uavs in smaller

Table 2.3: Analysis of current RF based UAV localisation systems under the proposed evaluation framework

System	Type	LA	L/U	SDE	AER	W/S	LCR	EC	SC
[27]	Wi-Fi/RSS	Meter	10Hz	L	M	L	M	M	L
[28]	Wi-Fi/RSS	Meter	N/A	L	H	L	M	M	M
[29]	Wi-Fi/RSS	Meter	N/A	L	M	L	M	M	L
[30]	Wi-Fi/RSS	Decimetre	N/A	M	H	L	M	M	M
[42]	Bluetooth/RSS	Meter	N/A	L	H	L	L	L	L
[43]	Bluetooth/RSS	Decimetre	N/A	L	N/A	L	L	L	L
[44]	Bluetooth/RSS	Decimetre	5Hz	L	N/A	L	L	L	L
[54]	Zigbee/RSS	Decimetre	N/A	L	M	L	L	L	L
[57, 58]	RFID	Centimetre	50Hz	L	M	L	L	L	L
[60]	RFID/RSS	Decimetre	N/A	L	H	L	L	L	L
[6]	UWB/TDOA	Centimetre	40Hz	M	M	L	L	M	M
[63]	UWB/TWR	Centimetre	40Hz	M	M	L	L	M	M
[64]	UWB/TWR	Decimetre	80Hz	M	M	L	L	M	M
[65]	UWB/TWR	Decimetre	20- 250Hz	M	M	L	L	M	M
[66]	UWB/DS- TWR	Decimetre	200Hz	M	M	L	L	M	M
[67]	UWB/SDS- TWR	Decimetre	N/A	M	H	L	L	M	M
[68]	UWB/SDS- TWR	Centimetre	65- 372Hz	M	H	L	M	M	M
[69]	UWB/TWR	Centimetre	N/A	M	M	L	L	M	M
[71, 72]	UWB/TWR	Meter	20Hz	M	L	L	M	M	M
[73–75]	UWB/TWR	Decimetre	N/A	M	N/A	L	M	M	M
[76]	UWB/TWR	Centimetre	N/A	N/A	L	L	L	M	M
[77]	UWB/DS- TWR	Decimetre	N/A	M	N/A	L	M	M	M
[78]	UWB/TWR	Decimetre	6.5-12ms	M	M	L	M	M	M
[79]	UWB/RGB- D	Decimetre	N/A	L	M	M	M	M	M
[80]	UWB/Vision	Decimetre	N/A	L	M	M	M	M	M
[81]	UWB/RGB- D	Decimetre	32Hz	L	M	M	M	M	M

indoor environment, where both [43] and [44] focused on the applications under this circumstance. Furthermore, the same as the previous conclusion, the low data rate feature of the Zigbee based system may cause the high localisation latency which runs counter to the requirements on UAV. Towards this end, only a few research [54] has been carried out, which means the Zigbee based system is not the ideal choice for UAV positioning. Similar to the Bluetooth based system, the weight and size of the sensor nodes, system cost and energy consumption of the RFID based system also remain low. But differently, the UHF RFID significantly improved the accuracy into the centimetre-level, and the tiny size of passive RFID nodes makes it possible to estimate the orientation information with multi sensor nodes equipped on UAV. However, the restricted communication range and NLOS sensitive characteristic still limit the applications of the RFID based UAV positioning system in smaller and open indoor environments. Finally, the UWB based system with the time based localisation mechanisms is highlighted here considering the existing characteristics and the focused application scenarios. The detailed analysis for each indicator individually will be given as follow to prove the conclusion.

- LA: As mentioned before, high time resolution is able to achieve with extremely short duration time of transmit signal for UWB based system. Thus, decimetre or centimetre-level localisation accuracy is simple to achieve for UWB based system with time based localisation mechanisms which is extremely important for UAV positioning in GPS-denied environments.
- L/U: For RF based localisation system, the localisation latency is closely related to the data transmission rate of each radio communication protocol.

Obviously, with the highest data transmission rate, UWB based system can achieve extremely low localisation latency which is much more suitable for UAV localisation compared with other radio communication protocols.

- SDE: With the extremely short duration time of transmit signal for UWB based system, it is much easier to identify the signals from different path which makes UWB based system can resist multipath fading. Therefore, the localisation performance of UWB based system is much more stable than other RF based systems in different operational environment, especially in cluttered environment.
- AER: The requirement for auxiliary components (anchor nodes) is the defect for almost all the RF based localisation technologies. However, with the high data transmission rate and ranging accuracy for UWB based system, it is possible to realise the relative localisation for UAV swarm to get rid of this limitation, as declared in the existing literature [73–76].
- W/S: For UWB based localisation system, the precise localisation is achieved by the compact and light weight wireless UWB sensor nodes, where the weight and size of the sensor nodes only have little impact on UAV [111,112].
- LCR: As aforementioned, the localisation coverage is related to the wireless communication protocols. Compared with other RF based localisation technologies, even UWB based sensor node is not the one with the widest communication range, but still keep large localisation coverage [111–113].
- EC: Compared with other RF based localisation systems like Bluetooth, Zigbee and Passive RFID, the energy consumption for UWB based system is much higher. But considering the application on UAV positioning, there

is no need to keep the sensor node working for months or years, keeping it alive during the operation process of UAV is enough. Thus, even UWB based system is not the one with lowest energy consumption, but still suitable for UAV positioning.

- SC: Due to the special requirements of UWB based system, the system cost is much higher than other RF based systems. But considering the application for UAV positioning in GPS-denied environments, there is no need for large-scale nodes (hundreds of wireless sensor nodes) for localisation. Thus, the system cost of UWB based system can be still kept in low level.

It is concluded that the UWB based system with time based localisation mechanisms is the best option for UAV positioning with RF based localisation technologies in GPS-denied and extremely confined environment.

## **2.6 Current challenges on UAV positioning with RF based localisation technologies**

Under the in-depth discussion and establishment of the evaluation framework for RF based localisation systems on UAV positioning, current challenges for designing or implementing high-performance RF based localisation system of UAV in GPS-denied environments will be discussed in this section to act as the guidance and lay fundamental base for subsequent research.

### **2.6.1 Unreasonable value**

Owing to the unpredictable working environment and communication condition between all sensor nodes. Considering the measurement noise from each sensor node is constantly changing due to the individual difference, the unreasonable value which denotes as the oscillation of localisation results may occur [63]. Generally, performance degradation caused by unreasonable value is not a sustained impact. Thus, for traditional applications, these values can be ignored directly. However, for UAV positioning, especially for the UAV applications in the extremely confined environment, even a short-term position drift can lead to the unstable control. Hence, before reaction of flight controller, localisation results must be smoothed or filtered to eliminate violent oscillation which makes unreasonable values become to a special challenge for UAV positioning.

### **2.6.2 Anchor self-positioning and relative localisation of UAV**

One of the fundamental requirements for the traditional RF based localisation systems is adequate anchor nodes with precise location. However, consider UAV application in GPS-denied environments, it is hard to measure the precise position information of anchor nodes before system operation. Under such circumstance, anchor self-positioning turns into one of the most concerned research questions in this area. In [114, 115], a source position estimation approach called source position estimation for anchor position uncertainty reduction (SPEAR) was proposed which achieved precise estimation of anchor position with existing RSS measurements. However, prior information for some anchor nodes is still required. Besides, the final estimation error is not acceptable for UAV localisation.

Differently, Großwindhager et al. [116] designed a single-anchor localisation system using multipath assistance (SALMA) for precise localisation. Thanks to the existing geometry for the building and the characteristics of the UWB signal, virtual anchor nodes are able to be built up with reflection between transmitter and receiver for precise localisation. Finally, a median error below 8cm with off-the-shelf UWB sensor node is garnered. However, in dynamic or unknown environment, this approach will lose effectiveness. In addition, another anchor self-localisation approach was proposed in [117] which exploited TOA measurements sequentially gathered from anchor nodes by moving quadcopter by hand and previous robust solvers to estimate anchor position for UAV localisation.

### 2.6.3 NLOS error

One of the fundamental challenges for precise localisation of UAV with RF based technologies in GPS-denied environments will be the abominable communication environment. It is always difficult to assess the communication condition, considering the dynamic characteristics of the working environment. Owing to the inherent nature of electromagnetic waves, to avoid reflect, refract and diffract of the communication signal between sensor nodes is impossible [118], that is where NLOS error comes from. NLOS error here denotes the localisation error caused by NLOS communication between sensor nodes, also treated as the excessive travelling distance. To be specific, the reflection or refraction of the signal will lead to the additional power loss, additional time-delay or incident angle change which all have the significant consequence on the localisation accuracy. Moreover, the multipath fading caused by the NLOS communication will also make it

challenging to distinguish the direct path. To remedy this, plenty of approaches have been presented. According to the method of dealing with NLOS error, these approaches can be divided into two categories, NLOS identification and NLOS mitigation.

The NLOS identification means to identify the NLOS path or measurement which are influenced by the NLOS error. In the last decade, hundreds of approaches have been developed in this area. The traditional approaches utilised the building methods or model and the existing LOS information to identify the NLOS path through the measured distance, signal strength or channel characteristics. The identification accuracy is relevant to the building methods or model and the existing LOS information. Different from the traditional approaches, the artificial intelligence (AI) based approach first utilises the RSS or channel state information (CSI) training data for feature extraction, then it is to distinguish the NLOS path. Even no identification model is required, however, the performance is restricted by the data volume. In this part, a brief overview for these two different NLOS identification approaches will be given.

In [119], Chan et al. proposed an identification approach to identify NLOS path through the designed residual test with measured TOA and successfully achieved over 90% accuracy. However, performance of the algorithm is restricted by the number of the base stations (anchor nodes) and LOS dimension for these nodes. The performance will drop sharply in terms of lack of LOS anchor nodes or if LOS dimension is under 4. Differently, another approach was proposed in [120] which exploited TOA-DOA fusion to precisely identify NLOS nodes and improve accuracy with reflection points served as reference nodes. In this approach, TOA

and DOA from the same target measured by different anchor nodes were applied to estimate multi-group position information, then to analyse estimation bias for distinguishing NLOS and LOS nodes. Moreover, a shared reflection point identification and localisation algorithm was presented to improve the positioning accuracy. However, their approach has the assumption that all reflection must be single bounce. Besides, the performance will be greatly restricted by accuracy of DOA and synchronisation between nodes. Similar to the above method, Zhang et al. [121] designed another approach which also utilised the measured angle information to transform the reflection points as reference nodes for localisation. Differently, this method could identify the multi reflection point through calculated possible region for target node from measured AOA, angle of departure (AOD) and TOA information. However, unless at least one single bounce reflection exists, the proposed approach is unable to identify multi reflection points. Besides, not only AOA, but also AOD is required which means for both target and anchor nodes high-performance antenna arrays are required to preserve the accuracy.

On the other hand, some other approaches exploiting machine-learning or deep-learning for the precise NLOS path identification were also proposed. The authors in [122] applied the non-parametric machine learning techniques for identification with no need of statistical characterisation for LOS and NLOS channels. Six different features were extracted directly from received waveform for classification through least square support vector machine (LS-SVM), owing to the characteristics of robustness, few requirements of user-defined parameters and superior performance. Due to the huge computational complexity of support vector machine (SVM), relevance vector machine (RVM) was exploited in [123] to iden-

tify and mitigate NLOS error with lower computational cost. They declared that an extremely smaller number of relevance vectors (RVs) of RVM were utilised for classification than support vectors (SVs) of SVM. Moreover, compared with SVM, RVM is able to estimate error bar for the improvement of localisation accuracy. In order to further reduce computational complexity, Yang et al. [124] proposed another NLOS identification approach based on import vector machine (IVM). During identification process, a feature selection strategy was designed to select optimal feature from the same six features to improve accuracy and reduce computational complexity. Moreover, comparison of SVM and RVM with proposed approaches was made to evaluate the effectiveness. In order to exclude human intervention, deep-learning based approaches for NLOS identification emerge recently. Bregar et al. [125] presented a convolutional neural network (CNN) based approach exploiting measured raw CIR for precise identification. The dimensionality of CNN was also reduced by filtering useful training data as small batches to significantly lower the complexity and improve the robustness of the algorithm. On the other hand, considering the insufficient information from single measurement and limitation of CIR, Choi et al [126] proposed another approach which applied a series of CSI to further improve the identification efficiency and accuracy by aid of recurrent neural network (RNN). However, all these data-aided methods are susceptible to unknown or dynamic environment due to the requirement of plenty measurements and training process for feature extraction. Moreover, for UAV applications, on-board identification is unrealistic owing to the limit power supply and high computational complexity. Therefore, further research is still necessary.

Compared with NLOS identification, NLOS mitigation is able to remedy the

lack of LOS anchor nodes problem to eliminate the influence of NLOS. The authors in [127] proposed two different convex relaxation approaches called as the semidefinite relaxation (SDR) and the second-order cone relaxation (SOCR) to mitigate the NLOS error precisely with the ability for solving non-convexity problem. They successfully mitigated NLOS error from measured TOA with no need of plenty statistical information. In addition, they also extended the above method to TDOA based localisation approach in [128]. At the same time, Marano et al. [122], Van Nguyen et al. [123] both designed the approach for NLOS error mitigation after identification with SVM and RVM. However, there is still restriction for NLOS mitigation. When compared with the identification approaches that remove NLOS nodes directly, mitigation approaches can only approximate LOS condition even in the ideal case. Therefore, NLOS mitigation approaches are only suitable for the applications with less LOS node exists.

#### **2.6.4 Node synchronisation**

Generally, in the ideal case, the clocks on all the sensor nodes are identical. However, considering the material, structure and manufacturing process, the clock of each sensor node is different. Additionally, to limit the system cost, the only low performance crystal oscillator can be provided for the wireless sensor nodes of the RF based localisation system. Therefore, with the extremely fast speed of electromagnetic waves, even a small difference between the local clock will have a huge impact on the localisation accuracy, especially for the time based localisation mechanisms. Hence, precise synchronisation will be the other grand challenge for precise localisation of UAV with RF based systems.

The current synchronisation approaches can be classified based on the method for handling the clock difference. One is to cancel out the clock difference through communication strategy or regulate clock difference with additional synchronisation server or node. The other is to achieve the relative synchronisation with the estimation of clock difference. As above mentioned, the localisation approaches such as TWR, DS-TWR and SDS-TWR all are synchronisation free which cancel out the clock difference by multi communication. However, the additional problems will be raised, like response delay, communication cost and high latency. The other conventional approach is leveraging additional synchronisation server or node to regulate clock difference. Lots of classical protocols or strategies on this side have been proposed over the past decades like timing-sync protocol for sensor networks (TPSN) [129], flooding time synchronisation protocol (FTSP) [130] and reference-broadcast synchronisation (RBS) [131] which are summarised in [132–135]. Nevertheless, performance for these approaches will be restricted by synchronisation server or node itself, also by the communication condition and synchronisation strategy. Meanwhile, with the extra components, energy consumption will also be the burning issue. Therefore, more attention will be given to the relative synchronisation with the estimation of clock difference. The classical approach was proposed in [136] which leveraged two-way exchange successfully estimate clock difference between sensor nodes with the known time delay. However, only clock offset is taken into account. For further research, authors in [137] designed a synchronisation protocol called asymmetrical time-stamping and passive listening (ATPL) utilised the same two-way exchange strategy. Differently, passive listened message from other nodes was considered to estimate relative clock skew and offset, also to reduce communication cost.

However, with the same strategy, even communication cost is reduced, but still keep high-level. Meanwhile, LOS paths between each sensor node are required to keep precise synchronisation. Likewise, Wang et al. [138] proposed another clock skew and offset estimation approach, which also utilised the same strategy and overhearing message. But different from the aforementioned approaches, only two-way exchange between the chosen two sensor nodes is required and no prior position information, response time or transmit time from responder needed. Therefore, communication cost of this approach is significantly reduced. But LOS paths are still required. On the other hand, Xiong et al. [139, 140] proposed another robust clock synchronisation approach which only requires periodic broadcast signal from each anchor node to estimate relative clock skew and offset. Even communication cost is reduced compared with all the aforementioned approaches, but with the additional communication between anchor nodes, LOS path between these nodes must be guaranteed. For further research, Wang et al. [141] proposed a revised synchronisation approach with unknown position information of anchor nodes followed by Xiong's [139, 140] work, which is much more suitable for UAV localisation in unknown environment.

### **2.6.5 Signal block or interference between localisation server or ground station and UAV**

Currently, there are two patterns for RF based UAV localisation system, the off-board pattern and on-board pattern. For off-board pattern, the localisation algorithm will be deployed on an additional localisation server (ground station), which is responsible for the complex computing. Thus, for off-board pattern, the

computational complexity and the system energy consumption only have little impact on localisation latency and UAV operation time. However, the additional process to send back the estimated position to UAV is required. Considering the applications in GPS-denied environments, the potential signal interference or block for the additional process may cause the position loss or low position update rate of UAV. Moreover, to avoid signal interference or block between UAV and ground station is not only the primary challenge for precise localisation, but also extremely significant for stable control of UAV.

### **2.6.6 Energy consumption**

As aforementioned, different from the off-board pattern, instead of the additional localisation server, an on-board processor will be equipped on UAV which is responsible for position estimation. Apparently, for on-board pattern, the computational complexity of the algorithm and energy consumption of the processor will all have great influence on the operation time of UAV. To lower the energy consumption, lots of approaches through different perspectives have been proposed. However, balance between energy consumption, computational complexity and localisation accuracy to preserve the stability of UAV requires to be taken into consideration, where at least decimetre-level accuracy with high update rate should be ensured, then to consider the lowest energy consumption to keep UAV alive for longer time.

### **2.6.7 Summary and discussion on the current challenges of the RF based UAV localisation technologies**

A detailed discussion on current solutions of the challenges for UAV localisation with RF based localisation technologies is provided in Table 2.4. The advantages and disadvantages for each solution under the consideration of the evaluation framework proposed in Section 2.5 are also generalised which can give a clear guidance for subsequent research.

## **2.7 Summary**

In this chapter, a comprehensive analysis and overview have been presented for the RF based UAV localisation technologies with different radio communication protocols under different localisation mechanisms to demonstrate the current circumstance of the RF based UAV localisation technologies in GPS-denied environments and to serve as the guidance for further research. Firstly, the pros and cons of the existing RF based UAV localisation technologies with different radio communication protocols (Wi-Fi, Bluetooth, Zigbee, RFID and UWB) were discussed. Later on, the classical localisation mechanisms (RSS, AOA, TOF/TOA, TDOA and Fingerprint) widely used on the RF based localisation systems and the effectiveness of each for UAV positioning in GPS-denied environments were reviewed. Thirdly, the evaluation framework to assess the system performance was established, aiming at the special demand for UAV positioning in GPS-denied environments. With the established framework, all the RF based localisation systems with the specific localisation mechanisms were analysed to find the suitable

Table 2.4: Discussion on current challenges for UAV positioning with RF based localisation technologies

Current Challenges	Current Solutions	Advantage	Disadvantage
Unreasonable Value	Identify the unreasonable value Smooth the result	No prior information required, stable performance Implementation simplicity	High computational complexity, identification fail Previous result required, additional equipment required
Anchor Self-positioning and Relative Localisation	Leveraging auxiliary nodes With the appropriate strategy Relative localisation	Implementation simplicity, low communication cost No prior information and extra equipment required No auxiliary nodes required	Prior information and additional equipment required Auxiliary nodes required, high communication cost Prior information required, high computational complexity
NLOS Error	NLOS Identification: Signal changing detection NLOS Mitigation: With appropriate model	Stable performance, immune to NLOS path, implementation simplicity No statistical and prior information required, acceptable accuracy	Statistical information required, potential lose effectiveness High computational complexity, unstable under extreme case
Node Synchronisation	Utilising communication strategy Additional synchronisation node/server	Implementation simplicity, low computational complexity Implementation simplicity, acceptable accuracy, low computational complexity	Suffering from response delay or clock drift, high communication cost Restricted by synchronisation node/server, high communication cost
Signal Block or Interference	Relative synchronisation Relay stations Multi-hop communication with specific strategy	No additional components required, acceptable accuracy Stable communication condition No extra equipment required	High computational complexity, require LOS path Additional auxiliary nodes required, difficult to implement Unstable performance, high energy consumption
Energy Consumption	Reduce computational complexity and communication cost Additional localisation server	No extra equipment required, easy to implement, low localisation latency High accuracy and stable performance, no need to consider energy consumption	Localisation accuracy degradation High latency, suffer from signal block or interference, additional equipment required, high system cost

application scenarios. According to the analysis, except the Zigbee based systems, all the other RF based localisation systems are able to be applied on UAV positioning. Within these, the Wi-Fi based systems with the RSS based localisation mechanisms are more suitable for the UAV positioning in outdoor environment. Both the Bluetooth and RFID based localisation systems are more effective for the applications on MAVs or micro-uavs in smaller indoor environment. Particularly, the UWB based system with the time based localisation mechanisms are highlighted for UAV positioning under the consideration of the proposed evaluation framework, which can be the best option for UAV positioning with the RF based systems. Finally, key issues and challenges for UAV positioning with the RF based system in GPS-denied environments were discussed which is served as the guidance for the following researches.

## Chapter 3

# UWB based UAV positioning technology

### 3.1 Introduction

According to the comprehensive overview for the existing UAV based localisation technologies, the UWB based system with the time based localisation mechanism can be the ideal candidate to remedy the existing issues for the high accuracy and precision UAV positioning in GPS-denied and extremely confined environments. Therefore, in this chapter, the description for the proposed MLE UAV positioning algorithm based on the UWB localisation system will be given. Followed by, considering the huge performance influence from the distribution of the fixed anchor nodes and the extremely confined space in the focused application scenarios, the investigation on the anchor distribution strategy will be provided help to find the suitable geometry configurations of the fixed anchor nodes to keep the best performance in focused environments.

### 3.2 MLE based UAV positioning algorithm

In order to avoid the requirement of strict clock synchronisation between the UWB sensor nodes, and provide high accuracy positioning performance for the UAV, the TW-TOF based localisation scheme with the MLE based positioning algorithm is investigated and exploited. It is clear from Fig. 2.5, during the localisation process, the position request packet will be transmitted by the tag node equipped on UAV at time  $l_{Du}$ . Anchor node  $i$  ( $i = 1, 2, \dots, n$ ) involved in this round will receive the request and record the timestamp as  $l_{Ai}$  after a transmission delay. After a response delay caused by the data processing, anchor node  $i$  will respond to the request by transmitting back a response packet with the time departure stamp  $l_{Di}$ . Finally, the tag node will receive the response packet and record the TOA as  $l_{Au}$  after a same transmission delay.

Assume that TOA and TOD for the communication signal between two sensor nodes be written as

$$l_A = \tilde{l}_A + \tau, \quad (3.1)$$

$$l_D = \tilde{l}_D + \tau, \quad (3.2)$$

where,  $\tau$  is supposed to be the measurement noise of the UWB sensor node modelled as the AWGN with zero mean and  $\sigma_\tau^2$  variance,  $\tilde{l}_A$  and  $\tilde{l}_D$  represent the true value of TOA and TOD between tag node (equipped on UAV) and anchor node. The measurement noise is mainly comes from the UWB sensor node itself during the measurement process. Thus, according to the arithmetic theory of TW-TOF, the transmission delay between tag node and anchor node can be expressed as

$$d_i = l_i c = [(l_{Au} - l_{Du}) - (l_{Di} - l_{Ai})]c/2. \quad (3.3)$$

In the equation,  $d_i$  and  $l_i$  are defined as the measured distance and signal transmission delay between anchor node  $i$  and UAV.  $c$  is the velocity of electromagnetic wave. The equation can be further updated with the measurement noise from the UWB sensor nodes,

$$d_i = [(\tilde{l}_{Au} - \tilde{l}_{Du}) - (\tilde{l}_{Di} - \tilde{l}_{Ai})]c/2 + \eta_i. \quad (3.4)$$

Within the equation,  $\eta_i$  is the distance measurement noise between UAV and anchor node  $i$  which can be expressed as

$$\eta_i = [(\tau_{Du} - \tau_{Di}) + (\tau_{Ai} - \tau_{Au})]c/2. \quad (3.5)$$

Accordingly, the true value for the distance between UAV and anchor node  $i$  is able to be calculated by the coordinates of these sensor nodes. Therefore, the following equation can be derived

$$\begin{cases} d_1 = \|\mathbf{p} - \mathbf{p}_1\| + \eta_1 \\ d_2 = \|\mathbf{p} - \mathbf{p}_2\| + \eta_2 \\ \vdots \\ d_n = \|\mathbf{p} - \mathbf{p}_n\| + \eta_n \end{cases}, \quad (3.6)$$

where,  $\mathbf{p} = [x, y, z]^T$  and  $\mathbf{p}_i = [x_i, y_i, z_i]^T$  represent the position matrix of UAV and anchor node  $i$ . Then, by extending the equation into matrix form,

$$\mathbf{Z} = f(\mathbf{p}) + \boldsymbol{\eta}. \quad (3.7)$$

Among the above equation,  $\mathbf{Z}$ ,  $f(\mathbf{p})$  and  $\boldsymbol{\eta}$  represent the measured distance information matrix, real distance information matrix and measurement noise matrix which are known as

$$\mathbf{Z} = [d_1, d_2, \dots, d_n]^T, \quad (3.8)$$

$$f(\mathbf{p}) = [\tilde{d}_1, \tilde{d}_2, \dots, \tilde{d}_n]^T, \quad (3.9)$$

$$\boldsymbol{\eta} = [\eta_1, \eta_2, \dots, \eta_n]^T = (\mathbf{C}_0\boldsymbol{\tau} + \mathbf{C}_1\boldsymbol{\tau})c/2, \quad (3.10)$$

where,  $\tilde{d}_i = \|\mathbf{p} - \mathbf{p}_i\|$  is the real distance between UAV and anchor node  $i$ ,  $\boldsymbol{\tau} = [\tau_p, \tau_1, \tau_2, \dots, \tau_n]^T$  is defined as the measurement noise matrix,  $C_0$  and  $C_1$  are the coefficient matrix which can be written as

$$\mathbf{C}_0 = \begin{bmatrix} -1 & 1 & 0 & \cdots & 0 \\ -1 & 0 & 1 & \cdots & 0 \\ \vdots & \vdots & \vdots & \ddots & \vdots \\ -1 & 0 & 0 & \cdots & 1 \end{bmatrix}_{n \times (n+1)}, \quad (3.11)$$

$$\mathbf{C}_1 = \begin{bmatrix} 1 & -1 & 0 & \cdots & 0 \\ 1 & 0 & -1 & \cdots & 0 \\ \vdots & \vdots & \vdots & \ddots & \vdots \\ 1 & 0 & 0 & \cdots & -1 \end{bmatrix}_{n \times (n+1)}. \quad (3.12)$$

Thus, the covariance matrix of  $\boldsymbol{\eta}$  can be calculated as follows

$$\mathbf{Q}_\eta = c(\mathbf{C}_0\mathbf{Q}_\tau\mathbf{C}_0^T + \mathbf{C}_1\mathbf{Q}_\tau\mathbf{C}_1^T), \quad (3.13)$$

where,  $\mathbf{Q}_\tau$  is the covariance matrix of measurement noise matrix  $\boldsymbol{\tau}$ .

Finally, the likelihood function can be derived from the above-mentioned equations

$$p(\mathbf{Z}, \mathbf{p}) = \frac{1}{(2\pi)^{\frac{n}{2}} \det(\mathbf{Q}_\eta)^{\frac{1}{2}}} \cdot \exp\left[-\frac{1}{2}(\mathbf{Z} - f(\mathbf{p}))^T \mathbf{Q}_\eta^{-1}(\mathbf{Z} - f(\mathbf{p}))\right] \quad (3.14)$$

Considering the existing characteristics, including the implementation simplicity, asymptotically unbiased and high efficiency [142, 143], the MLE approach is selected to estimate the position information of UAV. Through (3.14), the MLE of  $\mathbf{p}$  can be obtained

$$\hat{\mathbf{p}} = \arg \min [(\mathbf{Z} - f(\mathbf{p}))^T \mathbf{Q}_\eta^{-1}(\mathbf{Z} - f(\mathbf{p}))]. \quad (3.15)$$

However, due to the nonlinearity of the real distance matrix  $f(\mathbf{p})$ , a closed-form solution for (3.15) does not exist. Therefore, a numerical minimisation method [139, 142–145] will be introduced to approach the real solution.

Firstly, the estimation of  $\mathbf{p}$  and the iteration factor at  $j$ th iteration is defined as  $\hat{\mathbf{p}}(j)$  and  $\mathbf{\Delta}(j)$ . It can be seen that

$$\mathbf{p} = \hat{\mathbf{p}}(j) + \mathbf{\Delta}(j). \quad (3.16)$$

Thus,  $f(\mathbf{p})$  can be linearised around  $\hat{\mathbf{p}}(j)$ , yielding

$$f(\mathbf{p}) = f(\hat{\mathbf{p}}(j)) + G(\hat{\mathbf{p}}(j))\mathbf{\Delta}(j), \quad (3.17)$$

where,  $G(\hat{\mathbf{p}}(j))$  is the Jacobian matrix

$$G(\mathbf{p}) = \frac{\partial f(\mathbf{p})}{\partial \mathbf{p}}. \quad (3.18)$$

From (3.9), the partial derivative of  $f(\mathbf{p})$  with respect to  $\mathbf{p}$  can be derived

$$\frac{\partial f_i(\mathbf{p})}{\partial \mathbf{p}} = \frac{\partial \tilde{d}_i}{\partial \mathbf{p}} = \frac{(\mathbf{p} - \mathbf{p}_i)}{\|\mathbf{p} - \mathbf{p}_i\|}. \quad (3.19)$$

Substituting (3.19) into (3.18), the Jacobian matrix can be written as

$$G(\mathbf{p}) = \left[ \frac{(\mathbf{p} - \mathbf{p}_1)}{\|\mathbf{p} - \mathbf{p}_1\|}, \frac{(\mathbf{p} - \mathbf{p}_2)}{\|\mathbf{p} - \mathbf{p}_2\|}, \dots, \frac{(\mathbf{p} - \mathbf{p}_n)}{\|\mathbf{p} - \mathbf{p}_n\|} \right]^T. \quad (3.20)$$

Combining (3.15) and (3.17), the estimation of the iteration factor can be calculated

$$\begin{aligned} \hat{\Delta}(j) = & [G^T(\hat{\mathbf{p}}(j))\mathbf{Q}_\eta^{-1}G(\hat{\mathbf{p}}(j))]^{-1} \\ & \cdot G^T(\hat{\mathbf{p}}(j))\mathbf{Q}_\eta^{-1}(\mathbf{Z} - \mathbf{f}(\hat{\mathbf{p}}(j))). \end{aligned} \quad (3.21)$$

Finally, the estimate coordinate matrix of UAV at  $(j + 1)$ th iteration will be

$$\hat{\mathbf{p}}(j + 1) = \hat{\mathbf{p}}(j) + \hat{\Delta}(j). \quad (3.22)$$

In order to make it clear to understand, the structure for the MLE based UAV positioning algorithm has been given in Fig. 3.1.

With the numerical minimisation method, the position information of UAV can be estimated. However, two additional problems, including the local minimum and the non-convergence problems which lead by the estimation method cannot be ignored. Clearly from (3.21), with a small  $G^T(\hat{\mathbf{p}}(j))\mathbf{Q}_\eta^{-1}G(\hat{\mathbf{p}}(j))$ , a

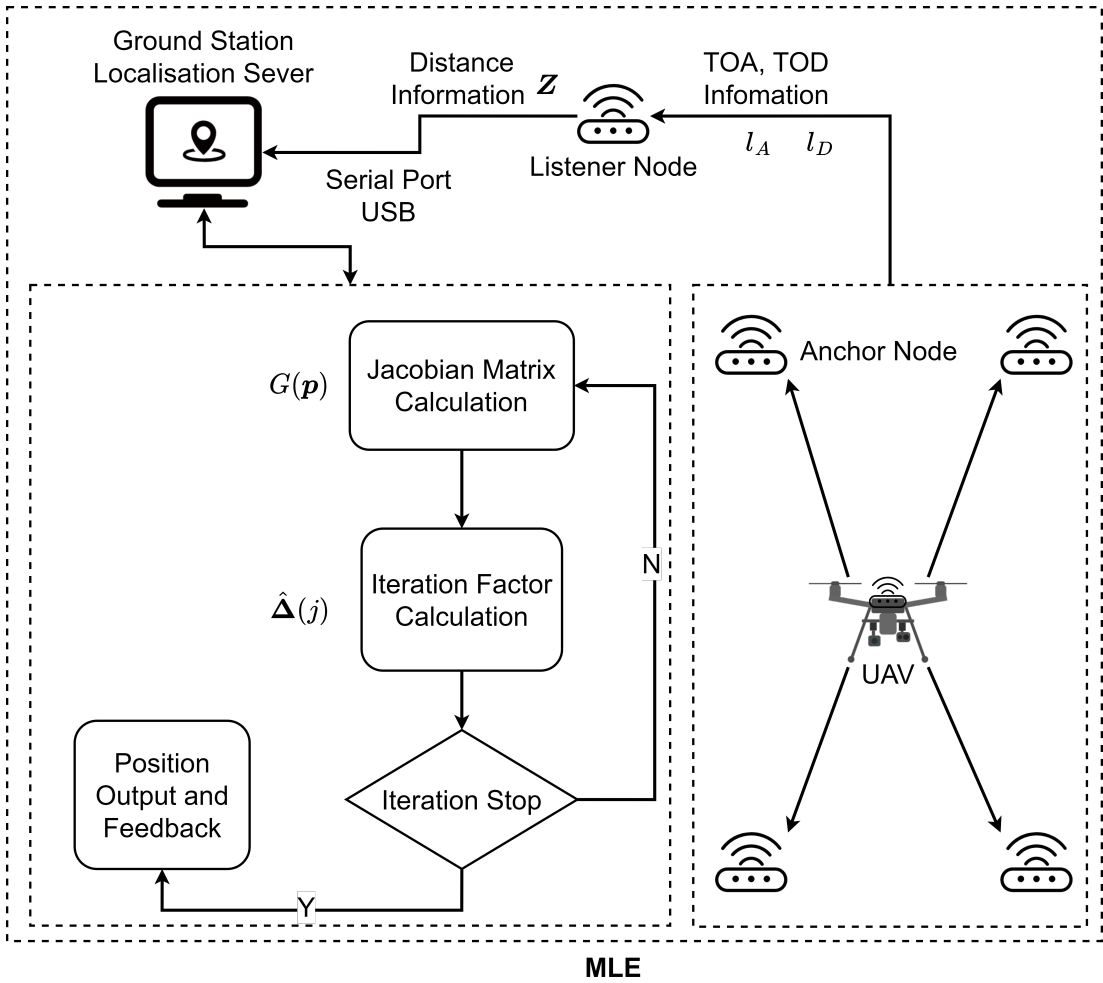


Figure 3.1: Structure for the MLE based positioning algorithm.

large oscillation for the iteration factor may occur. This may cause the estimation stopped at a local minimum or even the non-convergence for the estimator [139, 142–144]. To prevent the aforementioned issue, an appropriate initial guess close to the true value is required. Therefore, considering the UAV is moving continuously, the previous estimation of the UAV position information will be served as the initial guess to avoid the iteration stopped at a local minimum, the non-convergence of the estimator and to reduce the iterations.

### 3.3 Anchor distribution strategy

Clearly from the positioning scheme and localisation equation shown in Fig. 2.5 and (3.6), the number of anchor nodes in the system and their locations will have tremendous impact on the localisation performance. In addition, considering applications in extremely confined environments, such as a small storage tank or pressure vessel, which is hard to access, the anchor nodes can only be deployed near the entrance of the area inside that space. To be specific, the quantity and deployment area of anchor nodes are always limited in such environments. Consequently, the deployment strategies or layouts of the anchor nodes become particularly important to the localisation performance. Towards this end, the analysis on anchor deployment strategies to achieve high precision localisation of UAV in extremely confined environments is carried out in this section.

In order to quantitatively analyse the localisation performance under different geometry configurations of anchor nodes, geometric dilution of precision (GDOP) is introduced. GDOP is a significant metric to evaluate the precision of model parameters before positioning estimation [146]. It reflects the geometry configuration quality of anchor nodes. Here, suppose the covariance matrix of the unbiased estimation  $\hat{\mathbf{p}}$  to be  $Cov(\hat{\mathbf{p}})$ . Then GDOP can be defined as

$$GDOP = \frac{\sqrt{tr(Cov(\hat{\mathbf{p}}))}}{c\sigma_\tau}, \quad (3.23)$$

where,  $tr(\cdot)$  denotes matrix trace. The trace of the covariance matrix is related to the Cramér–Rao lower bound (CRLB) of the localisation algorithm.

According to the definition of CRLB, it is the inverse of the Fisher information

matrix (FIM) [147]. Under Gaussian noise, FIM can be calculated through

$$J(\mathbf{p}) = G^T(\mathbf{p})\mathbf{Q}_\eta^{-1}G(\mathbf{p}). \quad (3.24)$$

Thus, CRLB of the localisation algorithm can be represented as

$$\bar{\sigma}_{\mathbf{p}}^2 = \sum_{n=1}^3 [J^{-1}(\mathbf{p})]_{nn}, \quad (3.25)$$

where,  $[J^{-1}(\mathbf{p})]_{nn}$  denotes as the  $n$ th diagonal element of  $J^{-1}(\mathbf{p})$ .

Substituting (3.25) into (3.23), GDOP of the localisation algorithm can be computed by

$$GDOP = \frac{\bar{\sigma}_{\mathbf{p}}}{c\sigma_\tau}. \quad (3.26)$$

### 3.4 Performance evaluation in the simulation environment

Considering the safety reason for flying UAV in the real experiment before the verification of the algorithm and strategy, the simulation is firstly carried out to prove the effectiveness of these. In order to comprehensively validate the localisation performance of the MLE based positioning algorithm and its performance under different anchor deployment strategies, four different types of geometry configurations for the anchor nodes shown in Fig. 3.2 are simulated in the Matlab environment. This is the under the consideration that the anchor nodes can only be deployed near the entrance of the confined space. The coordinates of each anchor node under different geometry configurations are listed in Table 3.1, and the entrance of this confined space is supposed at the central area of the X-Z

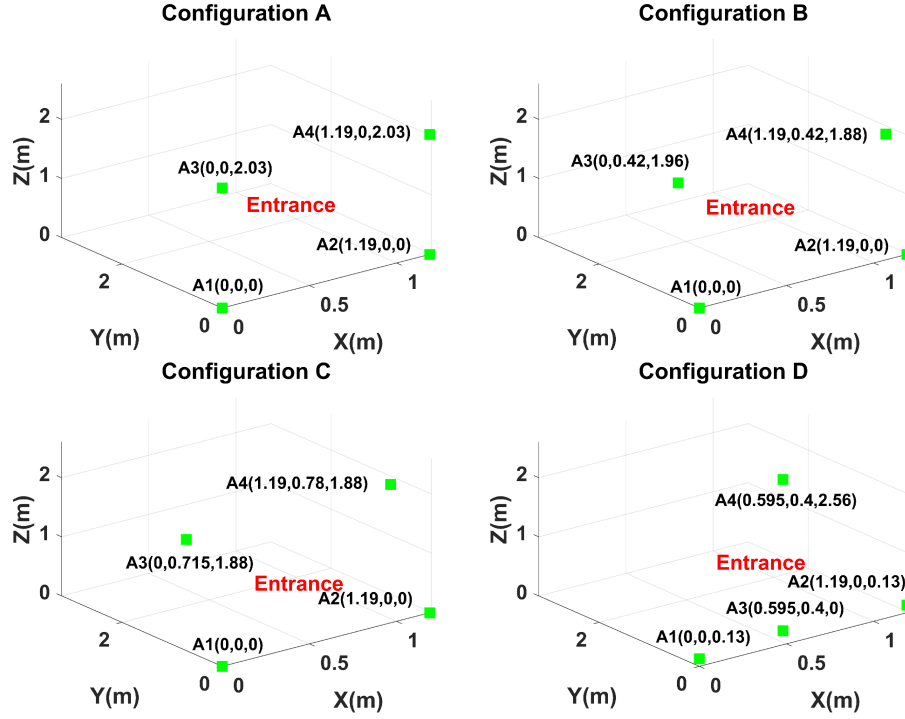


Figure 3.2: Geometry configurations of anchor nodes.

plane. The localisation area is set within a narrow space ( $1.2\text{m} \times 3.2\text{m} \times 2.6\text{m}$ ) which is the same as the actual experiment area for this approach, where X-axis is set as the width direction, Y-axis is parallel to the depth direction, while Z-axis denotes the altitude. Only four anchor nodes are considered in the simulation due to the difficulty for anchor deployment in the confined space. Moreover, considering the anchor nodes can only be deployed near the entrance of the confined space, the simulation will pay more attention to the performance change with the Y coordinate variation. Different Y coordinates of the target are taken into account for the performance evaluation. In the simulation, the standard deviation (STD) of the measurement noise is set to be  $0.1\text{ns}$  [148, 149].

As shown in Fig. 3.3, Fig. 3.4, Fig. 3.5 and Fig. 3.6, GDOP of the algo-

Table 3.1: Coordinates of anchor nodes under different geometry configurations

Geometry Configuration	Anchor 1	Anchor 2	Anchor 3	Anchor 4
A	(0,0,0)m	(1.19,0,0)m	(0,0,2.03)m	(1.19,0,2.03)m
B	(0,0,0)m	(1.19,0,0)m	(0,0.42,1.96)m	(1.19,0.42,1.88)m
C	(0,0,0)m	(1.19,0,0)m	(0,0.715,1.88)m	(1.19,0.78,1.88)m
D	(0,0,0.13)m	(1.19,0,0.13)m	(0.595,0.4,0)m	(0.595,0.4,2.56)m

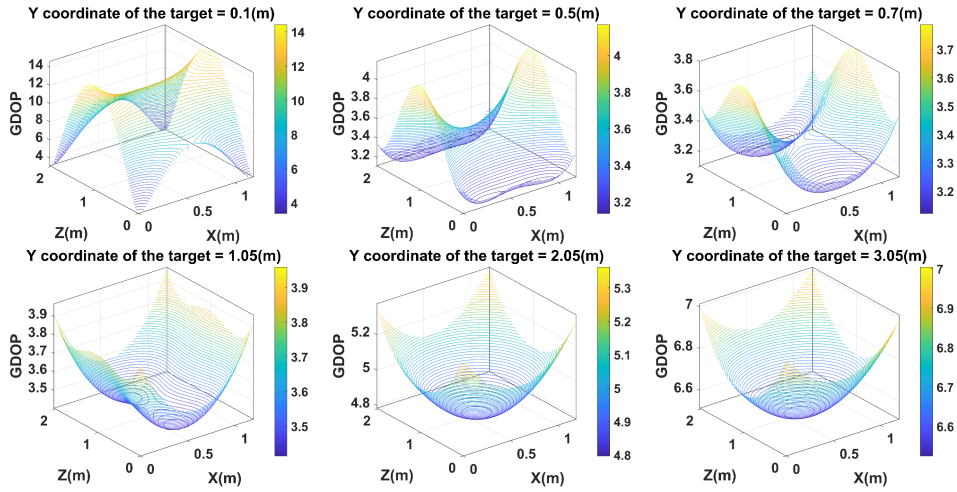


Figure 3.3: GDOP under configuration A of anchor nodes.

rithm under four different geometry configurations of anchor nodes with UAV at different position are simulated. From all the simulation results under different geometry configurations, it can be observed that with the increasing of the Y coordinate, the value of GDOP go up, which means a drop-off for the localisation accuracy. The performance drop-off is associated with the measurement noise of sensor nodes and the distribution of anchor nodes on the Y-axis. With the increasing distance between anchor nodes and UAV, the measurement noise will have greater impact on the localisation accuracy. The accuracy descending rate is different for each geometry configuration. Configuration A holds the biggest accuracy descending rate compared with B and C with all the anchor nodes being

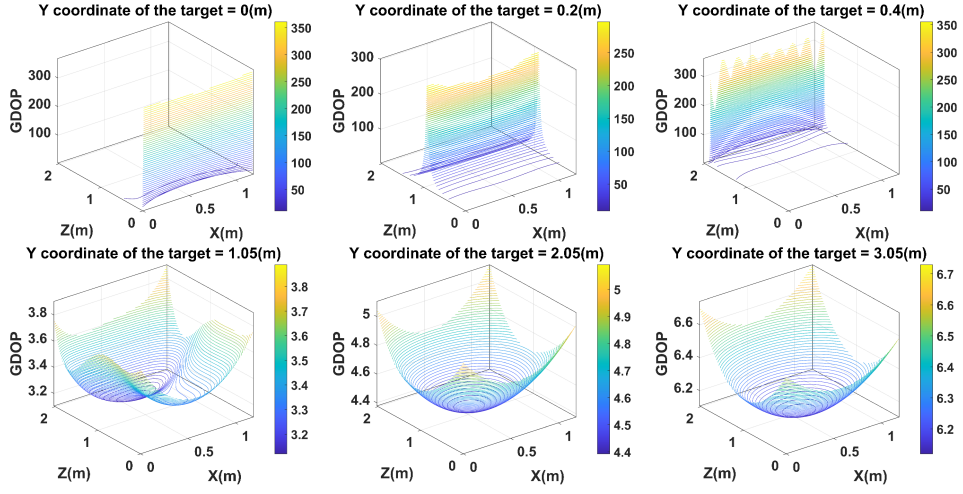


Figure 3.4: GDOP under configuration B of anchor nodes.

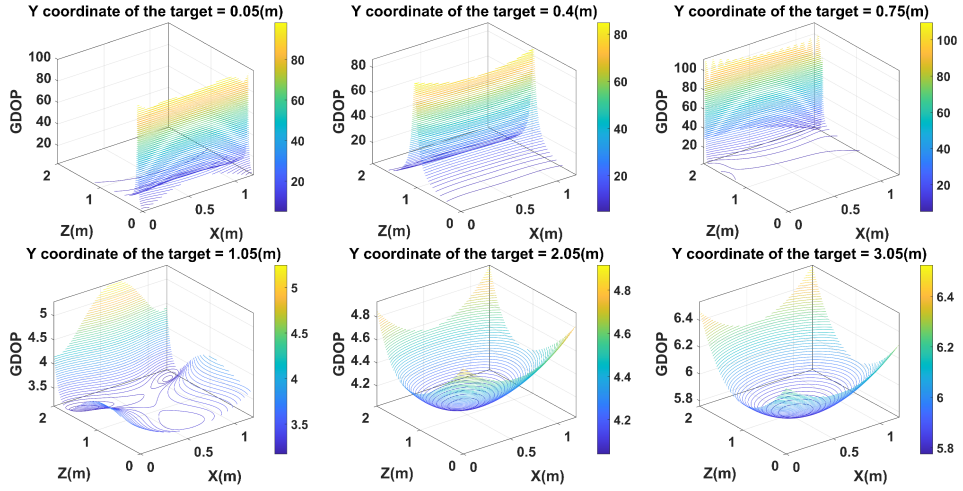


Figure 3.5: GDOP under configuration C of anchor nodes.

deployed on the X-Z plane. From (3.20) and (3.24), FIM can be reshaped as

$$FIM = \frac{1}{c^2 \sigma_\eta^2} \sum_{i=1}^n \frac{(\mathbf{p} - \mathbf{p}_i) (\mathbf{p} - \mathbf{p}_i)^T}{\|\mathbf{p} - \mathbf{p}_i\| \|\mathbf{p} - \mathbf{p}_i\|}. \quad (3.27)$$

Considering the anchor nodes are all deployed on the X-Z plane, when UAV is

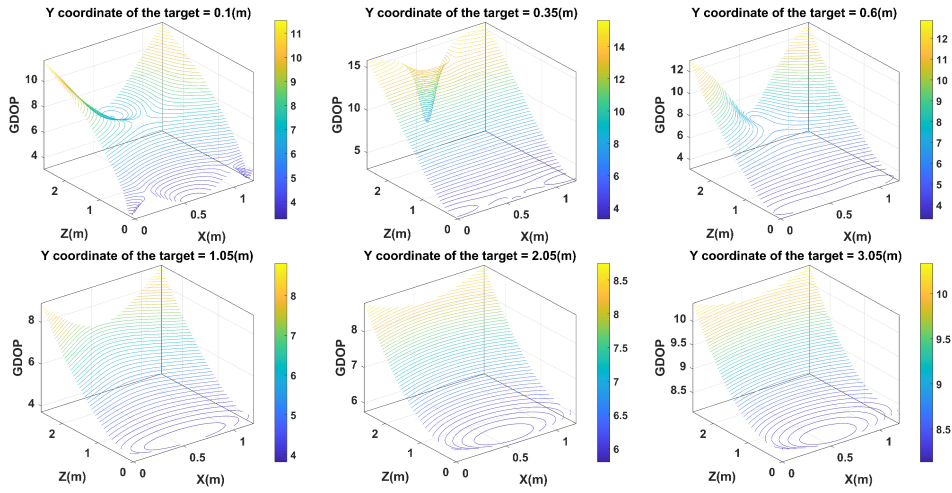


Figure 3.6: GDOP under configuration D of anchor nodes.

on the same plane, FIM will be singular. This means no unbiased estimator for  $\mathbf{p}$  exists with a finite variance [150] and the algorithm will lose its effectiveness. Moreover, it appears that GDOP becomes larger with UAV close to the X-Z plane, especially for the centre of the plane under configuration A. For configuration B, where anchor 3 and anchor 4 are deployed a little deeper in the area with the same Y coordinate, the accuracy descending rate successfully decreased as shown in Fig. 3.4. GDOP becomes larger when UAV is approaching the plane composed of four anchor nodes. Clearly, within the composed plane, Y coordinate of UAV is able to be expressed linearly by X and Z coordinates. Thus, the inverse matrix of FIM does not exist, which will result in the lose effectiveness of the algorithm. Similar to configuration B, anchor 3 and anchor 4 are also deployed a little deeper in the area, but with the different Y coordinate for configuration C. As apparent from Fig. 3.5, the accuracy is further improved with the increasing of the Y coordinate in contrast to configuration B. Whereas, the precision degradation still exists when UAV is close to the planes composed of any three anchor nodes. Completely

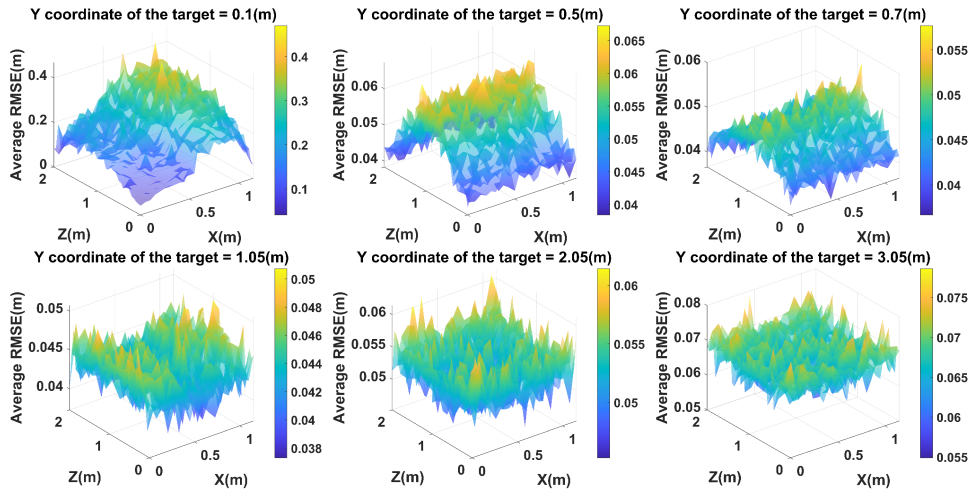


Figure 3.7: RMSE under configuration A of anchor nodes.

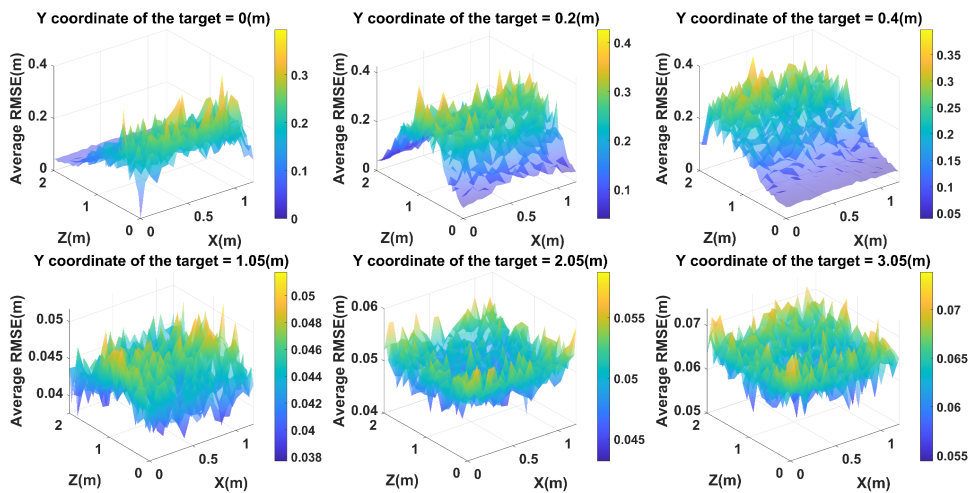


Figure 3.8: RMSE under configuration B of anchor nodes.

different from all the aforementioned deployment strategies, two anchor nodes are deployed on the top and bottom of the confined space for configuration D which is analysed in Fig. 3.6. Localisation performance becomes worse with the increasing of the Z coordinate under different Y coordinates, associated with the small distribution of anchor nodes on Z-direction.

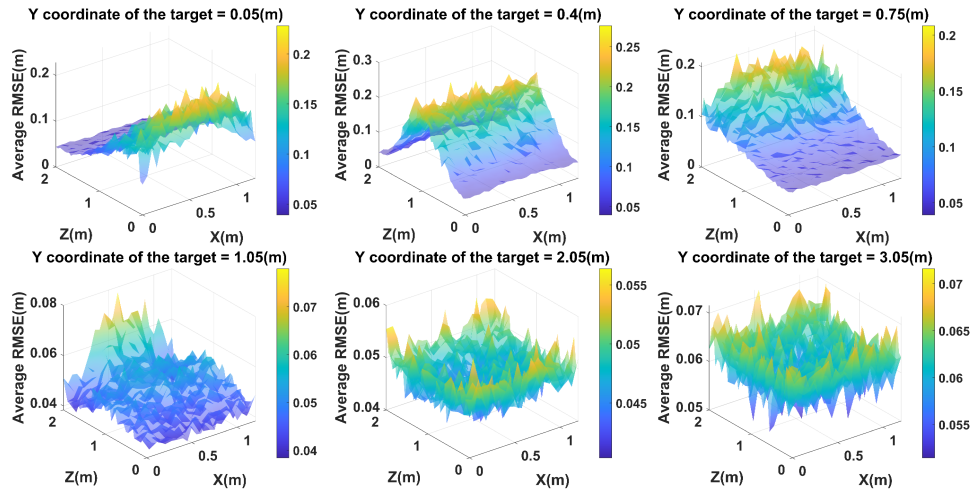


Figure 3.9: RMSE under configuration C of anchor nodes.

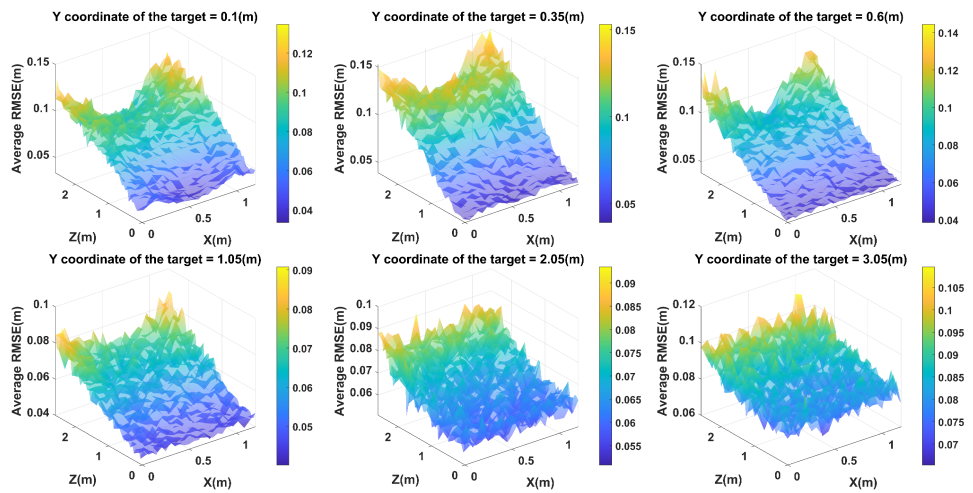


Figure 3.10: RMSE under configuration D of anchor nodes.

To further evaluate the localisation performance under different deployment strategies, RMSE of the algorithm under these four geometry configurations are given in Fig. 3.7, Fig. 3.8, Fig. 3.9 and Fig. 3.10. Here, some declaration should be made before the simulation results analysis. For this simulation, the input is the ranging information between tag node and anchor nodes, the output is the

estimated position information for the UAV and the iteration will stop when the difference between two round iterations less than 1mm. Furthermore, for each of the test point, 100 simulations have been done to comprehensively evaluate the performance. Clearly, RMSE becomes larger with the increasing of the Y coordinate when the UAV is not moving towards the anchor nodes deployment area, and configuration A holds the biggest descending rate of localisation accuracy compared with B and C. For configuration A, the same result can be obtained that when UAV is close to the X-Z plane, especially the centre of the plane, there will be a sharp drop-off for the accuracy. When UAV flies away from the plane, the influence will be eased. On the other hand, considering the RMSE distribution under configuration B and C. It appears that with UAV flying within the area composed of these four anchor nodes, there will be performance oscillation which has the same conclusion in contrast to the analysis on GDOP. The localisation performance is better than configuration A when out of the area constituted by these anchor nodes. Finally, from Fig. 3.10, it is clear to find that, even an accurate result can be obtained with a small Z coordinate for configuration D, the overall accuracy is still kept in low level in contrast to the other three geometry configurations.

In conclusion, according to the simulation results, the following summary can be given. For the geometry configuration A of the anchor nodes, it is more suitable for applications in the space with the smaller value in depth direction. For the space with a relatively larger size in depth direction, the geometry configuration B and C can provide more accurate positioning performance. However, the performance degradation still exists when the UAV move towards the anchor nodes deployment area.

### 3.5 System implementation and experiment setup

To evaluate the localisation performance under these four geometry configurations of anchor nodes in actual environment, experiments are performed with a hybrid UAV localisation system consisting of UWB based sensor nodes designed by Pozyx and a commercial low cost mini quadcopter - DJI Tello EDU. For the UWB based sensor nodes, considering the stability and accuracy of the localisation performance, channel 2 is selected which is defined by the IEEE 802.15.4 standard [151]. The centre frequency is 3993.6 MHz and the bandwidth is 499.2 MHz. The localisation area is set within a narrow space ( $1.2\text{m} \times 3.2\text{m} \times 2.6\text{m}$ ) in lab environment with four anchor nodes existing as depicted in Fig. 3.12. The UAV localisation system has three main modules: UWB based localisation module, ground station (localisation server) and UAV. The system structure and diagrams of each module are given in Fig. 3.11 and Fig. 3.13. During the localisation process, a position request will be sent out from the tag node equipped on UAV. Afterwards, the recorded information from the communication between sensor nodes will be transmitted to the ground station (localisation server) for position estimation. The localisation server and ground station is a laptop where the localisation algorithm and position controller are implemented. With the estimated position information, the response command will be given by the controller and encapsulated as a ROS package. Finally, the package will be transmitted to UAV for position update. Here needs to declare that, in the system, each sensor node is able to power itself with its on-board battery which has no impact on the operation time of the UAV. Moreover, considering the UWB based system cannot provide the attitude information for the UAV, the attitude information

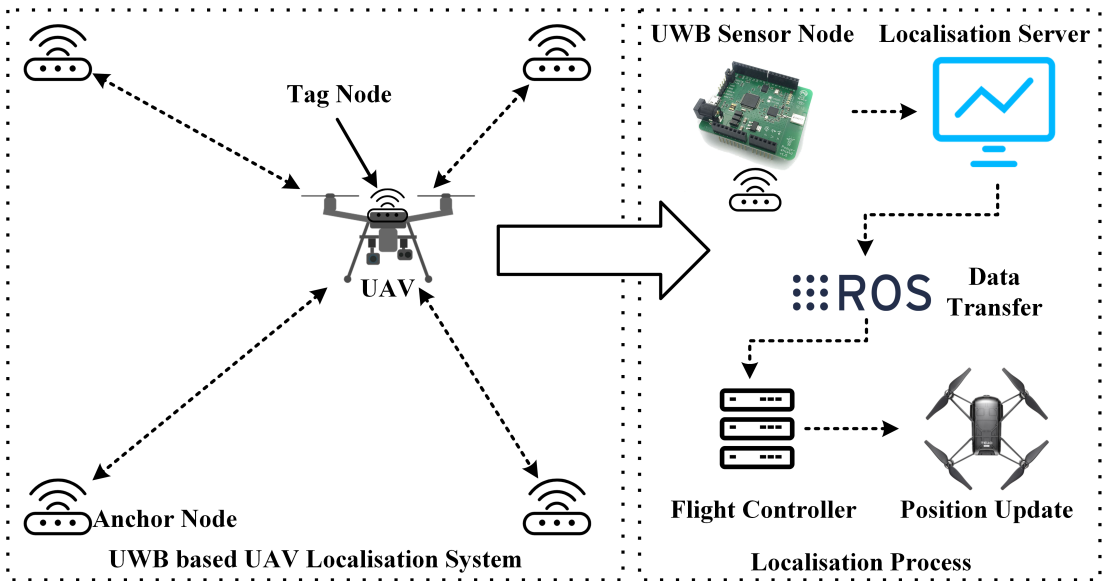


Figure 3.11: Localisation structure for the pure UWB based UAV localisation system.

utilised for this system is directly measured by the IMU attached on the UWB tag node.

### 3.6 Performance evaluation in the experiment environment

In order to validate the localisation performance comprehensively, the experiments are divided into two parts, the static experiments and flight tests. Firstly, the performance testing was done at some representative points statically without UAV flying under different anchor deployment strategies. These experiments pay more attention to analyse the impact of different anchor deployment strategies on localisation performance in actual environments. The true location of each test point was measured manually. For each test point, 100 measurements were repeated to eliminate the influence of unreasonable values on positioning. The

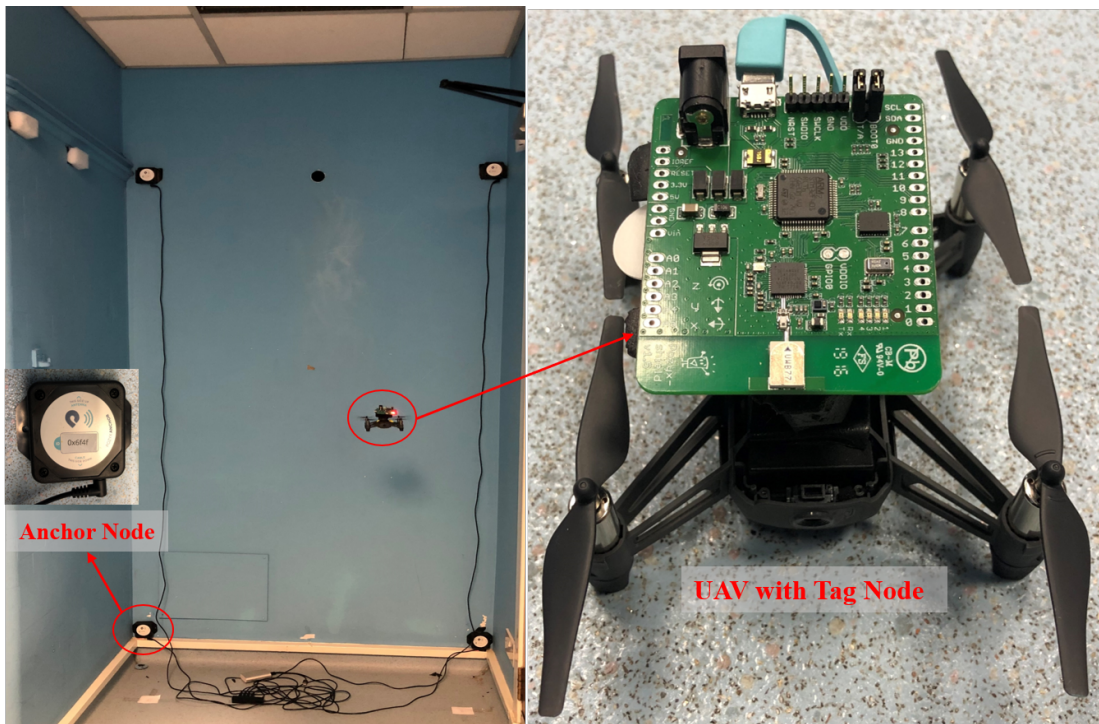


Figure 3.12: Laboratory experiment environment for the pure UWB based localisation system and the DJI Tello EDU.

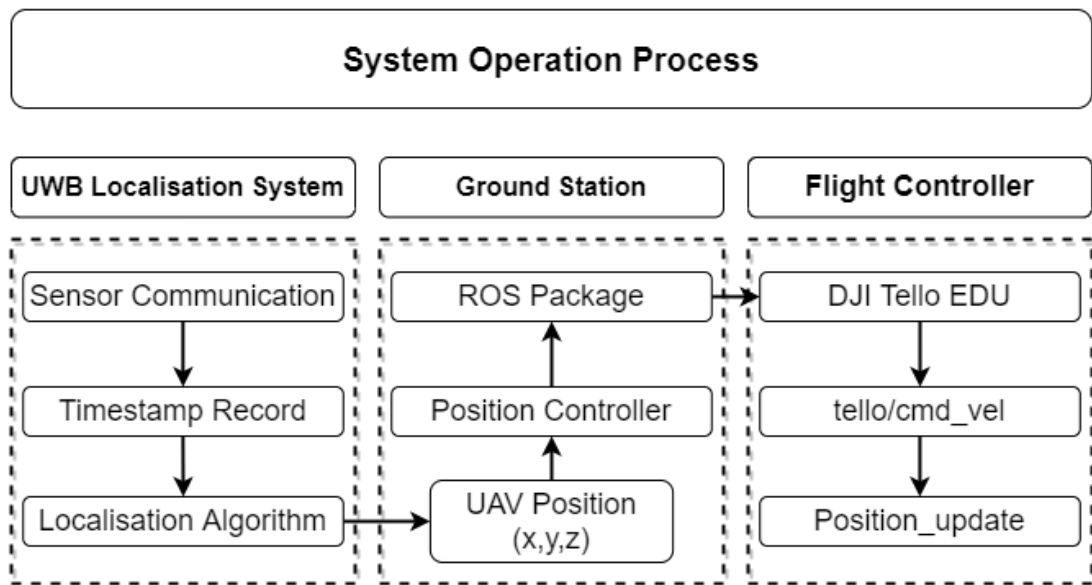


Figure 3.13: Operational process for the pure UWB based system.

average RMSE and STD of the 100 RMSE for each test point under four geometry configurations of anchor nodes are presented in Fig. 3.14 and Fig. 3.15. Where  $X(m)$ ,  $Y(m)$  and  $Z(m)$  represent the coordinate of the test points, the colour bar is denoted as the distribution of average RMSE and the STD of RMSE. Moreover, the empirical cumulative distribution function (eCDF) of the localisation error at four representative test points under different geometry configurations are shown in Fig. 3.16. The median and 95<sup>th</sup> percentile localisation errors are given in Table 3.2. Within Fig. 3.16 and Table 3.2, the coordinates of these test points are, test point 1:  $[0.59,0.550,0.99]m$ , test point 2:  $[0.59,1.050,0.99]m$ , test point 3:  $[0.59,2.050,0.99]m$  and test point 4:  $[0.59,2.550,0.99]m$ . Furthermore, these experiments are also utilised to measure the noise level of the UWB distance measurements.

From the results, it can be found out that, high accuracy result with an average RMSE under 0.15m can be obtained with Y coordinate of the target within  $[0.5,2]m$  for configuration A. The average STD of RMSE keeps below 0.07m which also means a high precision performance. However, with the Y coordinate larger than 2m, average RMSE is increased to 0.26m which is significantly inferior to configuration B and C. For configuration B and C, with the same Y coordinate, the accuracy is improved with the average RMSE less than 0.23m and 0.21m. Whereas, it appears that when the target is near the plane consisting of anchor nodes, the violent oscillation can be observed in Fig. 3.14 and Fig. 3.15 with the average RMSE and STD larger than 0.35m. But the average RMSE and STD are still kept below 0.2m and 0.07m for most test points with configuration B and C. Particularly, the STD of RMSE for configuration C is even lower than 0.04m excluding the test points aforementioned. Moreover, it is clear to find out that

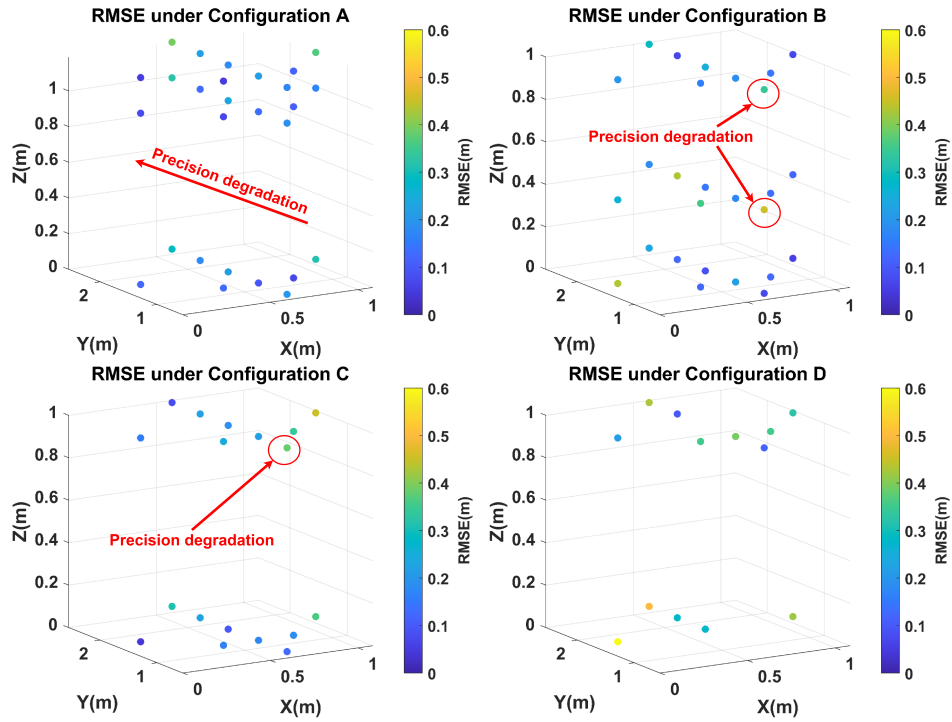


Figure 3.14: RMSE under different geometry configurations of anchor nodes.

configuration D holds the worst performance with the average RMSE larger than 0.3m.

On the other hand, from Table 3.2 and Fig. 3.16, it appears that for test point 1 and 2 with a smaller Y coordinate (0.550m and 1.050m), configuration A holds the great performance with median error less than 0.19m. However, with the increased Y coordinate for test point 3 (2.050m) and test point 4 (2.550m), the median error and 95<sup>th</sup> percentile error are all increased. Another key observation is that for test point 3 and test point 4, configuration B and C can achieve higher accuracy. Especially for configuration C at test point 4, the localisation error is significantly decreased with a 0.07m median error and 0.15m 95<sup>th</sup> percentile error. Nevertheless, the performance oscillation can be observed for these two geometry

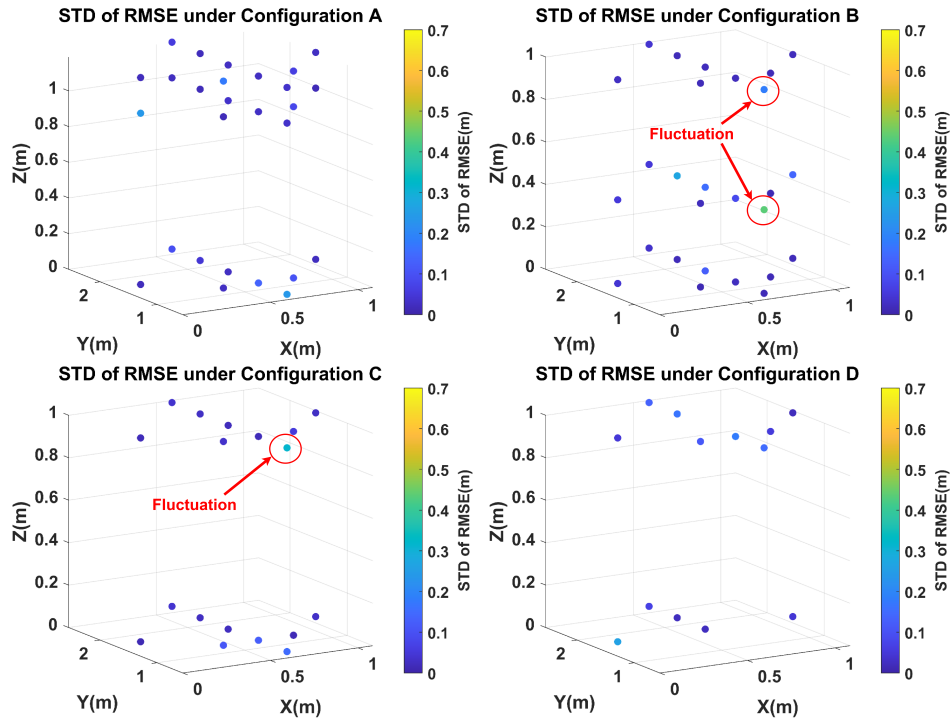


Figure 3.15: STD of RMSE under different geometry configurations of anchor nodes.

configurations with the target near the entrance of the confined environment at test point 1. Interestingly, for test point 1, configuration D holds the best performance with the median error and 95<sup>th</sup> percentile error to be 0.09m and 0.20m. Whereas, the localisation performance is unstable with the STD larger than 0.13m for all the test points under configuration D. Meanwhile, for test point 2 and test point 4, the median errors are increased to 0.50m and 0.44m which is unacceptable for UAV positioning in extremely confined environments.

To further evaluate the localisation performance and illustrate the effectiveness of the proposed approach, flight tests under different geometry configurations of anchor nodes were carried out with UAV flying along a planned trajectory. The planned trajectory with the estimated position under different geometry

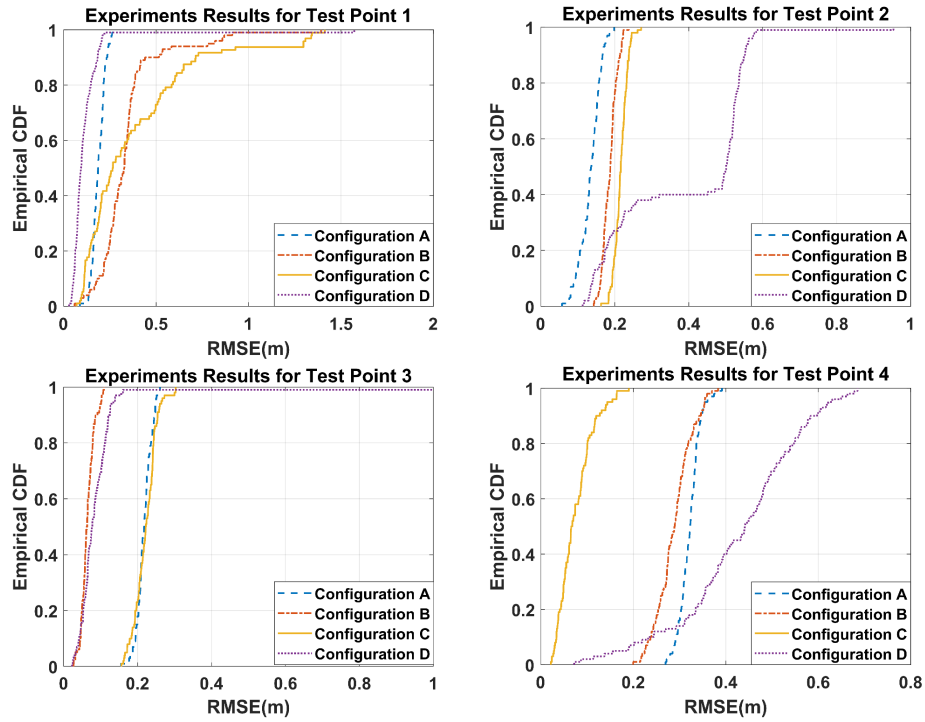


Figure 3.16: eCDF for representative test points under different geometry configurations of anchor nodes.

configurations of anchor nodes is given in Fig. 3.17. Therein, the flight tests were only performed with configuration A, B and C, considering the unacceptable and unstable accuracy for configuration D. As apparent from the localisation results, the same conclusion can be made in contrast to the results from simulation and static experiments.

In conclusion, from the experimental results, it can be determined that in the space with a small size in depth direction (less than 2m), configuration A is able to provide precise and accurate localisation for UAV with the average RMSE and STD under 0.15m and 0.07m, respectively. On the contrary, configuration B and C are much more suitable to be applied in the area with a larger size in depth

Table 3.2: Localisation error for representative test points

Geometry Configuration	Median Error (m)	95 <sup>th</sup> Error (m)	Average STD (m)
A-Test 1	0.19	0.24	0.03
A-Test 2	0.14	0.17	0.03
A-Test 3	0.22	0.25	0.02
A-Test 4	0.32	0.35	0.02
B-Test 1	0.33	0.78	0.18
B-Test 2	0.19	0.22	0.02
B-Test 3	0.06	0.10	0.02
B-Test 4	0.29	0.35	0.04
C-Test 1	0.27	1.30	0.31
C-Test 2	0.22	0.24	0.02
C-Test 3	0.22	0.27	0.03
C-Test 4	0.07	0.15	0.04
D-Test 1	0.09	0.20	0.15
D-Test 2	0.50	0.56	0.18
D-Test 3	0.08	0.13	0.17
D-Test 4	0.44	0.62	0.13

direction, especially for configuration C where higher accuracy can be provided. However, performance drop-off will be noticed when the UAV is approaching the entrance of the area (near the anchor nodes deployment area). Moreover, with the proposed algorithm and the developed system, the position update around 25Hz can be obtained.

For the focused application scenarios in extremely confined environments, one of the most important indexes for UAV positioning is the STD for the localisation error. This is also known as the precision or the level of performance oscillation for the system. The precision will have a huge impact on the stability of UAV in such environments. Considering the dimensions of the DJI Tello (98mm  $\times$  92.5mm  $\times$  41mm), the precision less than 0.098m is acceptable for the focused applications which can be attained with the suitable geometry configuration of anchor nodes.

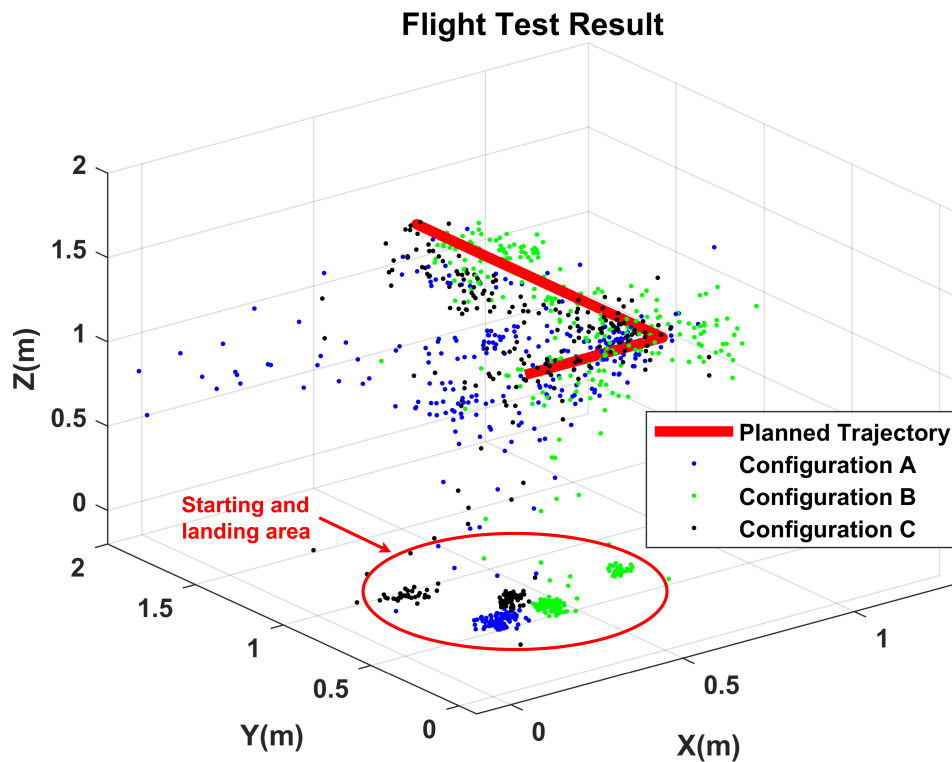


Figure 3.17: Localisation results for the flight tests with the MLE based UWB localisation system.

On the other hand, regarding to the absolute accuracy, this index is relevant to the situation that whether UAV can fly along with the planned trajectory and hit the targeted points or not. Owing to the air flow disturbance, in such environments, UAV cannot fly too close to the wall for inspection, in case of the instability control or crash down. Therefore, a safety distance is required when planning the trajectory or target points. Meanwhile, the system is developed for smart inspection, even UAV cannot hit every target point accurately, the camera can still record the video or picture in that area for further inspection. Thus, the average RMSE less than 0.2m is acceptable for the focused applications. In conclusion, with the proposed MLE based localisation approach, the precise UAV

positioning can be achieved in extremely confined environments under different circumstances.

### 3.7 Summary

In this chapter, the investigation and research on the UWB based UAV positioning technology has been made. Firstly, in order to solve the issues for the existing UAV localisation technologies such as the vision based, LiDAR, ultrasonic and infrared, including the performance influence from different illumination conditions, the extremely high system cost, the high energy consumption, the unacceptable weight and size for the components, the restricted localisation area and the vulnerable performance in different operational environments, the MLE localisation algorithm based on the UWB localisation system was proposed. To avoid the strict clock synchronisation between UWB sensor nodes, the TW-TOF ranging scheme was applied in the proposed algorithm. In addition, for the UWB based localisation system the distribution of the fixed anchor nodes also has the great impact on the positioning performance. Therefore, the anchor distribution strategy has been investigated in this chapter help to find the suitable geometry configurations of the fixed anchor nodes to keep the best localisation performance. Finally, the simulation and real-world tests have been carried out to validate the performance of the proposed algorithm and strategy. As shown in the results, the algorithm can provide precise 3D UAV positioning with a decimetre-level accuracy and centimetre-level precision, and the suitable geometry configurations of the anchor nodes can be found by the proposed strategy to keep these performance under different circumstances. In conclusion, with the proposed MLE

### Chapter 3. UWB based UAV positioning technology

based localisation algorithm and the presented anchor distribution strategy, a high level positioning performance can be achieved for the pure UWB based system under difference circumstances to support the UAV autonomous inspection in extremely confined environments.

## Chapter 4

# UWB and IMU based EKF sensor fusion UAV positioning technology

### 4.1 Introduction

As declared in Chapter 3, with the MLE based localisation algorithm and UWB based localisation system, the UAV positioning in GPS-denied and extremely confined environments can be achieved. Nevertheless, the restriction still exists for the UWB based localisation technology which limits its applications on UAV in such environments. Owing to the inherent properties of the RF signal, the additional propagation delay and changing measurement noise caused by the unpredictable propagation condition and the time varying operational environment always exist which will lead to the localisation performance oscillation and may result in the instability of UAV.

Under such circumstances, plenty of researches have been carried out. Among them, the KF based sensor fusion localisation algorithms which integrated the IMU and the UWB have been investigated and extensively utilised for UAV positioning due to the implementation simplicity and sufficient accuracy. In [63], the EKF based sensor fusion algorithm was exploited for the low cost UAV positioning. The additional measurement calibration and outlier detection methods were proposed to resist the performance influence from the unreasonable values. Similarly, Li et al. [64] proposed an EKF based IMU and UWB localisation system which successfully achieved the 80Hz 3D positioning of the MAV swarm. The same research has also been carried out by Strohmeier et al. [66], but differently, excluding the UAV position, the angular rate was considered in the prediction model to estimate the precise orientation information for performance improvement. Whereas, with the utilisation of the first order Taylor expansion for the EKF, the neglected high order terms still limit its performance. To remedy this, the advanced KF algorithms were proposed. Instead of linearising the transition matrix, the system state can be approximated by the sampling points for the UKF. According to the UAV flight test results in [69], the performance of the UKF based system was significantly improved 70% compared with the pure UWB based system. Yet, considering the focused applications in extremely confined environments, where it is difficult to collect the UAV after crash, the priority for the positioning system is to prevent any positioning failure. Thus, the increased probability for filtering divergence and computational complexity of the UKF based approaches restrict the applications in the focused scenarios [152]. Excluding EKF and UKF, the particle filter (PF) based sensor fusion algorithm also attract lots of attention in this area, since it can provide optimal estimation in

nonlinear non-Gaussian state-space models and does not require any hypothesis for the probability density function of the measurements [153–155]. However, the performance of it is high relevant to the number of particles in the system, and the high accuracy of the algorithm is at the expense of the computational complexity of the system [156]. This runs counter to the focused applications in this thesis. In order to achieve the high accuracy and precision UAV positioning with low computational complexity and prevent the positioning failure, the EKF based sensor fusion based algorithm becomes the ideal candidate for the focused applications in this thesis.

Yet, one critical issue still exists which restrict the performance of the EKF based algorithm is the requirement of the prior information. The accuracy for the prior information, including the process and measurement noise covariance matrices, highly affects the performance of the EKF based sensor fusion approach. Inappropriate value can cause the sharp performance degradation, even the filtering divergence. For the IMU and UWB based UAV positioning, since the propagation condition and operational environment are unpredictable and time varying during the flight of UAV, the performance oscillation or degradation may appear, with the constant and inaccurate noise covariance matrices for the traditional EKF based sensor fusion approaches. Furthermore, the potential drift for the attitude information caused by the magnetometer on the IMU will also have the great impact on the localisation performance. To remedy the existing problems and provide accurate noise covariance matrices for performance improvement, the AEKF and TC-AEKF based sensor fusion algorithms are proposed in this chapter.

## 4.2 Coordinate system transformation

In order to appropriately describe the motion of UAV, a suitable coordinate system is required. For traditional applications of UAV, the local navigation coordinate system is often set to be north-east-down (NED) coordinate system, then convert the position information from NED to the body frame of UAV for position control. However, for the focused applications, the local navigation coordinate system is determined by UWB anchor nodes, there is no need to transform the coordinate system into NED. Therefore, to convert the acceleration from IMU in its coordinate system to the local navigation frame established by UWB anchor nodes shown in Fig. 4.1 is sufficient for the focused applications. Afterwards, the position information still needs to be transformed into the body frame of UAV for position control.

In the system, the IMU is attached on the UWB tag node which is determined as the right-handed coordinate system. Here, the coordinate system of IMU is set to be  $OX_{IMU}Y_{IMU}Z_{IMU}$ , and the local navigation coordinate system is assumed as  $OX_NY_NZ_N$ . It was known that the quaternion method is the most widely utilised method to represent the attitude information and the rotation of UAV, in order to prevent the gimbal lock issue. However, considering the focused application is the detailed inspection in the extremely confined environments, which means that the UAV could only fly slowly to do the inspection. Under such circumstances the rotation in Pitch and Roll direction are always within  $\pm 10^\circ$  according to the experiment in lab environment. Thus, the gimbal lock issue can be ignored for the focused application. As a result, the Euler angle method is still leveraged here to make the whole conversion and estimation process more

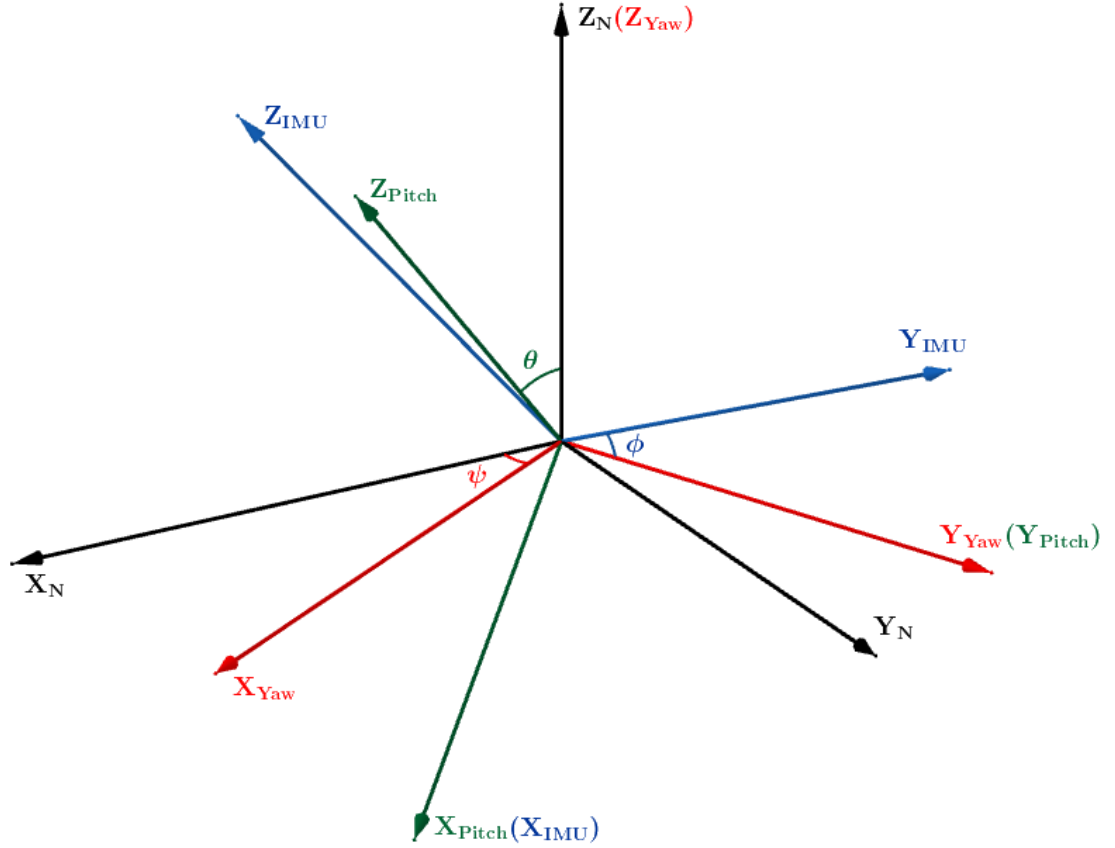


Figure 4.1: Transformation of the coordinate system.

clearly. The detailed information will be given as follows.

As from Fig. 4.1, the three angles between the local navigation frame and IMU frame including Roll, Pitch and Yaw have been defined as  $\phi$ ,  $\theta$  and  $\psi$ . Firstly, rotate the acceleration from the IMU frame into the Pitch frame. Here, let  $\mathbf{C}_{IP}$  represents the transformation matrix between these two frames. Thus, the acceleration  $\mathbf{a}^P$  in the Pitch frame can be derived through the acceleration  $\mathbf{a}^{IMU}$  in the IMU frame

$$\mathbf{a}^P = \mathbf{C}_{IP}\mathbf{a}^{IMU}. \quad (4.1)$$

Within the equation, the transformation matrix  $\mathbf{C}_{IP}$  is expressed as

$$\mathbf{C}_{IP} = \begin{bmatrix} 1 & 0 & 0 \\ 0 & \cos \phi & -\sin \phi \\ 0 & \sin \phi & \cos \phi \end{bmatrix}_{3 \times 3} . \quad (4.2)$$

Afterwards, leveraging the same conversion principle, the acceleration in the Pitch frame can be transformed into the Yaw frame, then into the local navigation frame for UAV positioning. Where the derivation process is given as follow

$$\mathbf{a}^Y = \mathbf{C}_{PY} \mathbf{a}^P, \quad (4.3)$$

$$\mathbf{C}_{PY} = \begin{bmatrix} \cos \theta & 0 & \sin \theta \\ 0 & 1 & 0 \\ -\sin \theta & 0 & \cos \theta \end{bmatrix}_{3 \times 3} , \quad (4.4)$$

$$\mathbf{a}^N = \mathbf{C}_{YN} \mathbf{a}^Y, \quad (4.5)$$

$$\mathbf{C}_{YN} = \begin{bmatrix} \cos \psi & -\sin \psi & 0 \\ \sin \psi & \cos \psi & 0 \\ 0 & 0 & 1 \end{bmatrix}_{3 \times 3} . \quad (4.6)$$

In the above equation,  $\mathbf{a}^Y$  and  $\mathbf{a}^N$  are supposed as the acceleration in Yaw frame and local navigation frame.  $\mathbf{C}_{PY}$  and  $\mathbf{C}_{YN}$  denote the transformation matrices between these coordinate systems, respectively. Finally, throughout the transformation process, the conversion equation from IMU frame to the local navigation frame can be derived

$$\mathbf{a}^N = \mathbf{C}_{YN} \mathbf{C}_{PY} \mathbf{C}_{IP} \mathbf{a}^{IMU}. \quad (4.7)$$

If the gravitational acceleration  $g$  is not removed in the local navigation frame, then the equation should be re-derived as

$$\mathbf{a}^N = \mathbf{C}_{YN}\mathbf{C}_{PY}\mathbf{C}_{IP}\mathbf{a}^{IMU} + \begin{bmatrix} 0 \\ 0 \\ g \end{bmatrix}. \quad (4.8)$$

### 4.3 EKF based sensor fusion with the integration of IMU and UWB

In order to remedy the aforementioned issue, the IMU and UWB based EKF sensor fusion method will be introduced in this section. The IMU and UWB based EKF algorithm is presented to eliminate the performance influence from the unreasonable values within the ranging information from the UWB sensor nodes. To make it clear, the detailed operational process for the EKF based sensor fusion approach has been depicted in Fig. 4.2.

#### 4.3.1 State prediction

With the existing kinematic model of the UAV [157], the matrix form for the motion equation can be derived

$$\begin{cases} \hat{\mathbf{p}}_{k/k-1} = \mathbf{p}_{k-1} + \Delta T\mathbf{v}_{k-1} + \frac{\Delta T^2}{2}\mathbf{a}_{k-1}^N \\ \hat{\mathbf{v}}_{k/k-1} = \mathbf{v}_{k-1} + \Delta T\mathbf{a}_{k-1}^N \end{cases}, \quad (4.9)$$

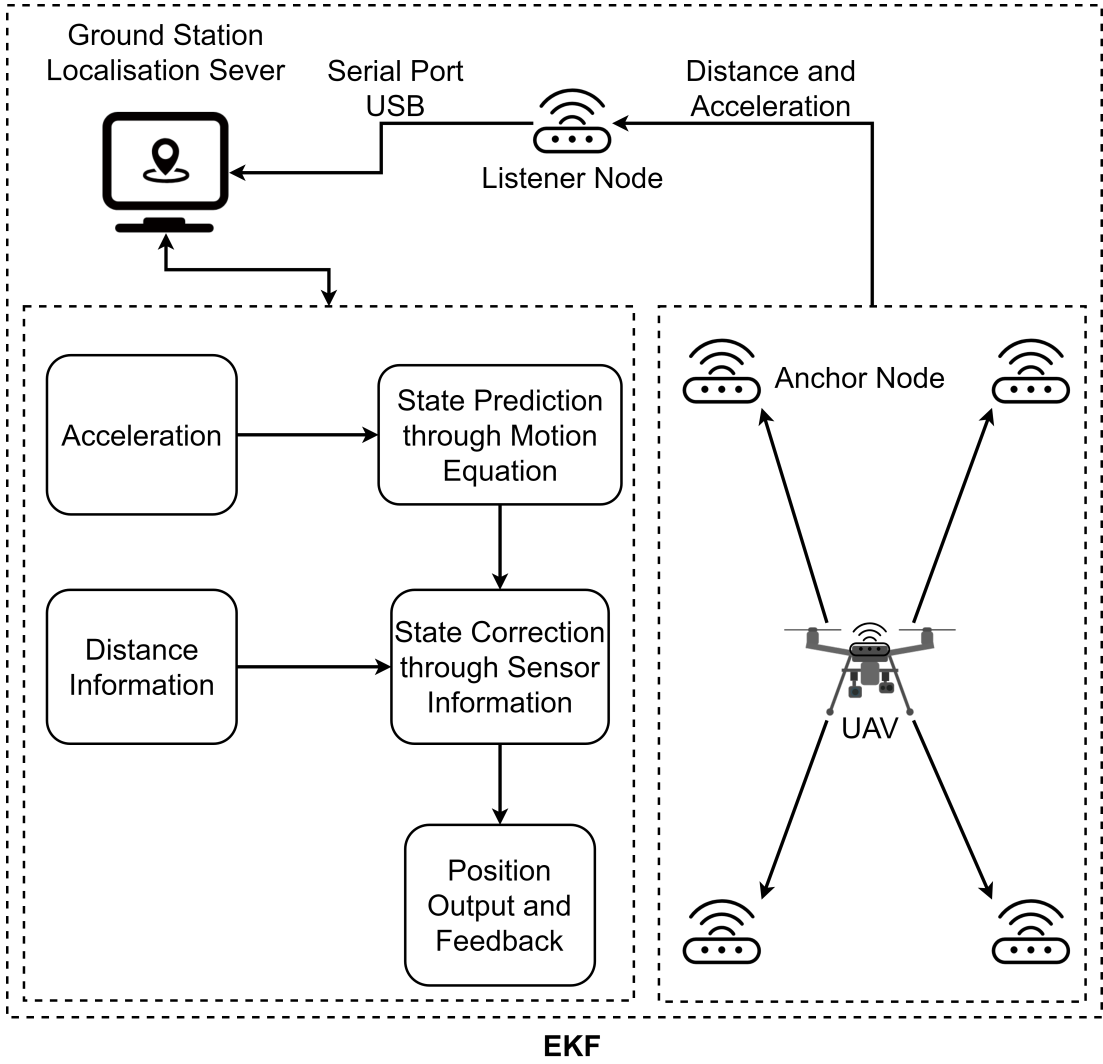


Figure 4.2: Structure for the EKF based algorithm.

within the equation, the UAV position information  $\mathbf{p} = [x, y, z]^T$  and the UAV velocity  $\mathbf{v} = [v_x, v_y, v_z]^T$  in each direction are the state information to be estimated.  $\Delta T$  denotes the time interval between two measurements of IMU and  $\mathbf{a}^N = [a_x^N, a_y^N, a_z^N]^T$  represents the measured and converted acceleration of UAV in local navigation frame all are the input variables. Considering the existing bias  $\mathbf{b}_a$  and the measurement noise  $\boldsymbol{\xi}$  for the accelerometer from IMU, the true value

for the acceleration can be represented as

$$\tilde{\mathbf{a}}^N = \mathbf{a}^N - \mathbf{b}_a - \boldsymbol{\xi}. \quad (4.10)$$

Corresponding to the literature in [158,159],  $\mathbf{b}_a$  is modelled as Gaussian random walk processes with zero mean and  $\mathbf{Q}_b$  covariance,  $\boldsymbol{\xi}$  is modelled as AWGN with zero mean and  $\mathbf{Q}_\xi$  covariance.

Then, transforming the equation into matrix form yields

$$\hat{\mathbf{u}}_{k/k-1} = \mathbf{F}_k \mathbf{u}_{k-1} + \mathbf{B}_k \mathbf{a}_{k-1}^N, \quad (4.11)$$

$$\hat{\mathbf{A}}_{k/k-1} = \mathbf{F}_k \mathbf{A}_{k-1} \mathbf{F}_k^T + \mathbf{Q}_k, \quad (4.12)$$

where,  $\mathbf{u} = [x, v_x, y, v_y, z, v_z]^T$  is the state vector,

$$\mathbf{F}_k = \mathbf{I}_3 \otimes \begin{bmatrix} 1 & \Delta T \\ 0 & 1 \end{bmatrix} \quad (4.13)$$

represents the state transition matrix,

$$\mathbf{B}_k = \mathbf{I}_3 \otimes \begin{bmatrix} \frac{\Delta T^2}{2} \\ \Delta T \end{bmatrix} \quad (4.14)$$

is the control matrix,  $\mathbf{I}_3$  denotes the  $3 \times 3$  identity matrix, “ $\otimes$ ” represents the Kronecker product,  $\mathbf{A}$  represents the covariance matrix and

$$\mathbf{Q}_k = \mathbf{B}_k \mathbf{Q}_b \mathbf{B}_k^T + \mathbf{B}_k \mathbf{Q}_\xi \mathbf{B}_k^T \quad (4.15)$$

is the process noise covariance matrix determined by the bias and measurement noise from accelerometer.

Leveraging the state prediction or motion equation, the position and velocity information of UAV can be estimated. However, considering the cumulative error from IMU, the estimated information requires to be corrected, which leads to an additional observation correction or updating process.

### 4.3.2 Observation correction

As aforementioned in Section 2.3.3 and Fig. 2.5, the distance information can be measured through the TW-TOF ranging protocol. Here, the measured distance information will be served as the observation information to further correct the estimated result to eliminate the cumulative error from IMU.

Suppose the distance measurements matrix to be  $\mathbf{Z}_k$ . Then the observation equation can be written as

$$\mathbf{Z}_k = \mathbf{H}_k \hat{\mathbf{u}}_{k/k-1} + \boldsymbol{\eta}_k, \quad (4.16)$$

where,  $\mathbf{H}_k$  denotes the observation matrix,  $\hat{\mathbf{u}}_{k/k-1}$  is the estimated information from state prediction process,  $\boldsymbol{\eta} \sim N(0, \boldsymbol{\sigma}_\eta^2)$  is the distance measurement noise from UWB sensor node, modelled as the AWGN with zero mean and  $\boldsymbol{\sigma}_\eta^2$  variance.

Considering  $\mathbf{Z}_k$  represents the distance measurements,  $\mathbf{H}_k \hat{\mathbf{u}}_{k/k-1}$  can be writ-

ten as

$$\mathbf{H}_k \hat{\mathbf{u}}_{k/k-1} = \begin{bmatrix} d_{1,k/k-1} \\ d_{2,k/k-1} \\ \vdots \\ d_{n,k/k-1} \end{bmatrix}_{n \times 1}, \quad (4.17)$$

where,  $d_{n,k/k-1}$  represents the estimated distance between UAV and anchor node  $n$  through the prediction process at round  $k$ , which can be calculated as

$$d_n = \sqrt{(x_n - \hat{x})^2 + (y_n - \hat{y})^2 + (z_n - \hat{z})^2}. \quad (4.18)$$

Due to the nonlinearity of (4.18), the first order Taylor expansion is exploited for the calculation of the observation matrix  $\mathbf{H}_k$ ,

$$\mathbf{H}_k = \begin{bmatrix} \frac{\partial d_{1,k/k-1}}{\partial \hat{x}_{k/k-1}} & 0 & \frac{\partial d_{1,k/k-1}}{\partial \hat{y}_{k/k-1}} & 0 & \frac{\partial d_{1,k/k-1}}{\partial \hat{z}_{k/k-1}} & 0 \\ \frac{\partial d_{2,k/k-1}}{\partial \hat{x}_{k/k-1}} & 0 & \frac{\partial d_{2,k/k-1}}{\partial \hat{y}_{k/k-1}} & 0 & \frac{\partial d_{2,k/k-1}}{\partial \hat{z}_{k/k-1}} & 0 \\ \vdots & \vdots & \vdots & \vdots & \vdots & \vdots \\ \frac{\partial d_{n,k/k-1}}{\partial \hat{x}_{k/k-1}} & 0 & \frac{\partial d_{n,k/k-1}}{\partial \hat{y}_{k/k-1}} & 0 & \frac{\partial d_{n,k/k-1}}{\partial \hat{z}_{k/k-1}} & 0 \end{bmatrix}_{n \times 6}. \quad (4.19)$$

In (4.19), the partial derivative of the estimated distance  $d_{n,k/k-1}$  can be represented as

$$\begin{cases} \frac{\partial d_{n,k/k-1}}{\partial \hat{x}_{k/k-1}} = \frac{\hat{x}_{k/k-1} - x_n}{\sqrt{(x_n - \hat{x}_{k/k-1})^2 + (y_n - \hat{y}_{k/k-1})^2 + (z_n - \hat{z}_{k/k-1})^2}} \\ \frac{\partial d_{n,k/k-1}}{\partial \hat{y}_{k/k-1}} = \frac{\hat{y}_{k/k-1} - y_n}{\sqrt{(x_n - \hat{x}_{k/k-1})^2 + (y_n - \hat{y}_{k/k-1})^2 + (z_n - \hat{z}_{k/k-1})^2}} \\ \frac{\partial d_{n,k/k-1}}{\partial \hat{z}_{k/k-1}} = \frac{\hat{z}_{k/k-1} - z_n}{\sqrt{(x_n - \hat{x}_{k/k-1})^2 + (y_n - \hat{y}_{k/k-1})^2 + (z_n - \hat{z}_{k/k-1})^2}} \end{cases}. \quad (4.20)$$

### 4.3.3 Position estimation

After the estimation of the observation matrix  $\mathbf{H}_k$  and the state covariance matrix  $\hat{\mathbf{A}}_{k/k-1}$ , the Kalman gain can be calculated

$$\mathbf{K}_{KF} = \hat{\mathbf{A}}_{k/k-1} \mathbf{H}_k^T (\mathbf{H}_k \hat{\mathbf{A}}_{k/k-1} \mathbf{H}_k^T + \mathbf{R}_k)^{-1}, \quad (4.21)$$

where,  $\mathbf{R}_k$  denotes the measurement noise covariance matrix which comes from the measurement noise of the UWB sensor nodes.

Then, the correction process can be proceeded with following equations to correct the estimated result and state covariance matrix from the state prediction process

$$\hat{\mathbf{u}}_k = \hat{\mathbf{u}}_{k/k-1} + \mathbf{K}_{KF} (\mathbf{Z}_k - \mathbf{H}_k \hat{\mathbf{u}}_{k/k-1}), \quad (4.22)$$

$$\hat{\mathbf{A}}_k = \hat{\mathbf{A}}_{k/k-1} - \mathbf{K}_{KF} \mathbf{H}_k \hat{\mathbf{A}}_{k/k-1}. \quad (4.23)$$

From the mathematical principle of the EKF based sensor fusion approach, with the participation of the acceleration information from IMU, it is clear that the localisation result can be smoothed to eliminate the unexpected oscillation and prevent the instability of UAV.

## 4.4 Adaptive EKF based sensor fusion

Even the unexpected performance oscillation can be eliminated by the EKF based sensor fusion approach. However, the unknown and constantly changing process noise covariance matrix  $\mathbf{Q}_k$  and measurement noise covariance matrix  $\mathbf{R}_k$  caused

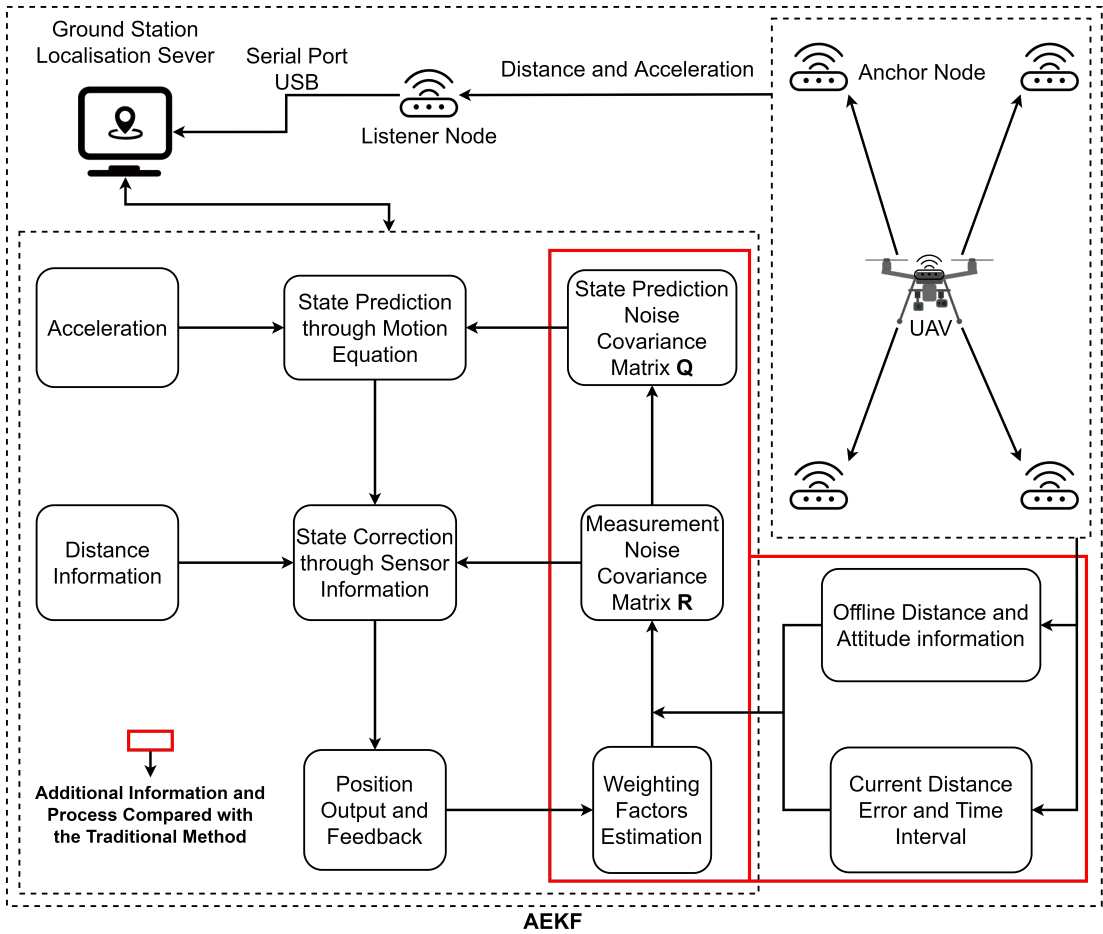


Figure 4.3: Structure for the AEKF based algorithm.

by the unpredictable propagation condition and the time varying operational environment still have huge impact on the localisation performance. Therefore, the AEKF based sensor fusion approach will be investigated to adaptively estimate these noise covariance matrices for the stable and reliable UAV positioning under different circumstances [160, 161]. In order to make it clear to understand the proposed AEKF sensor fusion algorithm before the detailed introduction, the structure of the algorithm has been provided in Fig. 4.3.

#### 4.4.1 Estimation of the noise covariance matrices

Accordingly, the difference between the distance measurements and the predicted information can be calculated through the observation measurements and the estimated information from the state prediction process

$$\mathbf{Z}'_k = \mathbf{Z}_k - \mathbf{H}_k \hat{\mathbf{u}}_{k/k-1}, \quad (4.24)$$

where,  $\mathbf{Z}'_k$  represents the difference between the observation measurements and the predicted value. Thus, the innovation covariance matrix  $\hat{\mathbf{C}}_{\mathbf{Z}'_k}$  can be derived

$$\hat{\mathbf{C}}_{\mathbf{Z}'_k} = \frac{1}{M} \sum_{i=k-M+1}^k \mathbf{Z}'_i \mathbf{Z}'_i{}^T, \quad (4.25)$$

where,  $M$  represents the window size or sampling number, which has the great impact on the estimation accuracy and stability. If a smaller  $M$  is selected, the computational complexity of the algorithm can be reduced, and the estimation process can be more adaptive to catch up the changes in the current process. However, the estimation process will become noisy and may lead to the filtering divergence. On the contrary, a larger  $M$  can improve the stability of the estimation process, which means a much smoother result. Nevertheless, the computational complexity will be increased, and the larger  $M$  may cause the adaptation ability lose of the algorithm. Considering all the existing issues, the  $M$  in the simulations and experiments is set as 10 through trial and error.

Then, the measurement noise covariance matrix  $\mathbf{R}_k$  can be obtained [160–162]

$$\mathbf{R}_k = \hat{\mathbf{C}}_{\mathbf{Z}'_k} - \mathbf{H}_k \hat{\mathbf{A}}_k \mathbf{H}_k^T. \quad (4.26)$$

On the other hand, from (4.10), (4.11) and (4.21), the state prediction noise at  $k$  round can be approximated as

$$\begin{aligned} \mathbf{B}_k \mathbf{b}_{ak} + \mathbf{B}_k \boldsymbol{\xi}_k &= \hat{\mathbf{u}}_k - \hat{\mathbf{u}}_{k/k-1} \\ &= \mathbf{K}_{KF}(\mathbf{Z}_k - \mathbf{H}_k \hat{\mathbf{u}}_{k/k-1}). \end{aligned} \quad (4.27)$$

Therefore, the process noise covariance matrix  $\mathbf{Q}_k$  can be derived as

$$\begin{aligned} \mathbf{Q}_k &= \mathbf{K}_{KF} E[\mathbf{Z}'_k \mathbf{Z}'_k{}^T] \mathbf{K}_{KF}^T \\ &= \mathbf{K}_{KF} \hat{\mathbf{C}}_{\mathbf{Z}'_k} \mathbf{K}_{KF}^T. \end{aligned} \quad (4.28)$$

With the estimated process noise covariance matrix  $\mathbf{Q}_k$  and measurement noise covariance matrix  $\mathbf{R}_k$ , the localisation performance can be further improved. However, considering the unpredictable propagation condition, operational environment and the varying time interval between two rounds acceleration measurements, the fluctuation exists for the measurements from the IMU and UWB sensor nodes. This fluctuation may lead to the inaccurate estimation of these two noise covariance matrices and will result in the localisation performance oscillation, even the filtering divergence. Therefore, the further limitation for this performance oscillation is still required.

#### 4.4.2 Estimation of weighting factors

In order to remedy the above mentioned issue, two different weighting factors  $\alpha$  and  $\beta$ , and the offline data  $\mathbf{R}_{off}$  and  $\mathbf{Q}_{off}$  will be introduced [161]. Here,  $\mathbf{R}_{off}$  and  $\mathbf{Q}_{off}$  are calculated through the captured offline data from sensor nodes

(UWB sensor nodes and IMU) with UAV statically at the original position before the flight of it.

Firstly, for the estimation of the measurement noise covariance matrix, a weighting factor  $\alpha$  is introduced to eliminate the influence of the varying measurement noise from UWB sensor nodes.

$$\mathbf{R}_{update} = (1 - \alpha)\mathbf{R}_{off} + \alpha\mathbf{R}_k. \quad (4.29)$$

As shown in the above equation, the weighting factor  $\alpha$  is added into the estimation process.  $\mathbf{R}_{update}$  is the estimated measurement noise covariance matrix limited by the additional weighting factor.  $\alpha$  is set within  $0 \leq \alpha \leq 0.5$  to prevent the filtering divergence caused by the unexpected oscillation of the current measurements. Clearly, with the increasing of  $\alpha$ , the estimation of  $\mathbf{R}_{update}$  will more rely on the current measurements, which means the oscillation of  $\mathbf{R}_{update}$ , but the system can react fast. However, the performance oscillation may occur and cause the divergence. On the contrary, the performance oscillation will be eased with a more stable estimation of  $\mathbf{R}_{update}$ , but the system will take more time to catch up the changes.

To adaptively estimate the weighting factor  $\alpha$ , the current difference between the observation measurements and the predicted value  $\mathbf{Z}'_k$ , and average difference  $Z'_{in}$  from the previous processes will be utilised. Where  $Z'_{in}$  is calculated through the recorded estimation results from the state prediction process and the correction process with UAV statically at fixed points before the flight of it.

Throughout these,  $\alpha$  can be adaptively estimated as

$$\alpha_{ad} = \frac{\frac{1}{n} \sum_{i=1}^n [\mathbf{Z}'_k]_{i1}}{\mathbf{Z}'_{in}} \alpha_{in}. \quad (4.30)$$

In which,  $n$  represents the number of anchor nodes in the system, and the initial guess  $\alpha_{in}$  is set to be 0.5. Clearly, with the augment of  $\mathbf{Z}'_k$ ,  $\alpha_{ad}$  will become larger, and the estimation of  $\mathbf{R}_{update}$  will more rely on the current measurements to catch up the changes. On the contrary, with smaller difference, the estimation of  $\mathbf{R}_{update}$  will give more credence on the previous measurements, which means a more stable value.

On the other hand, to prevent the performance oscillation and potential filtering divergence, another weighting factor  $\beta$  is introduced and adaptively estimated through the recorded average time interval  $\Delta T_{avg}$  between two rounds IMU acceleration measurements with UAV statically at fixed points, before the operation of the localisation system.

$$\mathbf{Q}_{update} = (1 - \beta)\mathbf{Q}_{off} + \beta\mathbf{Q}_k, \quad (4.31)$$

$$\beta_{ad} = \frac{\Delta T}{\Delta T_{avg}} \beta_{in}. \quad (4.32)$$

Similar to  $\alpha$ , the weighting factor  $\beta$  is also set within  $0 \leq \beta \leq 0.5$  to prevent the filtering divergence, and the initial guess  $\beta_{in}$  is given as 0.5. Throughout the estimation process, with a larger  $\Delta T$ , the estimation of  $\mathbf{Q}_{update}$  will more rely on the current measurements to catch up the changes. By contrast, the result can be smoother, but the performance degradation is inevitable. Moreover, since  $\mathbf{R}_k$  is calculated through two positive definite matrices as from (4.26), which may

lead to a negative estimation and cause the filtering divergence. Therefore, in the estimation process, if a negative estimation of  $\mathbf{R}_k$  is detected,  $\alpha$  in this round will be directly set to zero to prevent the potential filtering divergence.

Finally, with the estimated  $\mathbf{Q}_{update}$  and  $\mathbf{R}_{update}$ , the localisation result can be further updated.

## 4.5 Tightly coupled adaptive EKF based sensor fusion

With the adaptively estimated noise covariance matrices, the localisation performance for the UAV in the focused applications can be further improved. However, for UAV applications, rule out of the position information, the attitude information also has the great impact on the stable control of the UAV. For the current UWB based systems, the attitude information is measured by the equipped IMU on the UAV. Yet, the potential drift for the attitude information from the IMU caused by the magnetometer always exists which may have the impact on the localisation performance. Therefore, in this chapter, in order to overcome this issue, the TC-AEKF based sensor fusion algorithm is proposed. To comprehensively describe the operational process of the TC-AEKF based sensor fusion approach, the structure for the algorithm is depicted in Fig. 4.4.

### 4.5.1 State prediction

Similar to the description of the EKF based approach in Section 4.3.1, the motion equation of the UAV can be derived through the existing kinematic model in [157]. But differently, the angular rate is considered for the prediction of the at-

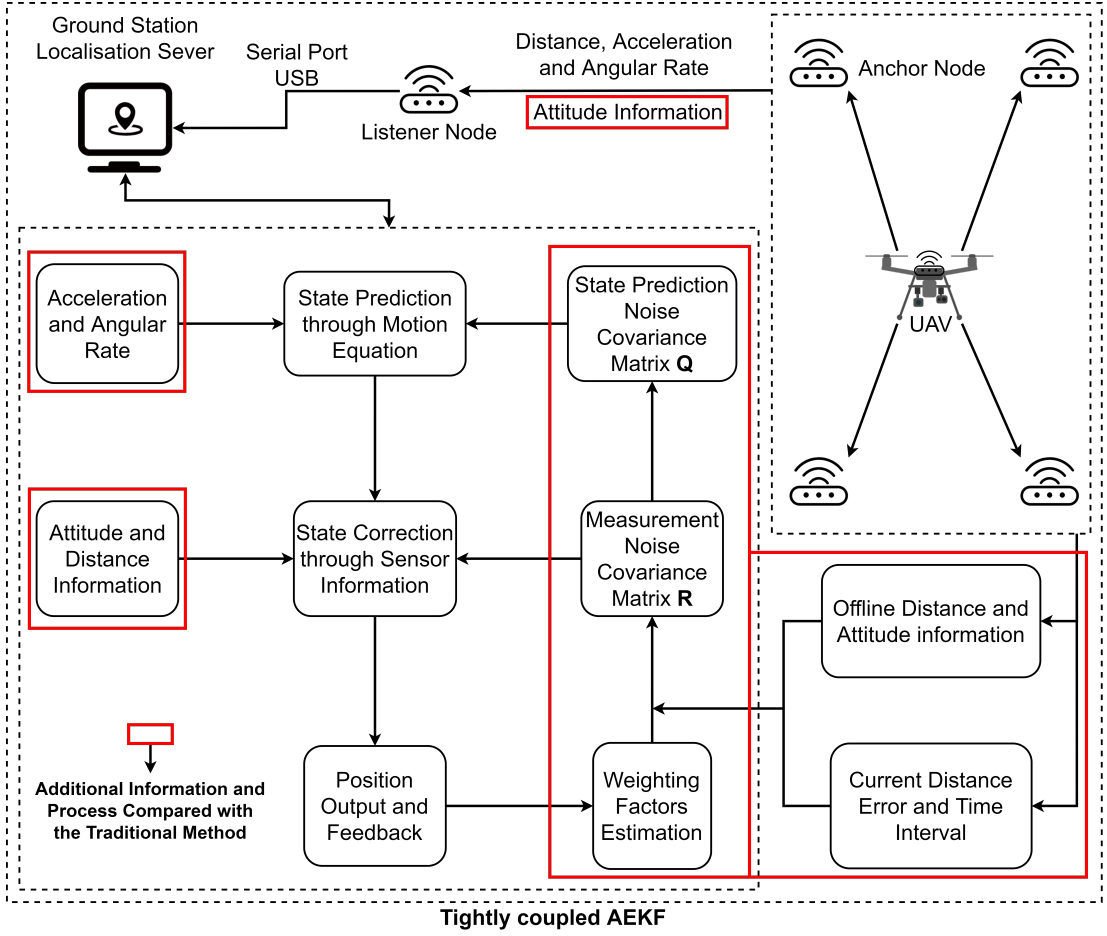


Figure 4.4: Structure for the TC-AEKF based algorithm.

Attitude information in the state prediction model of the TC-AEKF in this section.

Accordingly, it can be derived as

$$\begin{cases} \hat{\boldsymbol{\gamma}}_{k/k-1} = \boldsymbol{\gamma}_{k-1} + \Delta T \boldsymbol{\omega}_{k-1} \\ \hat{\boldsymbol{p}}_{k/k-1} = \boldsymbol{p}_{k-1} + \Delta T \boldsymbol{v}_{k-1} + \frac{\Delta T^2}{2} \boldsymbol{a}_{k-1}^N \\ \hat{\boldsymbol{v}}_{k/k-1} = \boldsymbol{v}_{k-1} + \Delta T \boldsymbol{a}_{k-1}^N \\ \boldsymbol{a}_{k-1}^N = \boldsymbol{C}_{k-1}^{YN} \boldsymbol{C}_{k-1}^{PY} \boldsymbol{C}_{k-1}^{IP} \boldsymbol{a}_{k-1}^{IMU} \end{cases}, \quad (4.33)$$

where,  $\boldsymbol{\gamma} = [\phi, \theta, \psi]^T$  is the attitude of UAV,  $\boldsymbol{\omega} = [\omega_\phi, \omega_\theta, \omega_\psi]^T$  is the angular rate,  $\boldsymbol{p} = [x, y, z]^T$  represents the UAV position information,  $\boldsymbol{v} = [v_x, v_y, v_z]^T$  is the velocity at X, Y and Z direction,  $\boldsymbol{a}^N = [a_x^N, a_y^N, a_z^N]^T$  is the acceleration at X, Y and Z direction in local localisation frame,  $\Delta T$  denotes the time interval between two round measurements. It is noted here that the acceleration and angular rate between two rounds are assumed as constant. Then, transforming the equation into matrix form yields

$$\begin{bmatrix} \hat{\boldsymbol{\rho}}_{k/k-1} \\ \hat{\boldsymbol{u}}_{k/k-1} \end{bmatrix} = \begin{bmatrix} \mathbf{F}_k^\rho & \mathbf{0} \\ \mathbf{0} & \mathbf{F}_k^u \end{bmatrix} \begin{bmatrix} \boldsymbol{\rho}_{k-1} \\ \boldsymbol{u}_{k-1} \end{bmatrix} + \begin{bmatrix} \mathbf{0} & \mathbf{0} \\ \mathbf{0} & \mathbf{B}_k^u \end{bmatrix} \begin{bmatrix} \mathbf{0} \\ \boldsymbol{a}_{k-1}^N \end{bmatrix}, \quad (4.34)$$

in which,  $\boldsymbol{\rho} = [\phi, \omega_\phi, \theta, \omega_\theta, \psi, \omega_\psi]^T$  represents the UAV attitude and angular rate information,  $\boldsymbol{u} = [x, v_x, y, v_y, z, v_z]^T$  consists of the position and velocity information in this round, the state transition matrix is composed of  $\mathbf{F}_k^\rho$  and  $\mathbf{F}_k^u$ ,

$$\mathbf{F}_k^\rho = \mathbf{F}_k^u = \mathbf{I}_3 \otimes \begin{bmatrix} 1 & \Delta T \\ 0 & 1 \end{bmatrix}, \quad (4.35)$$

the control matrix is constituted by  $\mathbf{B}_k^u$ ,

$$\mathbf{B}_k^u = \mathbf{I}_3 \otimes \begin{bmatrix} \frac{\Delta T^2}{2} \\ \Delta T \end{bmatrix}, \quad (4.36)$$

where,  $\mathbf{I}$  represents the identity matrix, “ $\otimes$ ” is the Kronecker product.

Same as the EKF based approach, the measurement noise and gyro bias for the measured information including the angular rate and acceleration should be

considered and represented as follows,

$$\boldsymbol{\omega} = \tilde{\boldsymbol{\omega}} + \mathbf{b}^\omega + \mathbf{e}, \quad (4.37)$$

$$\mathbf{a}^N = \tilde{\mathbf{a}}^N + \mathbf{b}^a + \boldsymbol{\xi}. \quad (4.38)$$

Where, all the measurement noise and the gyro bias are modelled as the AWGN with zero mean and variance,  $\mathbf{b}^\omega \sim N(\mathbf{0}, \sigma_{b^\omega}^2)$ ,  $\mathbf{b}^a \sim N(\mathbf{0}, \sigma_{b^a}^2)$ ,  $\mathbf{e} \sim N(\mathbf{0}, \sigma_e^2)$  and  $\boldsymbol{\xi} \sim N(\mathbf{0}, \sigma_\xi^2)$ .  $\tilde{\boldsymbol{\omega}}$  and  $\tilde{\mathbf{a}}^N$  are assumed as the true value of the angular rate and acceleration.  $\boldsymbol{\omega}$  and  $\mathbf{a}^N$  are supposed to be the measured value of them. Then, from (4.34), (4.37) and (4.38), the state covariance matrix can be derived

$$\begin{aligned} \hat{\mathbf{A}}_{k/k-1} = & \begin{bmatrix} \mathbf{F}_k^\rho & \mathbf{0} \\ \mathbf{0} & \mathbf{F}_k^u \end{bmatrix} \begin{bmatrix} \boldsymbol{\rho}_{k-1} \\ \mathbf{u}_{k-1} \end{bmatrix} \begin{bmatrix} \boldsymbol{\rho}_{k-1} \\ \mathbf{u}_{k-1} \end{bmatrix}^T \begin{bmatrix} \mathbf{F}_k^\rho & \mathbf{0} \\ \mathbf{0} & \mathbf{F}_k^u \end{bmatrix}^T \\ & + \begin{bmatrix} \mathbf{Q}_k^\rho + \mathbf{Q}_k^{b^\omega} & \mathbf{0} \\ \mathbf{0} & \mathbf{Q}_k^u + \mathbf{Q}_k^{b^a} \end{bmatrix}, \end{aligned} \quad (4.39)$$

where, the state process noise covariance matrix  $\mathbf{Q}$  is constituted by the noise and bias from IMU measurements,  $\mathbf{Q}_k^\rho = \mathbf{F}_k^\rho \mathbf{e}_k \mathbf{e}_k^T \mathbf{F}_k^{\rho T}$ ,  $\mathbf{Q}_k^{b^\omega} = \mathbf{F}_k^\rho \mathbf{b}_k^\omega \mathbf{b}_k^{\omega T} \mathbf{F}_k^{\rho T}$ ,  $\mathbf{Q}_k^u = \mathbf{B}_k^u \boldsymbol{\xi}_k \boldsymbol{\xi}_k^T \mathbf{B}_k^{u T}$  and  $\mathbf{Q}_k^{b^a} = \mathbf{B}_k^u \mathbf{b}_k^a \mathbf{b}_k^{a T} \mathbf{B}_k^{u T}$ .

Then, the position and attitude information of UAV can be predicted. However, the cumulative error from the IMU still requires to be taken into account, considering the increasing performance influence as time goes on. Therefore, an additional observation correction process is still needed to prevent this performance degradation.

### 4.5.2 Observation correction

In the observation correction process, with the measured precise distance information between the tag node attached on the UAV and fixed anchor nodes, and the attitude information provided by the IMU module equipped on the UAV, the predicted state information from the state prediction process can be corrected and updated to get rid of the cumulative error.

Assuming the attitude measurement matrix and the distance measurement matrix at  $k$  round to be  $\mathbf{Z}_k^\rho$  and  $\mathbf{Z}_k^u$ , the observation equation can be derived as

$$\begin{bmatrix} \mathbf{Z}_k^\rho \\ \mathbf{Z}_k^u \end{bmatrix} = \begin{bmatrix} \mathbf{H}_k^\rho & \mathbf{0} \\ \mathbf{0} & \mathbf{H}_k^u \end{bmatrix} \begin{bmatrix} \hat{\boldsymbol{\rho}}_{k/k-1} \\ \hat{\mathbf{u}}_{k/k-1} \end{bmatrix} + \begin{bmatrix} \boldsymbol{\epsilon}_k \\ \boldsymbol{\eta}_k \end{bmatrix}, \quad (4.40)$$

in which, the observation matrix is composed of  $\mathbf{H}_k^\rho$  and  $\mathbf{H}_k^u$ ,  $\boldsymbol{\epsilon} \sim N(\mathbf{0}, \boldsymbol{\sigma}_\epsilon^2)$  and  $\boldsymbol{\eta} \sim N(\mathbf{0}, \boldsymbol{\sigma}_\eta^2)$  are denoted as the attitude measurement noise and distance measurement noise which are all modelled as the AWGN. Owing to the observation information  $\mathbf{Z}_k^\rho$  measured from the IMU is the attitude, thus,  $\mathbf{H}_k^\rho$  can be represented as

$$\mathbf{H}_k^\rho = \mathbf{I}_3 \otimes \begin{bmatrix} 1 & 0 \end{bmatrix}. \quad (4.41)$$

Differently,  $\mathbf{Z}_k^u$  measured by the UWB sensor nodes is the distance information, therefore, a conversion is required. Since the distance information cannot be linearly represented by the position information, the first order Taylor expansion

is utilised,

$$\mathbf{H}_k^u = \begin{bmatrix} \frac{\partial d_{1,k/k-1}}{\partial \hat{x}_{k/k-1}} & 0 & \frac{\partial d_{1,k/k-1}}{\partial \hat{y}_{k/k-1}} & 0 & \frac{\partial d_{1,k/k-1}}{\partial \hat{z}_{k/k-1}} & 0 \\ \frac{\partial d_{2,k/k-1}}{\partial \hat{x}_{k/k-1}} & 0 & \frac{\partial d_{2,k/k-1}}{\partial \hat{y}_{k/k-1}} & 0 & \frac{\partial d_{2,k/k-1}}{\partial \hat{z}_{k/k-1}} & 0 \\ \vdots & \vdots & \vdots & \vdots & \vdots & \vdots \\ \frac{\partial d_{n,k/k-1}}{\partial \hat{x}_{k/k-1}} & 0 & \frac{\partial d_{n,k/k-1}}{\partial \hat{y}_{k/k-1}} & 0 & \frac{\partial d_{n,k/k-1}}{\partial \hat{z}_{k/k-1}} & 0 \end{bmatrix}, \quad (4.42)$$

where,  $n$  is supposed to be the number of fixed anchor nodes.

The Kalman gain can be obtained throughout the aforementioned processes and represented by

$$\begin{aligned} \mathbf{K}_{KF} = & \hat{\mathbf{A}}_{k/k-1} \begin{bmatrix} \mathbf{H}_k^\rho & \mathbf{0} \\ \mathbf{0} & \mathbf{H}_k^u \end{bmatrix}^T \\ & \cdot \left( \begin{bmatrix} \mathbf{H}_k^\rho & \mathbf{0} \\ \mathbf{0} & \mathbf{H}_k^u \end{bmatrix} \hat{\mathbf{A}}_{k/k-1} \begin{bmatrix} \mathbf{H}_k^\rho & \mathbf{0} \\ \mathbf{0} & \mathbf{H}_k^u \end{bmatrix}^T + \begin{bmatrix} \mathbf{R}_k^\rho & \mathbf{0} \\ \mathbf{0} & \mathbf{R}_k^u \end{bmatrix} \right)^{-1}, \end{aligned} \quad (4.43)$$

where, the combination of  $\mathbf{R}_k^\rho$  and  $\mathbf{R}_k^u$  is supposed to be the measurement noise covariance matrix  $\mathbf{R}$ .

Finally, the position and attitude information from the prediction process can be corrected, i.e.

$$\begin{bmatrix} \hat{\boldsymbol{\rho}}_k \\ \hat{\mathbf{u}}_k \end{bmatrix} = \begin{bmatrix} \hat{\boldsymbol{\rho}}_{k/k-1} \\ \hat{\mathbf{u}}_{k/k-1} \end{bmatrix} + \mathbf{K}_{KF} \left( \begin{bmatrix} \mathbf{Z}_k^\rho \\ \mathbf{Z}_k^u \end{bmatrix} - \begin{bmatrix} \mathbf{H}_k^\rho & \mathbf{0} \\ \mathbf{0} & \mathbf{H}_k^u \end{bmatrix} \begin{bmatrix} \hat{\boldsymbol{\rho}}_{k/k-1} \\ \hat{\mathbf{u}}_{k/k-1} \end{bmatrix} \right), \quad (4.44)$$

$$\hat{\mathbf{A}}_k = \hat{\mathbf{A}}_{k/k-1} - \mathbf{K}_{KF} \begin{bmatrix} \mathbf{H}_k^\rho & \mathbf{0} \\ \mathbf{0} & \mathbf{H}_k^u \end{bmatrix} \hat{\mathbf{A}}_{k/k-1}. \quad (4.45)$$

### 4.5.3 Estimation of the noise covariance matrices

Even the precise attitude and position information of the UAV can be attained, nevertheless, how to adjust or decide the  $\mathbf{Q}$  and  $\mathbf{R}$  matrices still have huge impact on the localisation performance. Thus, the TC-AEKF based approach is investigated in this section to adaptively estimate these matrices for performance improvement [160–162].

It can be observed that, through (4.40), the measurement noises can be approximated by the measured and the predicted information in this round,

$$\begin{bmatrix} \mathbf{Z}_k^{\rho'} \\ \mathbf{Z}_k^{u'} \end{bmatrix} = \begin{bmatrix} \mathbf{Z}_k^{\rho} \\ \mathbf{Z}_k^u \end{bmatrix} - \begin{bmatrix} \mathbf{H}_k^{\rho} & \mathbf{0} \\ \mathbf{0} & \mathbf{H}_k^u \end{bmatrix} \begin{bmatrix} \hat{\boldsymbol{\rho}}_{k/k-1} \\ \hat{\mathbf{u}}_{k/k-1} \end{bmatrix}. \quad (4.46)$$

Therefore, the innovation covariance matrix  $\hat{\mathbf{C}}_{\mathbf{Z}_k^{\rho'} \mathbf{Z}_k^{u'}}$  can be derived as

$$\hat{\mathbf{C}}_{\mathbf{Z}_k^{\rho'} \mathbf{Z}_k^{u'}} = \frac{1}{M} \sum_{i=k-M+1}^k \begin{bmatrix} \mathbf{Z}_i^{\rho'} \\ \mathbf{Z}_i^{u'} \end{bmatrix} \begin{bmatrix} \mathbf{Z}_i^{\rho'} \\ \mathbf{Z}_i^{u'} \end{bmatrix}^T, \quad (4.47)$$

where,  $M$  is the sampling number or window size. Then, the estimation of  $\mathbf{R}$  matrix can be obtained through (4.46) and (4.47)

$$\begin{bmatrix} \mathbf{R}_k^{\rho} & \mathbf{0} \\ \mathbf{0} & \mathbf{R}_k^u \end{bmatrix} = \hat{\mathbf{C}}_{\mathbf{Z}_k^{\rho'} \mathbf{Z}_k^{u'}} - \begin{bmatrix} \mathbf{H}_k^{\rho} & \mathbf{0} \\ \mathbf{0} & \mathbf{H}_k^u \end{bmatrix} \hat{\mathbf{A}}_k \begin{bmatrix} \mathbf{H}_k^{\rho} & \mathbf{0} \\ \mathbf{0} & \mathbf{H}_k^u \end{bmatrix}^T. \quad (4.48)$$

Similarly, the  $\mathbf{Q}$  matrix can also be approximated as

$$\begin{bmatrix} \mathbf{F}_k^\rho \mathbf{e}_k + \mathbf{F}_k^\rho \mathbf{b}_k^\omega \\ \mathbf{B}_k^u \boldsymbol{\xi}_k + \mathbf{B}_k^u \mathbf{b}_k^a \end{bmatrix} = \mathbf{K}_{KF} \cdot \left( \begin{bmatrix} \mathbf{Z}_k^\rho \\ \mathbf{Z}_k^u \end{bmatrix} - \begin{bmatrix} \mathbf{H}_k^\rho & \mathbf{0} \\ \mathbf{0} & \mathbf{H}_k^u \end{bmatrix} \begin{bmatrix} \hat{\boldsymbol{\rho}}_{k/k-1} \\ \hat{\mathbf{u}}_{k/k-1} \end{bmatrix} \right), \quad (4.49)$$

$$\begin{bmatrix} \mathbf{Q}_k^\rho + \mathbf{Q}_k^{b^\omega} & \mathbf{0} \\ \mathbf{0} & \mathbf{Q}_k^u + \mathbf{Q}_k^{b^a} \end{bmatrix} = \mathbf{K}_{KF} \hat{\mathbf{C}} \mathbf{Z}_k^{\rho'} \mathbf{Z}_k^{u'} \mathbf{K}_{KF}^T. \quad (4.50)$$

However, the estimation of the  $\mathbf{R}$  and  $\mathbf{Q}$  matrix still rely on the measured information which may result in the performance oscillation or filtering divergence due to the unpredictable propagation condition between the UWB sensor nodes and the changing operational environment. Thus, to remedy the existing issue, additional weighting factors are added in the approximation process to limit the estimation of these two noise covariance matrices.

#### 4.5.4 Estimation of weighting factors

Inspired by the estimation approach in [161] and in order to eliminate the performance degradation and prevent the potential filtering divergence. Four weighting factors  $\alpha$ ,  $\alpha'$ ,  $\beta$  and  $\beta'$ , plus with the offline data for these two noise covariance matrices  $\mathbf{R}_{off}$  and  $\mathbf{Q}_{off}$  estimated before the flight of UAV are introduced in the approximation process.

Firstly, for the estimation of the measurement noise covariance matrix, with the additional weighting factors  $\alpha$  and  $\alpha'$ , the offline data  $\mathbf{R}_{off}$  and the approxi-

mation equation from (4.48), it can be derived that

$$\begin{aligned} \mathbf{R}_{update} = & \begin{bmatrix} (1 - \alpha')\mathbf{R}_{off}^\rho & \mathbf{0} \\ \mathbf{0} & (1 - \alpha)\mathbf{R}_{off}^u \end{bmatrix} + \begin{bmatrix} \alpha' \\ \alpha \end{bmatrix} \\ & \cdot \left( \hat{\mathbf{C}}_{\mathbf{z}_k^{\rho'} \mathbf{z}_k^{u'}} - \begin{bmatrix} \mathbf{H}_k^\rho & \mathbf{0} \\ \mathbf{0} & \mathbf{H}_k^u \end{bmatrix} \hat{\mathbf{A}}_k \begin{bmatrix} \mathbf{H}_k^\rho & \mathbf{0} \\ \mathbf{0} & \mathbf{H}_k^u \end{bmatrix}^T \right). \end{aligned} \quad (4.51)$$

Apparently from (4.51), with the increasing of  $\alpha$  and  $\alpha'$ , more trust is given to the current measurements to catch up the changes caused by the changing environment or propagation condition. However, this may lead to the oscillation for the estimation of the  $\mathbf{R}$  matrix, which means the filtering divergence is more likely to happen. In contrast, the estimation of the  $\mathbf{R}$  matrix is relatively stable, but the system needs more time to catch up the changes, which means a long time performance degradation.

Same as the estimation of the  $\mathbf{R}$  matrix, the other two weighting factors  $\beta$  and  $\beta'$  are added in the estimation of the  $\mathbf{Q}$  matrix to avoid the performance degradation and filtering divergence. The estimation equation is written as

$$\mathbf{Q}_{update} = \begin{bmatrix} (1 - \beta')\mathbf{Q}_{off}^\rho & \mathbf{0} \\ \mathbf{0} & (1 - \beta)\mathbf{Q}_{off}^u \end{bmatrix} + \begin{bmatrix} \beta' \\ \beta \end{bmatrix} \mathbf{K}_{KF} \hat{\mathbf{C}}_{\mathbf{z}_k^{\rho'} \mathbf{z}_k^{u'}} \mathbf{K}_{KF}^T. \quad (4.52)$$

Similarly, with the augmentation of  $\beta$  and  $\beta'$ , the estimation of the  $\mathbf{Q}$  matrix more relies on the current measurements (acceleration and angular rate) to catch up the changes. Otherwise, greater proportion is given to the offline data to keep the estimation process relatively stable, but more time is required to catch up the changes.

Even with the additional weighting factors the estimation performance can be improved, nevertheless, the value of these weighting factors still have huge impact on the localisation performance. To overcome this, an adaptive estimation process is proposed for the estimation of these weighting factors.

Considering  $\alpha$  and  $\alpha'$  are added to limit the estimation of the measurement noise covariance matrix, thus,  $\alpha$  and  $\alpha'$  can be estimated through the difference between the current observation information and the predicted information from state prediction process

$$\begin{bmatrix} \alpha'_{ad} \\ \alpha_{ad} \end{bmatrix} = \begin{bmatrix} \frac{\frac{1}{3} \sum_{i=1}^3 [Z_k^{p'}]_{i1}}{Z_{in}^{p'}} \\ \frac{\frac{1}{n} \sum_{i=1}^n [Z_k^{u'}]_{i1}}{Z_{in}^{u'}} \end{bmatrix} \begin{bmatrix} \alpha'_{in} \\ \alpha_{in} \end{bmatrix}, \quad (4.53)$$

where,  $\alpha_{ad}$  and  $\alpha'_{ad}$  are the adaptively estimated weighting factors,  $\alpha_{in}$  and  $\alpha'_{in}$  are the initial value for each,  $Z_{in}^{p'}$  and  $Z_{in}^{u'}$  represent the initial value for the current difference which are measured through a set of observation and prediction information before the flight of UAV and  $n$  is the number of fixed anchor nodes in the system. Clearly, when the difference between the current observation information and the predicted value becomes larger,  $\alpha_{ad}$  and  $\alpha'_{ad}$  will also become larger to overtake the current changes. On the contrary,  $\alpha_{ad}$  and  $\alpha'_{ad}$  will be smaller to give more trust to the offline data to maintain a steady state. Here it needs to note that, in order to avoid the filtering divergence,  $\alpha$  is set within  $0 \leq \alpha \leq 0.5$ ,  $\alpha_{in}$  is supposed as 0.5, and  $\alpha'$  is set within  $0 \leq \alpha' \leq 0.1$ ,  $\alpha'_{in}$  is set to be 0.1. Considering the potential abrupt change for the observed attitude information from IMU in confined environments, a smaller value for the  $\alpha'$  is selected to prevent the sudden change for the estimated measurement noise covariance. Furthermore, since the estimation of the measurement noise covariance is from two positive definite ma-

trices, thus, a negative value is potentially be obtained. To prevent the filtering divergence caused by the negative value, if a negative value for the estimation is detected, the two weighting factors will be directly set to zero.

Based on the same principle,  $\beta$  and  $\beta'$  can also be estimated through the data from the previous process. But differently, as the time interval  $\Delta T$  has more impact on the prediction process, with a larger time interval between two rounds acceleration and angular rate, the noises from these information will have more influence on the prediction performance. Therefore, the estimation of  $\beta$  and  $\beta'$  will more rely on the time interval between two round estimations. Throughout the  $\mathbf{Q}_{off}$  offline data and the average time interval  $\Delta T_{avg}$  measured before the flight of UAV, the estimation equation can be derived

$$\begin{bmatrix} \beta'_{ad} \\ \beta_{ad} \end{bmatrix} = \frac{\Delta T}{\Delta T_{avg}} \begin{bmatrix} \beta'_{in} \\ \beta_{in} \end{bmatrix}, \quad (4.54)$$

in which,  $\beta_{ad}$  and  $\beta'_{ad}$  are the adaptively estimated results,  $\beta_{in}$  and  $\beta'_{in}$  denote the initial value for each. To prevent the filtering divergence, the same limitation has been made for  $\beta$  and  $\beta'$ .  $\beta$  is set within  $0 \leq \beta \leq 0.5$ ,  $\beta_{in}$  is supposed as 0.5,  $\beta'$  is set within  $0 \leq \beta' \leq 0.1$  and  $\beta'_{in}$  is set to be 0.1.

Finally, throughout the further limited estimation, the localisation performance can be further improved.

## 4.6 Performance evaluation in the simulation environment

### 4.6.1 Simulation configuration

Considering the safety reason for flying UAV in the extremely confined environment and to evaluate the performance of the proposed algorithms before the actual experiments, the simulations in Gazebo environment have been setup and carried out. In the simulation, the UAV is placed in a confined space ( $1.95\text{m} \times 3.0\text{m} \times 2.3\text{m}$ ) with four anchor nodes mounted on X-Z plane. This is to simulate the actual applications that all anchor nodes can only be deployed near the entrance of such space, due to the inaccessible and extremely confined features for the focused environments. The coordinates of each anchor node and the simulation environment are depicted in Fig. 4.5. In the simulation, the ground truth for the position information of the UAV is directly obtained from the simulation environment.

### 4.6.2 Simulation for the AEKF based sensor fusion approach

In order to evaluate the performance and prove the effectiveness of the proposed AEKF based sensor fusion approach compared with the MLE based localisation algorithm in Section 3.2 which known as the pure UWB based approach without the sensor fusion and the EKF based sensor fusion algorithm, the simulation in this section has been carried out. In this simulation, the flight path for the UAV is set as a reversed “S”. For each simulation and algorithm, the position information of over 5000 points has been estimated which makes it can represent the actual performance of these algorithms and prove the effectiveness of

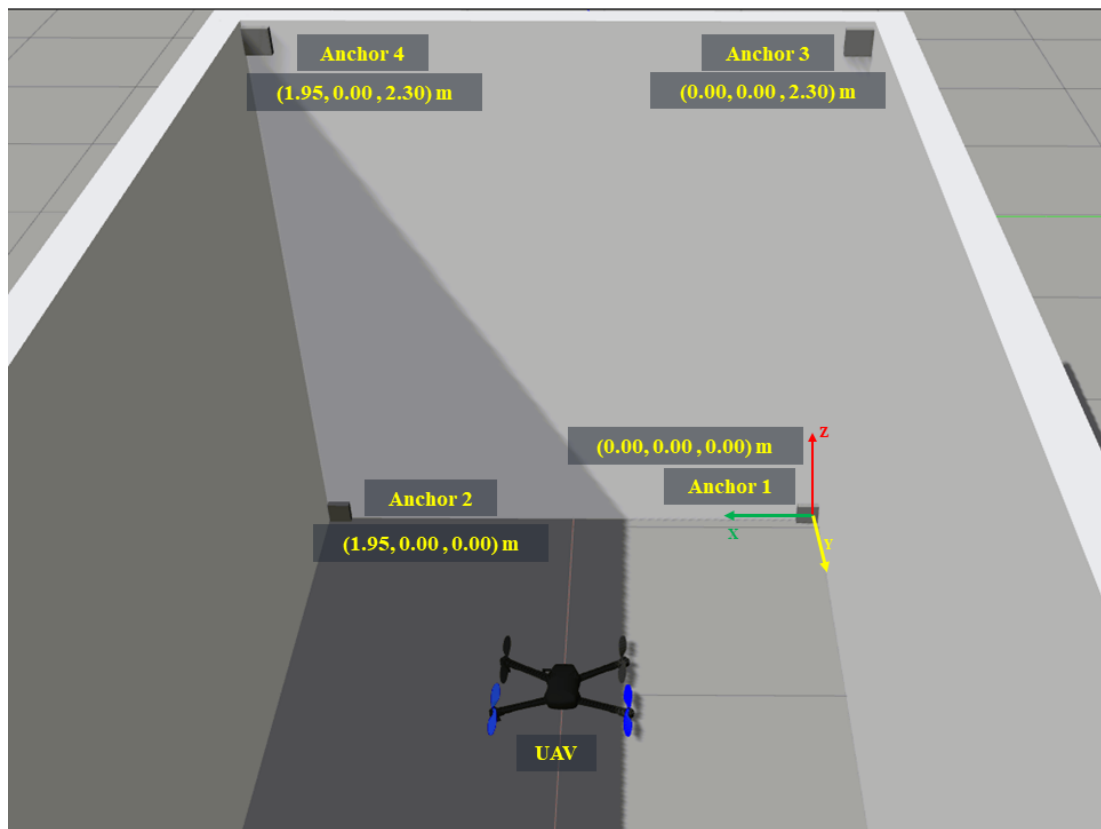


Figure 4.5: Simulation environment.

the proposed algorithm. Two simulations under different measurement noise of the acceleration and distance information have been carried out which is to exhaustively validate the effectiveness of the AEKF based approach. In the first simulation, the STD for the measurement noise of the simulated acceleration and distance information are assumed as constant and set to be  $0.5\text{m/s}^2$  and  $0.1\text{m}$ . In the second simulation, the STD for these two measurement noises is randomly set within  $[0,0.5]\text{m/s}^2$  and  $[0,0.2]\text{m}$  to simulate the variation of the operational environment. This is to validate the adaptive ability for the AEKF based approach under different circumstances. In these two simulations, the comparison for the algorithms including the MLE based localisation algorithm, the EKF based sensor fusion algorithm, the EKF based approach with the distance filter

Table 4.1: Detailed localisation results for the AEKF based sensor fusion approach with constant noise model in simulation 1

Algorithm	Median Error	Improved	95 <sup>th</sup> Error	Improved	Average STD	Improved
MLE	0.148m	N/A	0.271m	N/A	0.067m	N/A
EKF	0.087m	41.2%	0.235m	13.3%	0.069m	-3.0%
[63]	0.085m	42.6%	0.202m	25.5%	0.058m	13.4%
[66]	0.057m	61.4%	0.157m	42.1%	0.042m	37.3%
[159]	0.070m	52.7%	0.145m	46.5%	0.036m	46.3%
AEKF	<b>0.041m</b>	<b>72.3%</b>	0.133m	50.9%	0.035m	47.8%
( $\alpha = \beta =$ 0.3)						
AEKF	0.048m	67.6%	0.149m	45.0%	0.042m	37.3%
( $\alpha = \beta =$ 0.5)						
AEKF	0.042m	71.6%	<b>0.117m</b>	<b>56.8%</b>	<b>0.031m</b>	<b>53.7%</b>
(adaptive $\alpha, \beta$ )						

proposed by Guo et al. [63], the sensor fusion based approach presented in [66], the UWB and IMU based localisation approach designed by Li et al. [159], the AEKF based algorithm with different and constant weighting factors and the AEKF based algorithm with adaptive weighting factors has been done. Here it needs to mention that, considering it is difficult to evaluate the performance of the algorithms with the developed UAV system with the open source data set, the algorithms in [63], [66] and [159] were implemented by the author on the developed UAV platform according to their algorithm principle. The flight trajectories, flight trajectories in three directions, RMSE in the three directions, the eCDF and the detailed localisation error information for these two simulations have been provided in Fig. 4.6, Fig. 4.7, Table 4.1 and Table 4.2.

Firstly, for the localisation results of the simulation 1, when being focused on the positioning trajectory results in the first four figures in Fig. 4.6(a-d), it can be

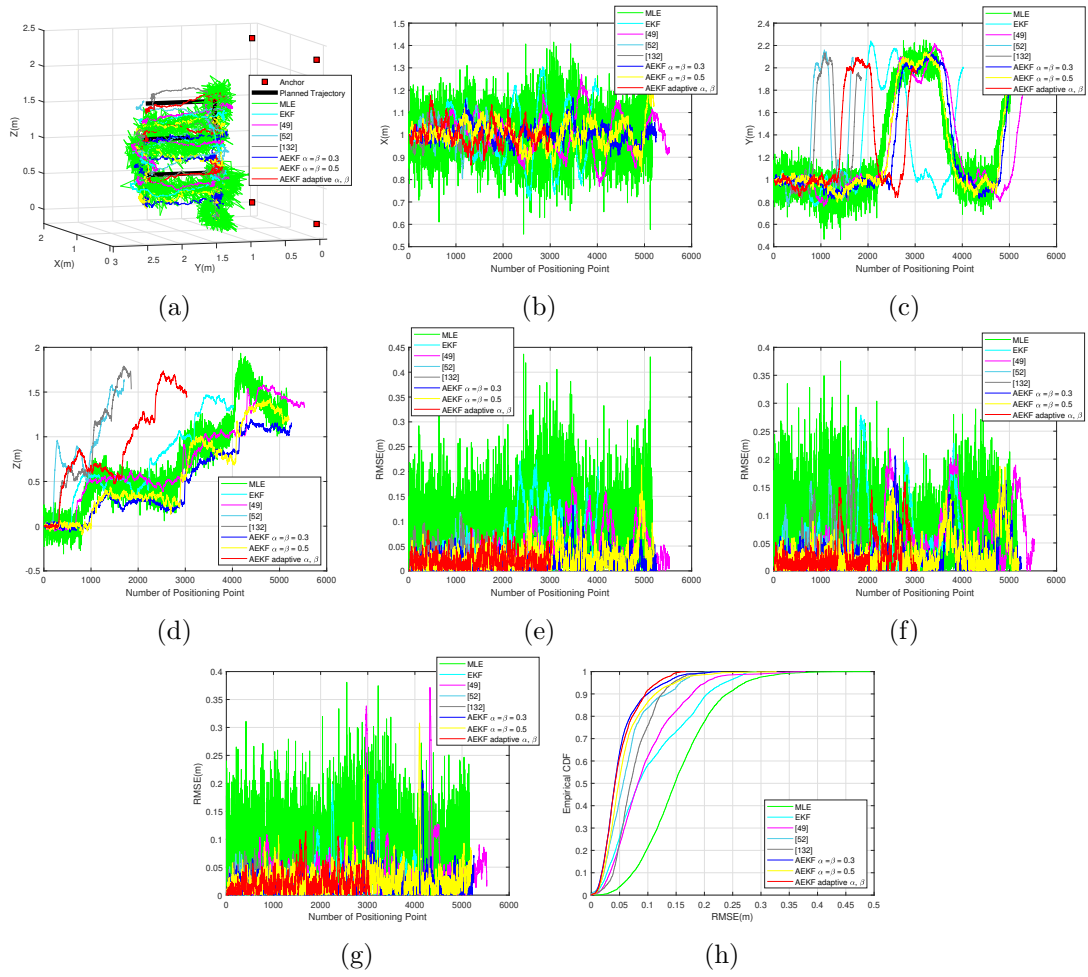


Figure 4.6: Simulation 1 flight results for the AEKF with constant noise model. (a) 3D trajectories. (b) X direction trajectories. (c) Y direction trajectories. (d) Z direction trajectories. (e) X direction RMSE (m). (f) Y direction RMSE (m). (g) Z direction RMSE (m). (h) eCDF.

observed that, the MLE based localisation algorithm holds the biggest oscillation in every direction due to the unreasonable value from the UWB sensor nodes. The unreasonable value within the UWB sensor nodes is led by the measurement noise and the unpredictable propagation condition. However, for all other sensor fusion based approaches, the trajectory results are significantly smoothed and improved. Meanwhile, in order to quantitatively assess the localisation performance of each algorithm, the RMSE for these algorithms in each direction plus with the eCDF

and the detailed localisation error of each are illustrated in Fig. 4.6(e-h) and Table 4.1. Specifically, from the RMSE simulation results, the same conclusion can be made. With the utilisation of the sensor fusion based approaches, the absolute accuracy and precision of the system are all improved significantly. For the approaches with the distance calibration and outlier detection methods in [63] and [159], when with the constant measurement noise STD, the performance is greatly improved with the average STD to be 0.058m and 0.036m. On the other hand, for the AEKF approaches, compared with the EKF sensor fusion algorithm and the three algorithms in [63], [66] and [159], with the estimated noise covariance matrices, the localisation performance is greatly improved with the median error, 95<sup>th</sup> percentile error and average STD around 0.044m, 0.133m and 0.036m, respectively. When doing the comparison within the AEKF approaches, it can be observed that, the larger weighting factors lead to the larger performance oscillation. This is caused by the constant noise model in the first simulation. As aforementioned in Section 4.4.2 with a larger  $\alpha$  and  $\beta$ , the estimation of  $\mathbf{R}_{update}$  and  $\mathbf{Q}_{update}$  will more rely on the current measurements, which means more changes on the estimation value of  $\mathbf{R}_{update}$  and  $\mathbf{Q}_{update}$ . Therefore, with the relatively stable measurement noise model, larger weighting factors will lead to the performance oscillation, which means the drop-off for the precision of the algorithm. Finally, when being focused on the proposed AEKF algorithm, obviously, with the estimated weighting factors, the proposed AEKF algorithm holds the high performance with 0.042m median error, 0.117m 95<sup>th</sup> percentile error and 0.031m average STD of the localisation error. Compared with the MLE based localisation algorithm, the performance is improved by 71.6%, 56.8% and 53.7%, respectively.

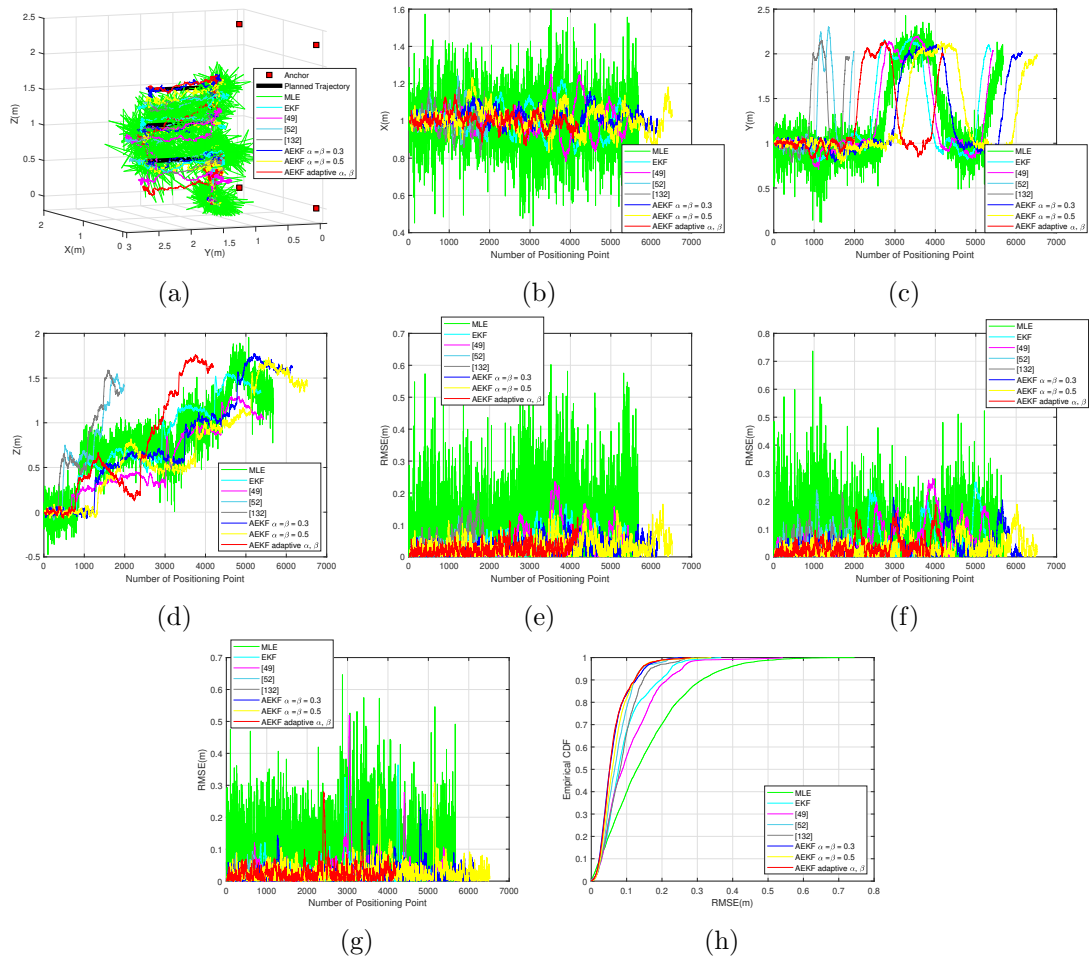


Figure 4.7: Simulation 2 flight results for the AEKF with changing noise model. (a) 3D trajectories. (b) X direction trajectories. (c) Y direction trajectories. (d) Z direction trajectories. (e) X direction RMSE (m). (f) Y direction RMSE (m). (g) Z direction RMSE (m). (h) eCDF.

In order to comprehensively validate the performance of the AEKF algorithm in the simulation environment, in the second simulation, the STD of these two measurement noises is randomly set within certain range. This is to simulate the variation of the operational environment. Same as the first simulation, the localisation performance for these algorithms in the second simulation has been demonstrated through different perspectives in Fig. 4.7 and summarised in Table 4.2. Clearly, with the sensor fusion based algorithms, the localisation results

Table 4.2: Detailed localisation results for the AEKF based sensor fusion approach with changing noise model in simulation 2

Algorithm	Median Error	Improved	95 <sup>th</sup> Error	Improved	Average STD	Improved
MLE	0.129m	N/A	0.381m	N/A	0.116m	N/A
EKF	0.077m	40.3%	0.226m	40.7%	0.064m	44.8%
[63]	0.088m	31.8%	0.258m	32.3%	0.079m	31.9%
[66]	0.066m	48.8%	0.143m	62.5%	0.042m	63.8%
[159]	0.082m	36.4%	0.167m	56.2%	0.050m	56.9%
AEKF	<b>0.052m</b>	<b>59.7%</b>	0.149m	60.9%	0.042m	63.8%
( $\alpha = \beta = 0.3$ )						
AEKF	0.060m	53.5%	<b>0.141m</b>	<b>63.0%</b>	0.042m	63.8%
( $\alpha = \beta = 0.5$ )						
AEKF	<b>0.052m</b>	<b>59.7%</b>	0.142m	62.7%	<b>0.041m</b>	<b>64.7%</b>
(adaptive $\alpha, \beta$ )						

are able to be greatly smoothed and improved. On the other hand, when being focused on the comparison between the AEKF based approaches and all other sensor fusion based approaches, a greatly performance improvement can be observed with AEKF approaches. This is because that the noise covariance matrices are adjusted manually and keep constant within the estimation process for all other sensor fusion based approaches, thus, when with the changing measurement noise model, the localisation performance can be significantly influenced. Meanwhile, for the two algorithms with the distance calibration and outlier detection methods in [63] and [159], the performance oscillation can be observed with the average STD dropped to 0.079m and 0.050m. This is also caused by the unsuitable calibration parameter led by the changing measurement noise model. Furthermore, different from the first simulation, the localisation performance for the AEKF algorithm with larger weighting factors is improved. With larger weighting factors,

Table 4.3: The probability for filtering divergence

AEKF Algorithms	Simulation 1	Simulation 2
$\alpha = \beta = 0.1$	0%	0%
$\alpha = \beta = 0.3$	0%	0%
$\alpha = \beta = 0.5$	0%	5%
$\alpha = \beta = 0.7$	40%	50%
$\alpha = \beta = 0.9$	90%	95%
Adaptive $\alpha, \beta$	0%	0%

more trust is given to the current measurement, which means that the offline data has less influence on the localisation performance, the estimated noise covariance matrices are much more accurate. Considering the measurement noise model is keep changing in the current simulation, the localisation performance can be improved with more accurate noise covariance matrices, especially for the 95<sup>th</sup> percentile error. Thus, larger weighting factors are more suitable for applications in the unstable operational environment. In addition, compared with all the other algorithms, the proposed AEKF algorithm still holds the high performance with 0.052m median error, 0.142m 95<sup>th</sup> percentile error and 0.041m average STD of the localisation error. It should be declared that even the proposed AEKF algorithm has not held the best performance within all these three indexes, but it always shows the capability for high accuracy and precision localisation under different circumstances of the measurement noise.

Moreover, rule out of the accuracy and precision of the algorithm, for UAV applications, the stability of the algorithm also needs to be considered. The filtering divergence for the proposed AEKF algorithm is more likely to happen with the keep changing noise covariance matrices, which may cause the position loss of UAV. For the purpose of verifying the stability of the proposed AEKF algorithm, the additional tests have been conducted. Two different simulations have been

carried out with the constant and changing measurement noise model same as the previous simulations. Here the AEKF algorithms with different weighting factors (0.1, 0.3, 0.5, 0.7 and 0.9) and the proposed AEKF algorithm have been tested. Each algorithm has been tested 20 times with the same path in the previous simulations. The probability of each algorithm for filtering divergence in two simulations are given in Table 4.3. According to the simulation results, with the weighting factors become larger, which means more changes for the noise covariance matrices, the filtering divergence is more likely to happen, especially with the suddenly changed acceleration. Besides, the changing measurement noise model in simulation 2 can also lead to the increasing probability of filtering divergence. For the proposed AEKF algorithm, considering the larger weighting factors will only be calculated when the big difference between the observation measurements and the predicted value, or between the recorded average time interval and current time interval is detected. And the calculated weighting factors are all limited within 0.5. Thus, the filtering divergence for the proposed AEKF algorithm can be ignored. This can also be proved by the simulation results in Table 4.3.

### **4.6.3 Simulation for the TC-AEKF based sensor fusion approach**

Same as the simulation for the AEKF based algorithm, before actual experiments, the simulations for the TC-AEKF based algorithm has also been carried out in the Gazebo environment. Similarly, within these, the UAV is deployed in the same extremely confined space with the same size, number of anchor nodes, coordinates of these anchor nodes to mock the actual operational environment. However, different from the previous simulations, in order to comprehensively validate the

performance of these algorithms, in the following simulations, the planned path for UAV is set as a rectangle. This is under the consideration that the reversed “S” flight path has already been selected in the previous section, thus, in order to comprehensively validate the performance of the algorithm with the different movement of the UAV including forward, backward, climbing and falling, the rectangle path is selected here. Different algorithms including the tightly coupled extended Kalman filter (TC-EKF), the algorithms in [66], [63] and [159], the TC-AEKF with constant weighting factors, the loosely coupled adaptive extended Kalman filter (LC-AEKF) and TC-AEKF are simulated. There are several points needs to be declared here. Firstly, considering the previous simulation results is enough to prove the effectiveness of the sensor fusion based approaches, thus, in the following simulations, more attention is given to the comparison between the tightly coupled approach and the loosely coupled approach. Secondly, in order to prevent ambiguity, the AEKF based sensor fusion approach in Section 4.4 is denoted as the LC-AEKF here. Thirdly, considering that the AEKF based approach is feasible for the application in changing environments, thus, in the following simulations, the standard deviation for the measurement noise of the distance information is randomly set within  $[0,0.2]$ m. The flight test results, including the 3D trajectories, trajectories in three directions, RMSE in three directions and the eCDF are depicted in Fig. 4.8. Moreover, to make it more intuitive, the detailed information including the localisation median error, 95<sup>th</sup> percentile error and the average STD for each algorithm have been summarised in Table 4.4. Within these, the numbers behind the TC-AEKF approach are the value for the weighting factors  $\alpha'$ ,  $\alpha$ ,  $\beta'$  and  $\beta$ , respectively.

From the simulation results, it can be observed that due to the changing

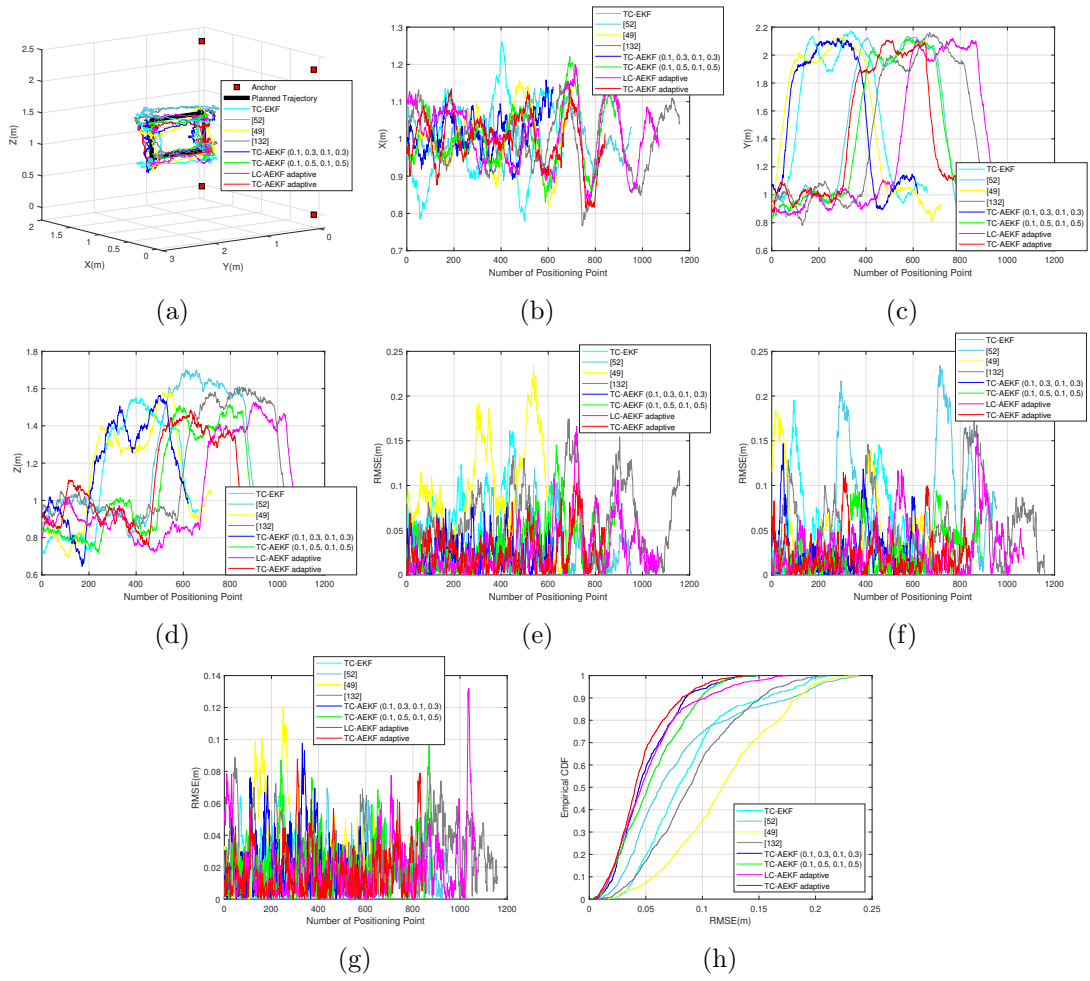


Figure 4.8: Simulation results for the TC-AEKF with changing noise model. (a) 3D trajectories. (b) X direction trajectories. (c) Y direction trajectories. (d) Z direction trajectories. (e) X direction RMSE (m). (f) Y direction RMSE (m). (g) Z direction RMSE (m). (h) eCDF.

measurement noise, the first four EKF based approaches with the constant noise covariance matrices always show worse performance when being compared with the AEKF based approaches. Especially, for the EKF based approaches in [63] and [159], due to the changing measurement noise, the unsuitable parameter is calculated for the distance calibration method which directly leads to the performance degradation. However, with the distance calibration and the outlier detection method, the average STD for [63] and [159] can still be improved to

Table 4.4: Detailed simulation results for the TC-AEKF based sensor fusion approach with changing noise model

Algorithm	Median Error	Improved	95 <sup>th</sup> Error	Improved	Average STD	Improved
TC-EKF	0.078m	N/A	0.183m	N/A	0.043m	N/A
[66]	0.063m	19.2%	0.200m	-9.3%	0.054m	-25.6%
[63]	0.117m	-50.0%	0.195m	-6.6%	0.047m	-9.3%
[159]	0.088m	-12.8%	0.170m	7.1%	0.042m	2.3%
TC-AEKF (0.1, 0.3, 0.1, 0.3)	0.044m	43.6%	0.105m	42.6%	0.027m	37.2%
TC-AEKF (0.1, 0.5, 0.1, 0.5)	0.052m	33.3%	0.110m	39.9%	0.030m	30.2%
LC-AEKF (adaptive weighting factors)	0.046m	41.0%	0.125m	31.7%	0.034m	20.9%
TC-AEKF (adaptive weighting factors)	<b>0.040m</b>	<b>48.7%</b>	<b>0.099m</b>	<b>45.9%</b>	<b>0.026m</b>	<b>39.5%</b>

0.047m and 0.042m, respectively. Then, when being focused on the AEKF approaches, through the adaptively estimated noise covariance matrices, the results are significantly smoothed and improved. Clearly, the best performance can be attained through the proposed approach with 0.097m median error, 0.167m 95<sup>th</sup> percentile error and 0.039m average STD. Meanwhile, compared with the TC-AEKF approach with larger weighting factors ( $\alpha = \beta = 0.5$ ), the one with smaller weighting factors ( $\alpha = \beta = 0.3$ ) holds the better performance. This is relevant to the measurement noise model in the current process, with relatively stable measurement noise model, small weighting factors will get better performance. Furthermore, through the performance comparison between the proposed TC-AEKF algorithm and the LC-AEKF, it can be observed that, the median error

for these two approaches are almost the same, but the proposed approach shows better performance for the 95<sup>th</sup> percentile error. However, considering the inaccurate attitude information caused by the geomagnetic disturbances is difficult to mock in the simulation environment, thus, in the simulation environment, the estimation error of the attitude information including the roll, pitch and yaw angle are almost the same for these two approaches.

## **4.7 Performance evaluation in the experiment environment**

### **4.7.1 System implementation and experiment setup**

In order to validate the effectiveness of the proposed algorithms in actual environment, an IMU and UWB based UAV positioning system is developed. The whole system is composed of six modules as depicted in Fig. 4.9. Firstly is the commercial low cost quadcopter known as Bebop 2 designed by Parrot. Secondly is the UWB system, which consists of four fixed anchor nodes, one tag node attached on UAV and one listener node to communicate with the ground station. Then there is an IMU module integrated within the UAV. Fourthly is the recording module (Insta360 go 2) for high quality video recording and image capturing. To achieve the stable control of the UAV, a ground station (laptop) is required for algorithm operation and command generation. Finally is the reference system (OptiTrack V120:Trio) to provide the ground truth for performance evaluation. The price, size and weight for each component are listed in Table 4.5. The cost for the IMU module is already included in the Bebop 2. The cost for the UWB

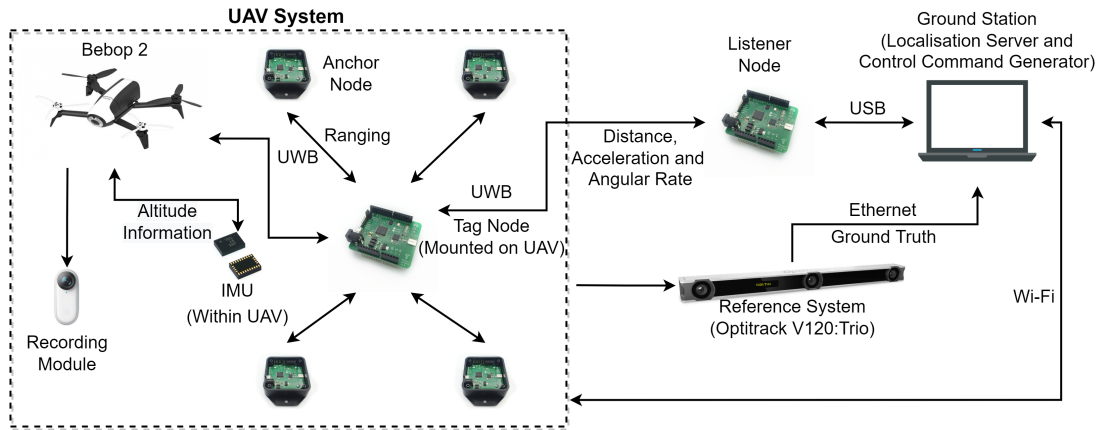


Figure 4.9: System structure.

Table 4.5: Size, weight and price for each component.

Name	Price (£)	Size (mm)	Weight (g)
Parrot Bebop 2	279.99	381 × 327.7 × 88.9	504
UWB System	583	60 × 53 × 1	12
Insta 360 go 2	294.99	52.9 × 23.6 × 20.7	26.5

system including one tag node, one listener node, four anchor nodes and relevant accessories. The size and weight for the UWB system in the table represents the size and weight for the tag node, considering only the tag node is equipped on UAV. The reference system is only exploited for the performance evaluation and the ground station does not belong to the UAV system, thus, the prices and size of these two modules are not considered.

As shown in Fig. 4.9, during the operational process, the acceleration and angular rate are firstly captured by the gyroscope on tag node and transmitted to the ground station through the listener node for the prediction of the position and attitude information. The listener node is directly connected with the ground station through USB cable. Simultaneously, the distance information and the attitude information are recorded and calculated by the UWB sensor nodes

and the IMU on UAV, then transmit to the ground station for the correction of the predicted information. In the system, the ground station also serves as the localisation server, which is responsible for the operation of the localisation algorithm. Finally, with the predicted and corrected information of UAV, the control command is generated by the ground station and sent back to the UAV via Wi-Fi for position and attitude control. During the process, the ground truth will be provided by the OptiTrack V120:Trio through the localisation of the markers attached on UAV. In the system, in order to keep a stable millimeter-level positioning accuracy, three markers are attached on Bebop 2. The position information of UAV from OptiTrack V120:Trio will be transmitted to the ground station via Ethernet in real-time for the performance evaluation.

In the experiment, in order to evaluate the performance of the proposed algorithms in the specified environment comprehensively, the experiment is performed within a confined space ( $1.95\text{m} \times 3.0\text{m} \times 2.3\text{m}$ ) in the laboratory to simulate the extremely confined space as depicted in Fig. 4.10. Similar to the simulation, all anchor nodes in the system are deployed on X-Z plane with the same coordinates to conform the application scenario where is difficult for human to access and the anchor nodes could only be deployed near the entrance of that extremely confined space.

#### **4.7.2 Performance evaluation for the AEKF based approach in the experiment environment**

In the experiments for the AEKF based sensor fusion approach, since the propagation condition and operational environment always have a great impact on the

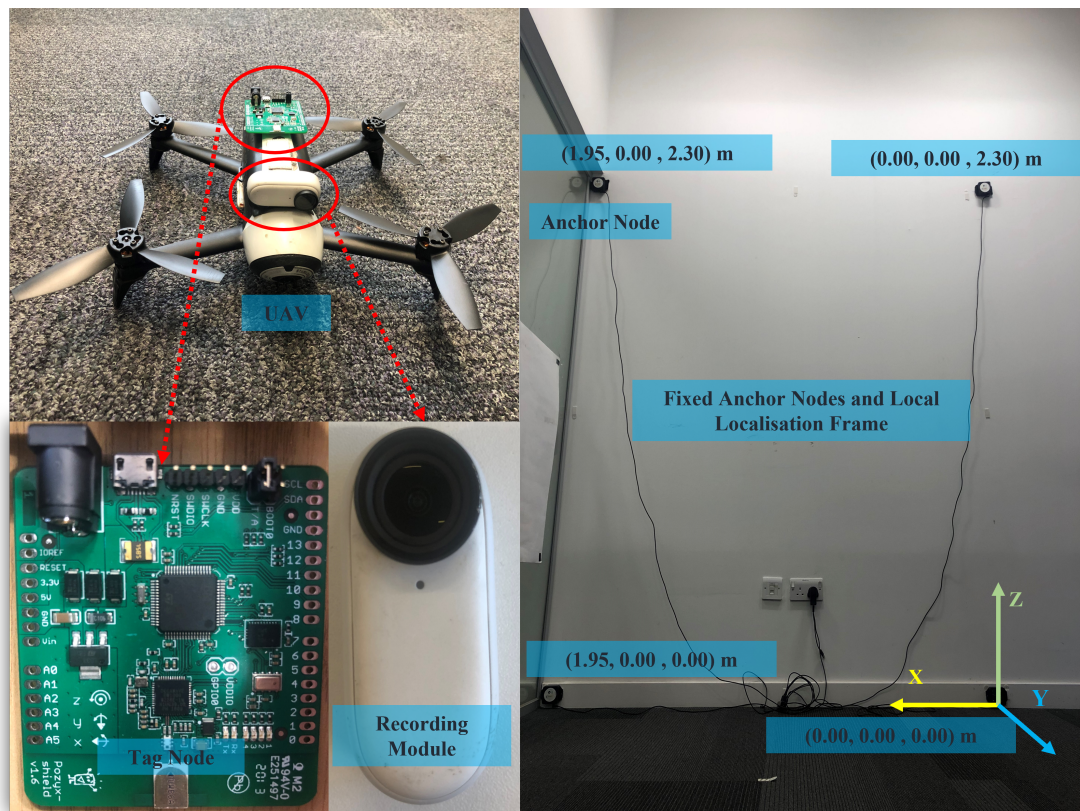


Figure 4.10: Experiment environment for the EKF, AEKF (LC-AEKF) and TC-AEKF based sensor fusion algorithms.

positioning performance which may cause the unexpected performance degradation, and in order to evaluate the adaptive ability for the AEKF approach, two different flight tests have been performed to get rid of this and comprehensively prove the effectiveness of the proposed AEKF algorithm under different operational circumstances. In the actual flight tests for the AEKF based sensor fusion approach, the planned trajectory is set as a reverse “S”. The STD for the measurement noise of IMU and UWB sensor nodes in the MLE based localisation algorithm and the sensor fusion based algorithms are also assumed as  $0.5\text{m/s}^2$  and  $0.1\text{m}$  which are estimated through 1000 recorded acceleration and distance measurements with UAV at the fixed point and adjusted manually through trial

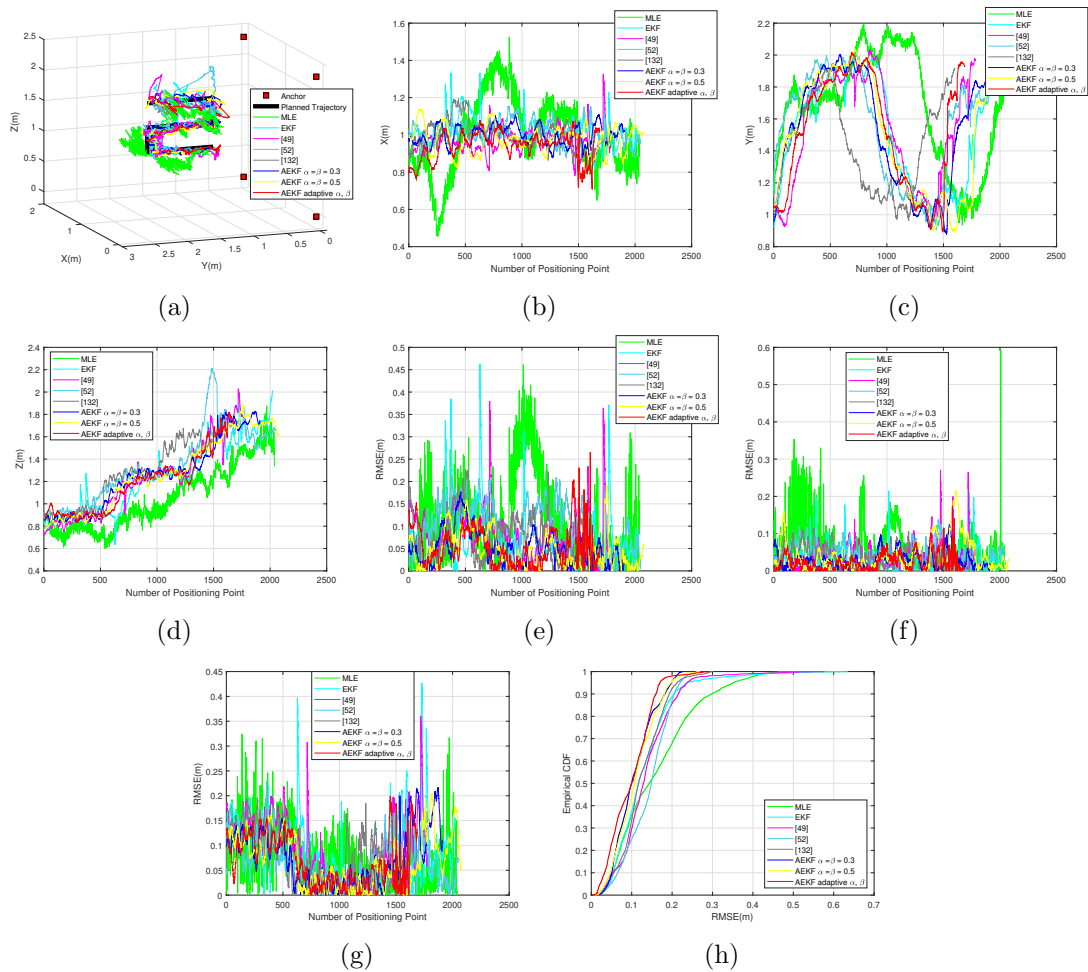


Figure 4.11: Experiment 1 flight test results for the AEKF. (a) 3D trajectories. (b) X direction trajectories. (c) Y direction trajectories. (d) Z direction trajectories. (e) X direction RMSE (m). (f) Y direction RMSE (m). (g) Z direction RMSE (m). (h) eCDF.

and error. For each experiment, over 1500 points' position information has been estimated to make the comprehensive performance evaluation of each algorithm.

In the flight test 1, the localisation performance of eight different types of algorithms same as the simulations have been demonstrated and listed in Fig. 4.11 and Table 4.6. Obviously, the same conclusion compared with the simulation can be made through the localisation results for the flight test 1, that the MLE based

Table 4.6: Detailed localisation results for the AEKF based sensor fusion approach in flight test 1

Algorithm	Median Error	Improved	95 <sup>th</sup> Error	Improved	Average STD	Improved
MLE	0.144m	N/A	0.351m	N/A	0.098m	N/A
EKF	0.116m	19.4%	0.239m	31.9%	0.075m	23.5%
[63]	0.129m	10.4%	0.237m	32.5%	0.067m	31.6%
[66]	0.149m	-3.5%	0.220m	37.3%	0.053m	45.9%
[159]	0.117m	18.8%	0.212m	39.6%	0.054m	44.9%
AEKF ( $\alpha = \beta = 0.3$ )	<b>0.099m</b>	<b>31.3%</b>	0.199m	43.4%	<b>0.048m</b>	<b>51.0%</b>
AEKF ( $\alpha = \beta = 0.5$ )	0.107m	25.7%	0.198m	43.6%	0.051m	48.0%
AEKF (adaptive $\alpha, \beta$ )	0.100m	30.6%	<b>0.170m</b>	<b>51.6%</b>	0.051m	48.0%

localisation algorithm holds the biggest performance oscillation. When being focused on the number of positioning points, with the MLE based localisation algorithm, much more time is required for UAV to hit the target points, which means that this oscillation also results in the instability of UAV. Thus, the results indicate that the measurement noise from the UWB sensor nodes has a great influence on the stability of UAV. However, this oscillation can be greatly limited through the sensor fusion based approaches. As listed in Table 4.6, in contrast with the MLE based localisation algorithm, the performance of other algorithms is all improved significantly, except the algorithm in [66]. However, there is still a great improvement on the 95<sup>th</sup> percentile error and the average STD of the algorithms in [66] compared with the MLE based localisation algorithm.

When being focused on the sensor fusion based approaches, the EKF algorithm and the algorithms in [63], [66] and [159] all exploited the manually adjusted and

constant noise covariance matrices for positioning. For the EKF algorithm, it can be observed that a high performance median error (0.116m) can be attained, nevertheless, the 95<sup>th</sup> percentile error and average STD of the localisation error still keep in high level when compared with the AEKF algorithms. Even the average STD is improved by the additional distance calibration and outlier detection methods in [63] and the 95<sup>th</sup> percentile error is enhanced by the additional angular rate in [66] and [159], however, a big gap still exists in contrast to the AEKF algorithms, due to the changing environment. For the AEKF algorithms, with the estimated noise covariance matrices  $\mathbf{R}_{update}$  and  $\mathbf{Q}_{update}$ , the median error, 95<sup>th</sup> percentile error and the average STD are all significantly improved with these around 0.102m, 0.189m and 0.05m, respectively. The AEKF algorithm with smaller weighting factors (0.3) holds the best performance on median error and average STD. But there is just a subtle difference for these compared with the proposed algorithm, and the proposed algorithm obtained the best performance on the 95<sup>th</sup> percentile error (0.170m).

As aforementioned, in order to eliminate the unexpected performance degradation and simulate the variation of the operational environment, another flight test has been conducted. In this flight test, obstacle is utilised to occlude one of the anchor nodes for a short time period during the flight to simulate the noise changing environment. Considering it is sufficient to prove the effectiveness of the sensor fusion based approaches in contrast with the MLE based localisation algorithm on UAV positioning, through the simulations and experiment results from the flight test 1. And to provide much more detailed information. In the flight test 2, only the experiments for the sensor fusion based approaches have been conducted and the results have been provided in Fig. 4.12 and Table 4.7.

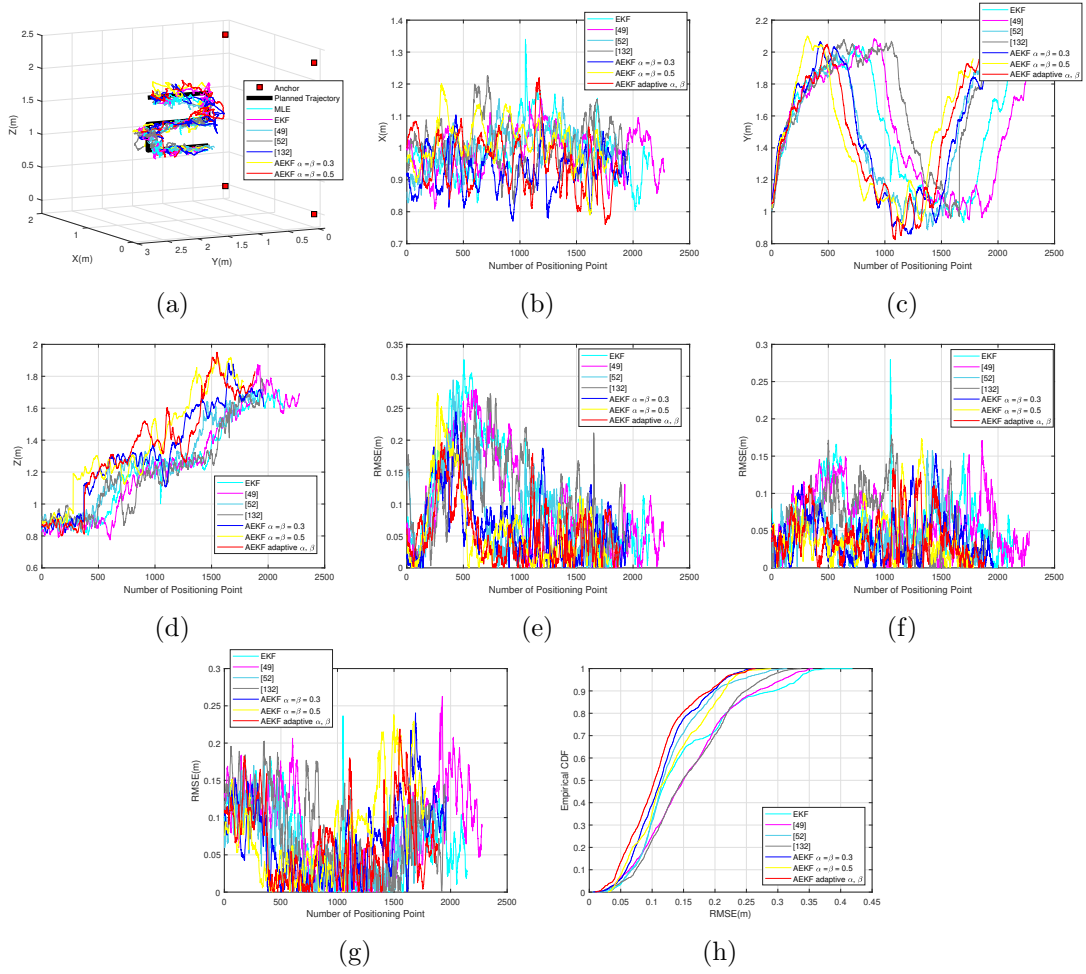


Figure 4.12: Experiment 2 flight test results for the AEKF. (a) 3D trajectories. (b) X direction trajectories. (c) Y direction trajectories. (d) Z direction trajectories. (e) X direction RMSE (m). (f) Y direction RMSE (m). (g) Z direction RMSE (m). (h) eCDF.

In the flight test 2, the degrading performance can be observed for almost all the algorithms due to the occluded anchor node during the flight test. Especially for the algorithms in [63] and [159], a great performance drop-off can be discovered. This is caused by the unsuitable calibration parameter led by the changing measurement noise. For the AEKF algorithms, obviously, in this flight test, the proposed algorithm holds the best performance on the median error (0.104m) and the 95<sup>th</sup> percentile error (0.213m). Owing to the changing measurement noise,

Table 4.7: Detailed localisation results for the AEKF based sensor fusion approach in flight test 2

Algorithm	Median Error	Improved	95 <sup>th</sup> Error	Improved	Average STD	Improved
EKF	0.133m	N/A	0.332m	N/A	0.082m	N/A
[63]	0.150m	-12.8%	0.309m	6.9%	0.076m	7.3%
[66]	0.122m	8.3%	0.240m	27.7%	0.054m	34.1%
[159]	0.148m	-11.3%	0.276m	16.9%	0.068m	17.1%
AEKF ( $\alpha = \beta = 0.3$ )	0.113m	15.0%	0.215m	35.2%	<b>0.050m</b>	<b>39.0%</b>
AEKF ( $\alpha = \beta = 0.5$ )	0.120m	9.8%	0.227m	31.6%	0.058m	29.3%
AEKF (adaptive $\alpha, \beta$ )	<b>0.104m</b>	<b>21.8%</b>	<b>0.213m</b>	<b>35.8%</b>	0.053m	35.4%

there is a performance degradation for the AEKF algorithm with the smaller weighting factors (0.3). When with smaller weighting factors, more trust will be given to the  $\mathbf{R}_{off}$  and  $\mathbf{Q}_{off}$  which means more stable performance. However, the system needs more time to catch up the changes, which may result in the accuracy degradation. This can also be proved by the localisation results in the flight test 2, that the median error (0.113m) and the 95<sup>th</sup> percentile error (0.215m) of the AEKF algorithm with smaller weighting factors (0.3) is worse than the proposed algorithm, but it still holds the best average STD (0.050m).

When combining the experiment results from all the flight tests, the following conclusion can be made that compared with the MLE based localisation algorithm, the EKF algorithm and the algorithms in [63], [66] and [159], the better performance can be attained by the AEKF algorithms under different conditions. For the comparison within the AEKF algorithms, even the localisation performance for the AEKF based algorithm with constant weighting factors may be

better than the proposed algorithm under certain conditions. However, the proposed algorithm always shows much more robust performance, the accuracy and precision always keep in high level with the median error around 0.102m, the 95<sup>th</sup> percentile error around 0.192m and the average STD around 0.052m. Furthermore, apart from the localisation accuracy and precision, the position update rate also has great influence on the stability of UAV in such environments due to the speed of it. Considering the limitation for the TW-TOF ranging protocol and the propagation speed of the electromagnetic wave, the position update rate for the MLE based localisation algorithm is restrained within 25Hz. This is significantly improved by the sensor fusion approaches which increased the update rate into 88Hz. This high position update rate will absolutely improve the stability of UAV in such environment. In conclusion, it can be proved that the proposed algorithm is capable for UAV applications in focused scenarios.

### **4.7.3 Performance evaluation for the TC-AEKF based approach in the experiment environment**

Similar to the simulation for the TC-AEKF based algorithm, in order to comprehensively validate the performance of the proposed algorithms, the planned path for UAV in this experiment is set as a rectangle. Same as the previous experiments, for each one, over 1500 points' position information has been estimated to make the comprehensive performance evaluation of each algorithm. Only the sensor fusion based algorithms have been tested is under the consideration of the comprehensive performance comparison for the EKF and AEKF based algorithms with the MLE based algorithm in the previous section. In the experiment, differ-

Table 4.8: Detailed experiment results for the TC-AEKF based sensor fusion approach

Algorithm	Median Error	Improved	95 <sup>th</sup> Error	Improved	Average STD	Improved
TC-EKF	0.147m	N/A	0.289m	N/A	0.080m	N/A
[66]	0.123m	16.3%	0.275m	4.8%	0.083m	-3.8%
[63]	0.183m	-24.5%	0.271m	6.2%	0.068m	15.0%
[159]	0.117m	20.4%	0.220m	23.9%	0.051m	36.3%
TC-AEKF (0.1, 0.3, 0.1, 0.3)	0.098m	33.3%	0.192m	33.6%	0.044m	45.0%
TC-AEKF (0.1, 0.5, 0.1, 0.5)	0.132m	10.2%	0.220m	23.8%	0.049m	38.8%
LC-AEKF (adaptive weighting factors)	0.099m	32.7%	0.180m	37.7%	0.050m	37.5%
TC-AEKF (adaptive weighting factors)	<b>0.097m</b>	<b>34.0%</b>	<b>0.167m</b>	<b>42.2%</b>	<b>0.039m</b>	<b>51.3%</b>

ent algorithms including the TC-EKF, the algorithms in [66], [63] and [159], the TC-AEKF with constant weighting factors, the LC-AEKF (AEKF with adaptive weighting factors in the previous section) and TC-AEKF have been tested. The flight test results, including the 3D trajectories, trajectories in three directions, RMSE in three directions and the eCDF are depicted in Fig. 4.13. Moreover, to make it more intuitive, the detailed information including the localisation median error, 95<sup>th</sup> percentile error and the average STD for each algorithm have been summarised in Table 4.8. Within these, the numbers behind the TC-AEKF approach are the value for the weighting factors  $\alpha'$ ,  $\alpha$ ,  $\beta'$  and  $\beta$ , respectively.

Similar to the simulation, the performance gap between the EKF and the AEKF based approaches still exists in the experiment results. But differently,

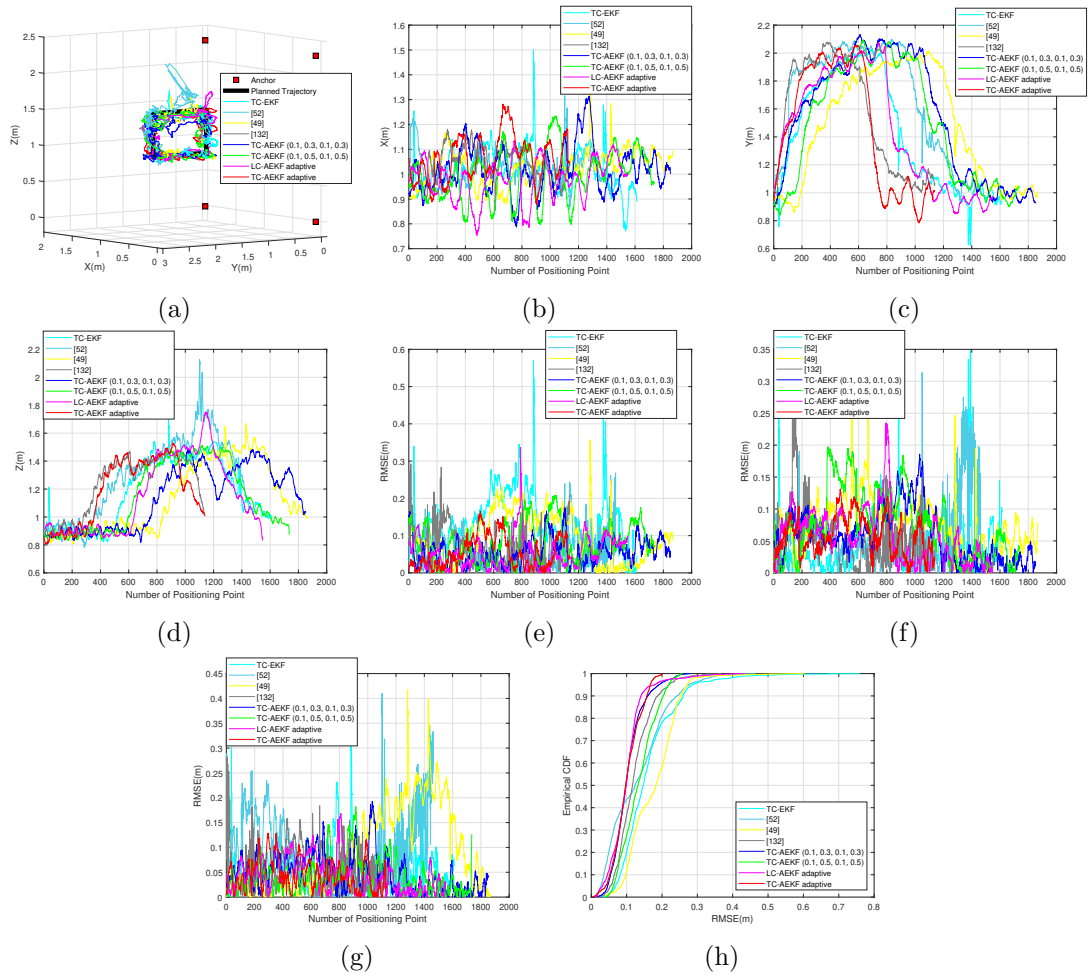


Figure 4.13: Experiment results for the TC-AEKF. (a) 3D trajectories. (b) X direction trajectories. (c) Y direction trajectories. (d) Z direction trajectories. (e) X direction RMSE (m). (f) Y direction RMSE (m). (g) Z direction RMSE (m). (h) eCDF.

with the suitable calibration parameter, the average STD and accuracy are greatly improved for [63] and [159]. When being focused on the AEKF based approaches, the TC-AEKF approach with smaller weighting factors (0.1, 0.3, 0.1, 0.3) holds the better performance than the one with relatively larger weighting factors. For the LC-AEKF algorithm, in the actual flight tests, more drift caused by the geomagnetic disturbances for the IMU measurements exist which directly lead to the degradation for the 95<sup>th</sup> percentile error and the precision (average STD)

of the algorithm, the performance oscillation is even larger than the two AEKF approaches with the constant weighting factors. For the proposed approach, it still holds the best performance with the median error, 95<sup>th</sup> percentile error and average STD to be 0.097m, 0.167m and 0.039m, respectively. The position update rate for the TC-AEKF is still keep in high level, which is 50Hz. In addition to the position estimation, in the actual flight tests, due to the influence from the magnetometer, the drift for the attitude information from the IMU can be observed with the estimation error of the roll, pitch and yaw angle to be 3.06°, 3.71° and 8.78°. Leveraging the proposed approach, this performance degradation is greatly limited with the estimation error to be 2.15°, 1.54° and 4.58°, which are improved 29.8%, 58.4% and 47.8%, respectively.

#### **4.7.4 Autonomous inspection flight test with the TC-AEKF algorithm**

Apart from the performance evaluation, in order to comprehensively validate the effectiveness of the proposed algorithm and the developed UAV system, the autonomous inspection flight test in the laboratory environment has been conducted. The planned path for UAV is calculated through the path planning algorithm to cover the whole area (X: 1.95m, Y: 3.0m, Z: 2.3m) for the autonomous inspection. Taking into account the complexity of the planned path, it is difficult to measure the ground truth during the flight, therefore, only the trajectory results are provided in Fig. 4.14. To make it clear, the video for the autonomous inspection flight test has been attached in Appendix A. Apparently, the proposed algorithm and the developed UAV system are capable of the autonomous

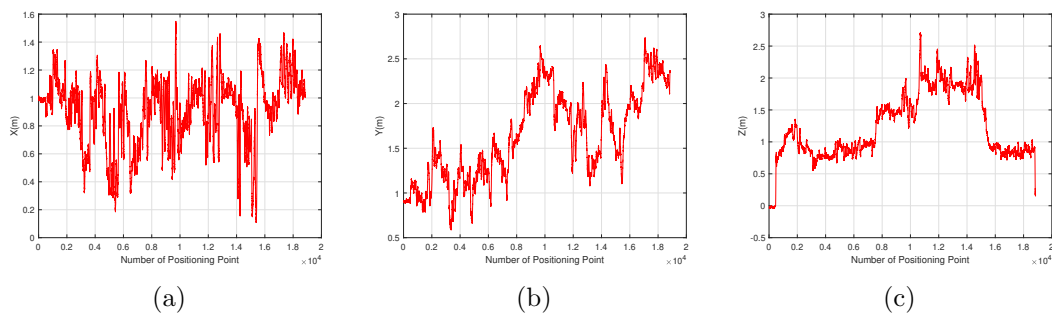


Figure 4.14: Flight trajectory for the TC-AEKF based autonomous inspection. (a) Trajectory in X(m) direction in the autonomous inspection flight test. (b) Trajectory in Y(m) direction in the autonomous inspection flight test. (c) Trajectory in Z(m) direction in the autonomous inspection flight test.

inspection in GPS-denied and extremely confined environments.

## 4.8 Summary

In this chapter, two adaptive sensor fusion based algorithms have been proposed focused on the UAV based autonomous inspection in GPS-denied and extremely confined environments. Firstly, the introduction and discussion about the pure UWB based localisation technology and algorithm in the previous chapter have been provided to point out the research questions including the potential performance influence caused by the unreasonable value within the ranging information and the low position update rate. Afterwards, the description for the EKF sensor fusion algorithm which based on the integration of the IMU and UWB has been provided. However, considering the unknown process and measurement noise covariance matrices, the performance oscillation still exists, and the precision and accuracy are insufficient for the stable flight of UAV in extreme cases. Therefore, the AEKF based sensor fusion approach was studied and proposed. With the measurements from previous processes, the process and measurement noise

covariance matrices can be adaptively estimated to relieve the performance oscillation. During the estimation process, two weighting factors  $\alpha$  and  $\beta$  were introduced and adaptively estimated through the recorded information to further limit the estimation of these matrices for performance improvement. Nevertheless, with the introduction of the IMU measurements, the potential drift for these measurements leading by the magnetometer on the IMU still limits the performance. To remedy this, the TC-AEKF based algorithm has been proposed in this chapter. With the consideration of the angular rate in the state prediction process and the ability to estimate the noise model, all the aforementioned issues can be solved. Finally, simulations and experiments have been carried out to comprehensively evaluate the performance of the proposed algorithms. From results, it is clear that, in contrast with the MLE based localisation algorithm, the EKF based approach, the algorithms in [63], [66] and [159], and the LC-AEKF and TC-AEKF based approach with constant weighting factors, the proposed two algorithms can always show better and robust performance. Furthermore, to validate the effectiveness of the developed system and the TC-AEKF based algorithm, the autonomous inspection test has been done in the laboratory environment, which can prove that the developed system and the TC-AEKF based algorithm is feasible for the autonomous inspection in GPS-denied and extremely confined environments.

## Chapter 5

# UWB and IMU based SRCKF sensor fusion UAV positioning technology

### 5.1 Introduction

With the proposed AEKF and TC-AEKF based algorithms, the performance oscillation leads by the unreasonable values within the ranging information can be significantly limited. During the estimation process, because of the nonlinearity of the transfer matrix in the correction process, the first order Taylor expansion has been applied for the linearisation. However, the neglected high order terms for the transfer matrix will still has the influence on the positioning performance. In order to remedy this, the investigation on the SRCKF based sensor fusion algorithm will be carried out. In addition, similar to the EKF based sensor fusion algorithm, the conventional SRCKF based algorithm still require the precise noise

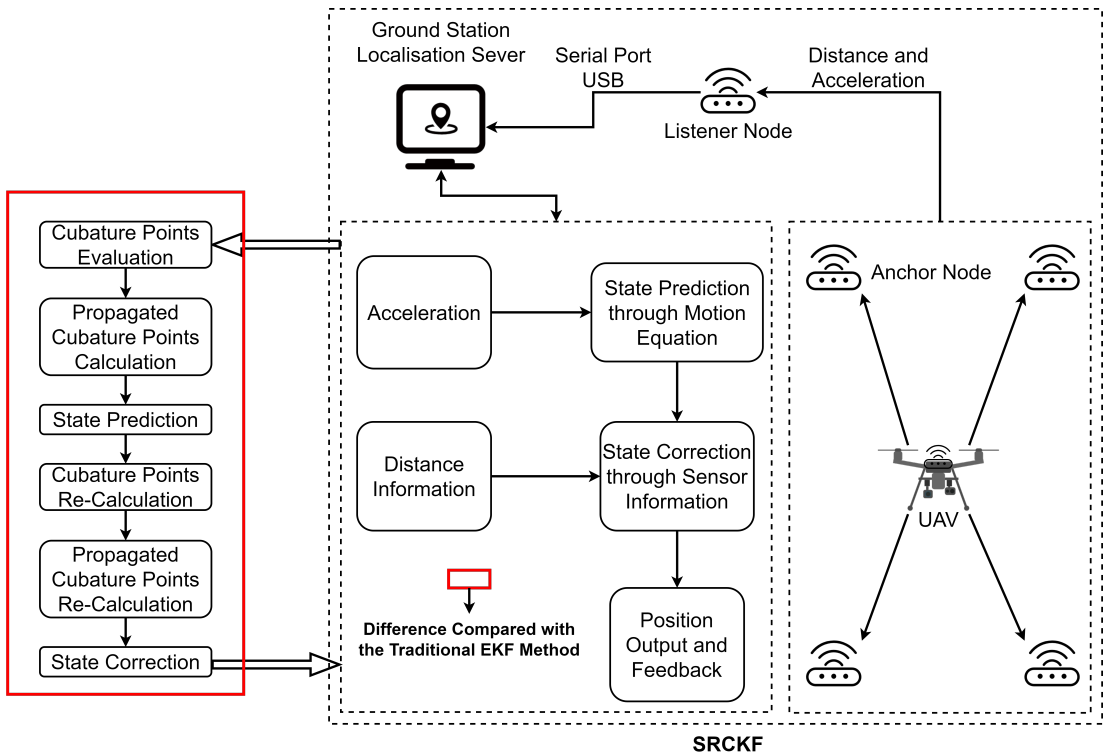


Figure 5.1: Structure for the SRCKF based algorithm.

model information to keep the high accuracy localisation performance. To deal with this, in this chapter, the ASRCKF based sensor fusion is proposed.

## 5.2 SRCKF based sensor fusion with the integration of IMU and UWB

To get rid of the performance influence caused by the linearisation of the observation matrix, the cubature rule is utilised by SRCKF to approximate the state posterior mean and covariance [163,164]. To make it clear, the operational process of the SRCKF based sensor fusion algorithm is depicted in Fig. 5.1.

Here, the estimation process of the SRCKF is given as follows.

### 5.2.1 State prediction

Firstly, the cubature points are evaluated through the state vector  $\mathbf{u}_{k-1}$  and  $\mathbf{S}_{k-1}$  from the  $k - 1$  round.

$$\mathbf{u}_{i,k-1} = \mathbf{S}_{k-1}\boldsymbol{\delta}_i + \mathbf{u}_{k-1}, i = 1, 2, \dots, 2m, \quad (5.1)$$

where,  $m$  represents the number of the state variables to be estimated in the state vector,  $\mathbf{u}_{k-1}$  is the state vector composed by the UAV position and velocity information (the definition for  $\mathbf{u}_{k-1}$  can also be found in Section 4.3.1),  $\mathbf{S}_{k-1}$  denotes the square root of the covariance matrix  $\mathbf{A}_{k-1}$  which can be calculated by the Cholesky decomposition

$$\mathbf{A}_{k-1} = \mathbf{S}_{k-1}\mathbf{S}_{k-1}^T, \quad (5.2)$$

$\boldsymbol{\delta}_i$  can be represented as

$$\boldsymbol{\delta}_i = \begin{cases} \sqrt{m}\mathbf{I}_{m,i}, i = 1, 2, \dots, m \\ -\sqrt{m}\mathbf{I}_{m,i-m}, i = m + 1, m + 2, \dots, 2m \end{cases}, \quad (5.3)$$

$\mathbf{I}_{m,i}$  is supposed as the  $i$ th column of the  $m \times m$  identity matrix.

Accordingly, the propagated cubature points can be calculated through (4.11) and (5.1) and represented as

$$\mathbf{u}_{i,k/k-1}^* = \mathbf{F}_k\mathbf{u}_{i,k-1} + \mathbf{B}_k\mathbf{a}_{k-1}^L, i = 1, 2, \dots, 2m. \quad (5.4)$$

Then, the predicted state vector and the square root of the covariance matrix can

be derived as

$$\hat{\mathbf{u}}_{k/k-1} = \frac{1}{2m} \sum_{i=1}^{2m} \mathbf{u}_{i,k/k-1}^*, \quad (5.5)$$

$$\mathbf{S}_{k/k-1} = \text{Tria}([\mathbf{\Gamma}_{k/k-1}^*, \mathbf{S}_Q]), \quad (5.6)$$

where,  $\text{Tria}(\cdot)$  denotes the QR decomposition,  $\mathbf{S}_Q$  is supposed as the square root of the process noise covariance matrix  $\mathbf{Q}$ ,  $\mathbf{\Gamma}_{k/k-1}^*$  can be represented as

$$\mathbf{\Gamma}_{k/k-1}^* = \frac{1}{\sqrt{2m}} [\mathbf{u}_{1,k/k-1}^* - \hat{\mathbf{u}}_{k/k-1}, \mathbf{u}_{2,k/k-1}^* - \hat{\mathbf{u}}_{k/k-1}, \dots, \mathbf{u}_{2m,k/k-1}^* - \hat{\mathbf{u}}_{k/k-1}] \quad (5.7)$$

### 5.2.2 Observation correction

During the correction process for the SRCKF algorithm, firstly, the cubature points can be calculated through the predicted state vector and the square root of the process noise covariance matrix from the prediction process and represented as

$$\mathbf{u}_{i,k/k-1} = \mathbf{S}_{k/k-1} \boldsymbol{\delta}_i + \hat{\mathbf{u}}_{k/k-1}, i = 1, 2, \dots, 2m. \quad (5.8)$$

Followed by, the propagated cubature points can be derived through the calculated cubature points

$$\mathbf{Z}_{i,k/k-1} = h(k, \mathbf{u}_{i,k/k-1}), i = 1, 2, \dots, 2m, \quad (5.9)$$

where,  $h(\cdot)$  is supposed as the observation transition function.

Then, the predicted measurement matrix can be expressed as

$$\hat{\mathbf{Z}}_{k/k-1} = \frac{1}{2m} \sum_{i=1}^{2m} \mathbf{Z}_{i,k/k-1}. \quad (5.10)$$

Throughout these, the square root of the innovation covariance matrix  $\mathbf{S}_{ZZ,k/k-1}$  and the cross covariance matrix  $\mathbf{S}_{uZ,k/k-1}$  can be calculated as follows

$$\mathbf{S}_{ZZ,k/k-1} = \text{Tri}a([\boldsymbol{\zeta}_{k/k-1}, \mathbf{S}_{R,k}]), \quad (5.11)$$

$$\mathbf{S}_{uZ,k/k-1} = \mathbf{\Gamma}_{k/k-1} \boldsymbol{\zeta}_{k/k-1}^T, \quad (5.12)$$

where,  $\mathbf{S}_R$  is assumed as the square root of the measurement noise covariance matrix  $\mathbf{R}$ ,  $\boldsymbol{\zeta}_{k/k-1}$  is able to be calculated by the propagated cubature points and the predicted measurement matrix

$$\begin{aligned} \boldsymbol{\zeta}_{k/k-1} = \frac{1}{\sqrt{2m}} & [\mathbf{Z}_{1,k/k-1} - \hat{\mathbf{Z}}_{k/k-1}, \mathbf{Z}_{2,k/k-1} - \hat{\mathbf{Z}}_{k/k-1}, \\ & \dots, \mathbf{Z}_{2m,k/k-1} - \hat{\mathbf{Z}}_{k/k-1}] \end{aligned}, \quad (5.13)$$

$\mathbf{\Gamma}_{k/k-1}$  can be represented as

$$\begin{aligned} \mathbf{\Gamma}_{k/k-1} = \frac{1}{\sqrt{2m}} & [\mathbf{u}_{1,k/k-1} - \hat{\mathbf{u}}_{k/k-1}, \mathbf{u}_{2,k/k-1} - \hat{\mathbf{u}}_{k/k-1}, \\ & \dots, \mathbf{u}_{2m,k/k-1} - \hat{\mathbf{u}}_{k/k-1}] \end{aligned}. \quad (5.14)$$

Finally, the Kalman gain  $\mathbf{K}_{KF}$ , corrected state vector  $\hat{\mathbf{u}}_k$  and the square root of the covariance matrix  $\hat{\mathbf{S}}_k$  can be calculated and estimated as

$$\mathbf{K}_{KF} = (\mathbf{S}_{uZ,k/k-1} / \mathbf{S}_{ZZ,k/k-1}^T) / \mathbf{S}_{ZZ,k/k-1}, \quad (5.15)$$

$$\hat{\mathbf{u}}_k = \hat{\mathbf{u}}_{k/k-1} + \mathbf{K}_{KF}(\mathbf{Z}_k - \hat{\mathbf{Z}}_{k/k-1}), \quad (5.16)$$

$$\hat{\mathbf{S}}_k = \text{Tri}a([\mathbf{\Gamma}_{k/k-1} - \mathbf{K}_{KF}\mathbf{\zeta}_{k/k-1}, \mathbf{K}_{KF}\mathbf{S}_{R,k}]). \quad (5.17)$$

### 5.3 Adaptive SRCKF based sensor fusion

With the ability to deal with the linearisation issue for the SRCKF algorithm, the localisation performance of the system can be further improved. However, owing to the variation of the operational environment, the changing for the process and measurement noise always exist which may lead to the performance degradation or even the filtering divergence when with the manually adjusted and constant noise covariance matrices [165]. Furthermore, the difficulty to manually adjust the noise covariance matrices in the focused environments should also be taken into account. Therefore, to overcome this, the ASRCKF based sensor fusion approach is investigated and proposed. To make it clearer about the structure of the ASRCKF based sensor fusion algorithm before the detailed introduction, the algorithm structure flow chart is provided in Fig. 5.2.

#### 5.3.1 Estimation of the noise covariance matrices

Firstly, for the estimation of the measurement noise covariance matrix  $\mathbf{R}$ . Traditionally, it can be estimated through the innovation sequence calculated through the difference between the predicted measurement matrix from (5.10) and the measurement matrix  $\mathbf{Z}_k$  in the current round [166]. Nevertheless, the negative estimation may exist which will directly lead to the filtering divergence. To remedy this, inspired by the approach in [161], the measurement filtering residual  $\mathbf{Z}'_k$

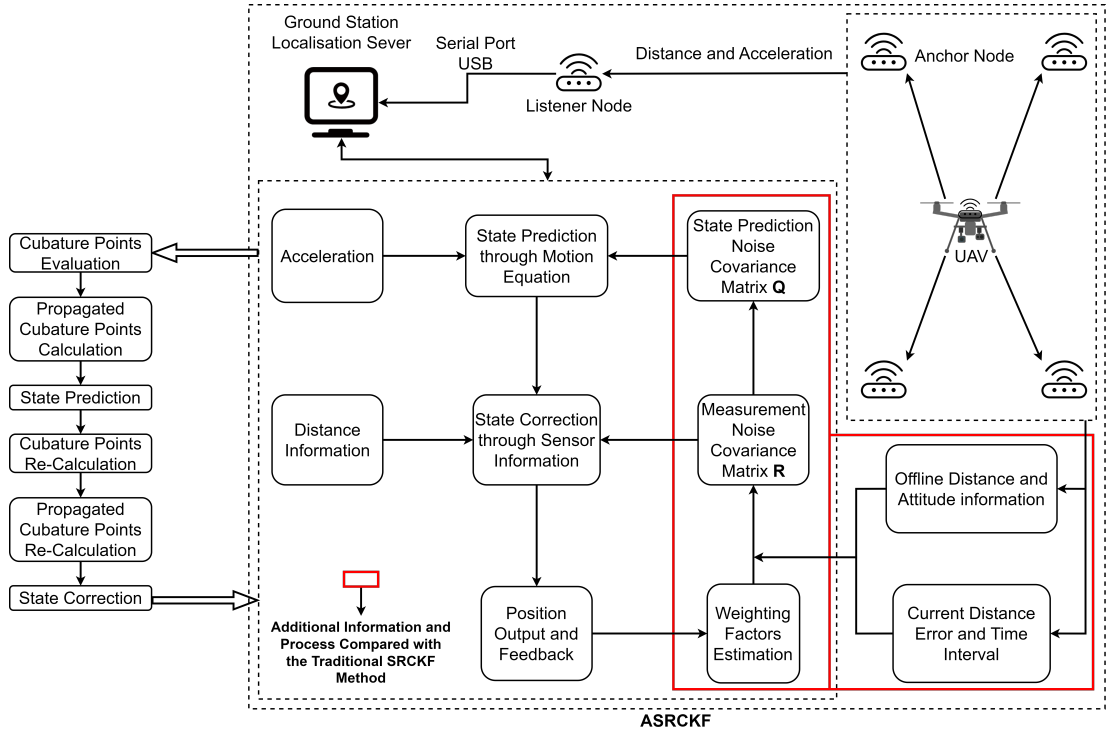


Figure 5.2: Structure for the ASRCKF based algorithm.

is calculated and exploited to estimate the measurement noise covariance matrix  $\mathbf{R}$  to prevent the negative estimation issue.

With the corrected state vector  $\hat{\mathbf{u}}_k$  in (5.16) and the measurement matrix  $\mathbf{Z}_k$  in the current round, the measurement filtering residual can be calculated and represented as

$$\mathbf{Z}'_k = \mathbf{Z}_k - h(k, \hat{\mathbf{u}}_k). \quad (5.18)$$

Then, the measurement noise covariance can be obtained

$$\mathbf{R}_k = \hat{\mathbf{Q}}_{\mathbf{Z}'_k} + \hat{\mathbf{Z}}_{k/k-1} \hat{\mathbf{Z}}_{k/k-1}^T, \quad (5.19)$$

where,  $\hat{\mathbf{Q}}_{\mathbf{Z}'_k}$  represents the residual covariance matrix which is calculated by the

residual  $\mathbf{Z}'_k$  from  $M$  rounds,

$$\hat{\mathbf{Q}}_{\mathbf{Z}'_k} = \frac{1}{M} \sum_{i=k-M+1}^k \mathbf{Z}'_i \mathbf{Z}'_i{}^T, \quad (5.20)$$

$M$  denotes the window size or sampling number. Larger  $M$  means the estimation of the residual covariance matrix will become stable and smooth, however, the adaptive ability will be reduced. On the contrary, smaller  $M$  will increase the adaptive ability, but it is at the expense of the stability of the algorithm.

Secondly, for the estimation of the process noise covariance matrix  $\mathbf{Q}$ . Through the mathematical model of the sensor fusion approach, it can be observed that the process noise  $\boldsymbol{\eta}$  comes from the bias and measurement noise of the acceleration information can be expressed as

$$\boldsymbol{\eta}_{k-1} = \hat{\mathbf{u}}_k - \hat{\mathbf{u}}_{k/k-1}, \quad (5.21)$$

where,

$$\hat{\mathbf{u}}_k - \hat{\mathbf{u}}_{k/k-1} = \mathbf{K}_{KF}(\mathbf{Z}_k - \hat{\mathbf{Z}}_{k/k-1}). \quad (5.22)$$

Accordingly, the process noise covariance matrix  $\mathbf{Q}$  can be derived

$$\mathbf{Q}_k = \mathbf{K}_{KF} \hat{\mathbf{C}}_{\mathbf{Z}''_k} \mathbf{K}_{KF}^T, \quad (5.23)$$

where,  $\hat{\mathbf{C}}_{\mathbf{Z}''_k}$  represents the innovation covariance matrix

$$\hat{\mathbf{C}}_{\mathbf{Z}''_k} = \frac{1}{M} \sum_{i=k-M+1}^k \mathbf{Z}''_i \mathbf{Z}''_i{}^T, \quad (5.24)$$

$\mathbf{Z}''_k$  denotes the innovation sequence which represents the difference between the

observation information in current round and the predicted measurements

$$\mathbf{Z}_k'' = \mathbf{Z}_k - \hat{\mathbf{Z}}_{k/k-1}. \quad (5.25)$$

With the adaptively estimated noise covariance matrices, the system is able to catch up the noise changes for performance improvement. Nevertheless, the changing of these noise covariance matrices may cause the instability of the filter and lead to the filtering divergence. The filtering divergence will directly cause the position loss of the UAV, which is unacceptable for the focused applications. Thus, an additional approach is required to limit the estimation of these noise covariance matrices to avoid the potential filtering divergence.

### 5.3.2 Additional weighting factors

In the estimation process, two additional weighting factors  $\alpha$  and  $\beta$ , and the offline data of the noise covariance matrices  $\mathbf{R}_{off}$  and  $\mathbf{Q}_{off}$  are introduced to against the potential filtering divergence of the ASRCKF algorithm and the position loss of the UAV. The offline data of these noise covariance matrices are estimated and recorded before the flight of UAV in offline phase through 50 rounds estimation results. It needs to declare here that the localisation process of the system can be divided into two parts, including the online phase and offline phase. During the offline phase, the localisation system will operate firstly with the UAV statically at the original point. This is to collect enough data for the calculation of the offline noise covariance matrices  $\mathbf{R}_{off}$  and  $\mathbf{Q}_{off}$ . After the offline phase, the system will go into the online phase which can provide the position information of the UAV to support the inspection mission.

For the estimation of the measurement noise covariance matrix, throughout the additional weighting factor  $\alpha$  and the offline data of the measurement noise covariance matrix  $\mathbf{R}_{off}$ , the limited measurement noise covariance matrix  $\mathbf{R}^{update}$  can be derived as

$$\mathbf{R}_{update} = (1 - \alpha)\mathbf{R}_{off} + \alpha\mathbf{R}_k. \quad (5.26)$$

Similarly, the limited process noise covariance matrix  $\mathbf{Q}^{update}$  can be calculated by the additional weighting factor  $\beta$  and the offline data of the process noise covariance matrix  $\mathbf{Q}_{off}$ ,

$$\mathbf{Q}_{update} = (1 - \beta)\mathbf{Q}_{off} + \beta\mathbf{Q}_k. \quad (5.27)$$

Obviously from (5.26) and (5.27), with the reduction of the weighting factors, the estimation of the limited noise covariance matrices will more rely on the offline data estimated during the offline phase. Which means that the estimation results will become relatively stable and smooth. The probability for the filtering divergence or position loss can be decreased. Nevertheless, this is at the expense of losing the adaptive ability. On the contrary, with the augment of the weighting factors, more changes for the estimation of these matrices will be brought by the current measurements to catch up the variation of the process and measurement noise in the current round. Which means that the localisation accuracy of the algorithm can be increased. Yet, the stability of the it will be influenced and may even cause the filtering divergence and position loss. Clearly, the value of the additional weighting factors greatly influences the performance and stability of the ASRCKF algorithm.

In order to find the suitable weighting factors, an adaptive estimation approach for these weighting factors is presented and given as follows. In the estimation process, the weighting factor  $\alpha$  is utilised to limit the estimation of the measurement noise covariance matrix. Which means that  $\alpha$  has the relationship with the measurement noise in the current round. Therefore, the following equation is given help for the estimation of it

$$\alpha_{ad} = \frac{\frac{1}{n} \sum_{i=1}^n [\mathbf{Z}_k'']_{i1}}{Z_{in}''} \alpha_{in}, \quad (5.28)$$

where,  $n$  represents the number of the fixed anchor nodes in the system,  $Z_{in}''$  denotes the calculated and recorded difference between the observation information and the predicted measurement in the offline phase and  $\alpha_{in}$  is the initial value of  $\alpha$ , which is set to be 0.2. The adaptively estimated  $\alpha_{ad}$  is set within  $[0,0.2]$ . The principle for selecting the initial value of  $\alpha$  and the range of  $\alpha_{ad}$  is provided in Section 5.4.

Apparently from (5.28), along with the increasing of the innovation sequence  $\mathbf{Z}_k''$ , which means larger difference between the predicted measurements and the observation information in the current round, the  $\alpha_{ad}$  will become larger to overtake the changes. Otherwise, the  $\alpha_{ad}$  will become smaller to give more trust to the offline data to keep the stable and smooth estimation of the measurement noise covariance matrix.

Similarly, the estimation of the weighting factor  $\beta$  can also be set up, according to the relationship with the process noise. Considering the time interval  $\Delta T$  between the two rounds acceleration measurements has the impact on the prediction process, where with the larger  $\Delta T$ , the influence of the process noise on the

Chapter 5. UWB and IMU based SRCKF sensor fusion UAV positioning technology prediction process will become larger, otherwise, the influence can be reduced. Thus, the relationship between the time interval in the current round and the average time interval  $\Delta T_{avg}$  calculated in the offline phase is utilised to estimate  $\beta$ . The calculation equation can be derived as follows

$$\beta_{ad} = \frac{\Delta T}{\Delta T_{avg}} \beta_{in}, \quad (5.29)$$

where,  $\beta_{in} = 0.2$  is the initial value of the weighting factor, the range of the  $\beta_{ad}$  is set within  $[0,0.2]$ . Similarly, the principle for selecting the initial value and the determination for the range of  $\beta_{ad}$  is given in Section 5.4.

Apparently, with a larger  $\Delta T$  which exceeds the  $\Delta T_{avg}$ , the process noise will have more impact on the prediction performance. Thus, a larger  $\beta_{ad}$  will be estimated to give more trust to the current estimation results. On the contrary, a smaller  $\Delta T$  means a smaller impact for the process noise on the prediction performance. Therefore, a smaller  $\beta_{ad}$  will be provided to keep a stable estimation.

## 5.4 Performance evaluation in the simulation environment

Under the consideration of the safety reason for the actual flight tests, the simulations for the proposed localisation algorithm on the UAV have been conducted. In order to mock the actual focused application scenarios such as the water tank or pressure vessel, the operational space of the UAV in the simulation environment is set as  $1.95 \times 3.0 \times 2.3$  (m). All anchor nodes in the system are disposed on the same plane near the entrance of the water tank or pressure vessel to mock the situation that the anchor nodes can be disposed without human enter that

Table 5.1: Coordinates of the anchor nodes.

Coordinates	Anchor 1	Anchor 2	Anchor 3	Anchor 4
X	0.00m	1.95m	0.00m	1.95m
Y	0.00m	0.00m	0.00m	0.00m
Z	0.00m	0.00m	2.30m	2.30m

space. The coordinates of each anchor node are provided in Table 5.1. The UAV flight path in the simulation is set as a reverse “S”, which is to comprehensively evaluate the performance of the proposed algorithms. Same as the previous simulation, for each algorithm in the simulation, the position information of over 5000 points has been estimated which makes it can represent the actual performance of these algorithms and prove the effectiveness of the proposed algorithm. The STD for the measurement noise of the ranging information from the UWB sensor nodes is supposed to be a randomly changing value from 0m to 0.2m, which is to mock the changing measurement noise caused by the variation of the operational environment and communication condition between the sensor nodes in actual environment. In the simulation, the performance comparison within seven algorithms including the MLE based localisation algorithm, EKF, SRCKF, ASRCKF with constant weighting factors, AEKF and ASRCKF with adaptive weighting factors have been made to comprehensively validate the effectiveness before the actual flight tests. The simulation results, e.g. the flight trajectories of the each algorithm, the flight trajectories in X, Y, Z directions, the RMSE of each algorithm in X, Y, Z directions and the eCDF of each have been depicted in Fig. 5.3. Furthermore, in order to provide a clear view for the localisation performance of each algorithm, the detailed performance information for each including the median error, 95<sup>th</sup> percentile error and the average STD of the RMSE has also been provided in Table 5.2.

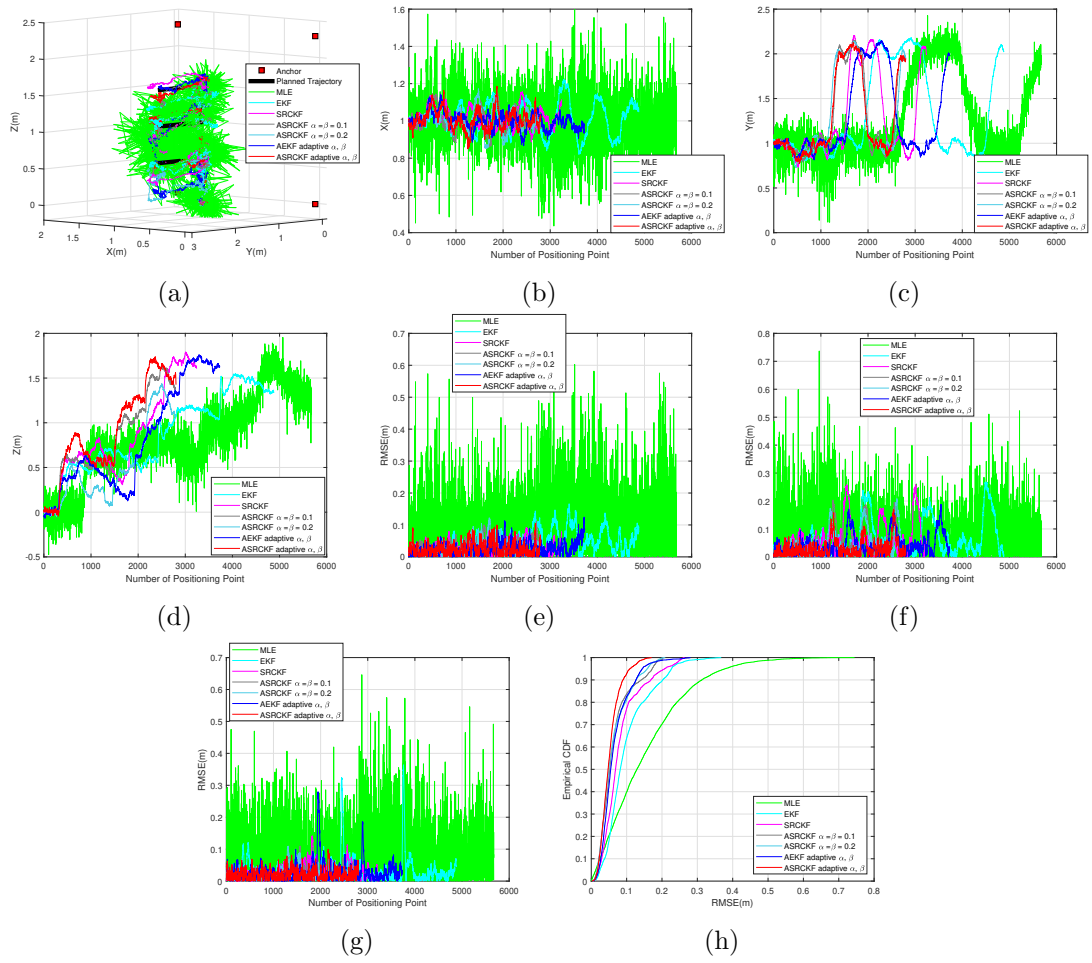


Figure 5.3: Simulation flight results for the SRCKF and ASRCKF with changing noise model. (a) 3D trajectories. (b) X direction trajectories. (c) Y direction trajectories. (d) Z direction trajectories. (e) X direction RMSE (m). (f) Y direction RMSE (m). (g) Z direction RMSE (m). (h) eCDF.

Obviously from the simulation results, the MLE based localisation algorithm holds the worst localisation performance due to the large measurement noise of the ranging information and the unreasonable value within it. With the integration of the IMU for the sensor fusion approaches such as the EKF, this performance influence is greatly reduced with 0.082m median error, 0.227m 95<sup>th</sup> percentile error and 0.063m average STD. However, the localisation performance is still limited by the neglected high order terms within the observation matrix and the

Table 5.2: Detailed simulation results for the SRCKF and ASRCKF based sensor fusion approaches with changing noise model

Algorithm	Median Error	Improved	95 <sup>th</sup> Error	Improved	Average STD	Improved
MLE	0.129m	N/A	0.380m	N/A	0.116m	N/A
EKF	0.082m	36.4%	0.227m	40.2%	0.063m	45.7%
SRCKF	0.069m	46.5%	0.208m	45.3%	0.054m	53.4%
ASRCKF	0.052m	59.7%	0.173m	54.5%	0.045m	61.2%
( $\alpha = \beta = 0.1$ )						
ASRCKF	0.050m	61.2%	0.160m	57.9%	0.042m	63.8%
( $\alpha = \beta = 0.2$ )						
AEKF	0.055m	57.4%	0.144m	62.1%	0.041m	64.7%
(adaptive weighting factors)						
ASRCKF	<b>0.047m</b>	<b>63.6%</b>	<b>0.110m</b>	<b>71.1%</b>	<b>0.028m</b>	<b>75.9%</b>
(adaptive weighting factors)						

manually adjusted and constant noise covariance matrices. To overcome these, leveraging the cubature rule, the state posterior mean and covariance can be approximated by the SRCKF for performance improvement, which successfully reduced the median error, 95<sup>th</sup> percentile error and average STD to 0.069m, 0.208m and 0.054m. Nevertheless, the SRCKF is still suffer from the performance influence led by the manually adjusted and constant noise covariance matrices. To remedy this, the adaptive sensor fusion based approach can be an ideal candidate. Here, two different adaptive sensor fusion approaches including the ASRCKF with constant weighting factors and the AEKF with the estimated weighting factors are tested and compared with the proposed ASRCKF algorithm with the adaptive weighting factors. Obviously, with the estimated noise covariance matrices for these adaptive sensor fusion based approaches, the localisation performance is

Chapter 5. UWB and IMU based SRCKF sensor fusion UAV positioning technology

significantly improved with the median error around 0.05m, the 95<sup>th</sup> percentile error around 0.160m and the average STD around 0.040m. Especially for the proposed ASRCKF algorithm, with the ability to deal with the linearisation issue for the observation matrix, the adaptively estimated noise covariance matrices and the estimated weighting factors, the best performance can be obtained by the proposed ASRCKF algorithm with the median error, 95<sup>th</sup> percentile error and average STD to be 0.047m, 0.110m and 0.028m, respectively. Compared with the MLE based localisation algorithm, these three indexes are improved 63.6%, 71.1% and 75.9%, respectively. However, it still needs to declare that only the smaller constant weighting factors (0.1 and 0.2) selected here is under the consideration of the stability of the algorithm. Larger weighting factors means the estimation results for the noise covariance matrices will more rely on the current estimation results, which will lead more changes for the noise covariance matrices and may cause the filtering divergence. According to the simulation results, with the ASRCKF algorithm, when the weighting factors exceed 0.5, the probability for filtering divergence will be increased significantly. Even with the relatively smaller weighting factors (0.3 or 0.4), the filtering divergence still exists under certain circumstances. Since the primary objective for the UAV localisation system in extremely confined environment is to prevent any positioning failure, the relatively smaller weighting factors (0.1 and 0.2) are selected, the estimation results for the weighting factors of the proposed ASRCKF algorithm are limited within [0,0.2] and the initial value of these are set as 0.2.

## **5.5 Performance evaluation in the experiment environment**

### **5.5.1 Experiment setup**

For the purpose of further evaluating the performance of the SRCKF and ASRCKF based algorithm, the actual experiments in the laboratory environment have been conducted. Similarly, the localisation area for the actual experiments for these algorithms has the same size ( $1.95 \times 3.0 \times 2.3$  (m)) compared with the previous experiments, which is to mock the extremely confined environments. The geometry configuration for the anchor nodes also keep as the same on the X-Z plane to conform that the anchor nodes can be deployed without human access in such environment. The clear view about the laboratory experiment environment, geometry configuration of the anchor nodes and the components utilised in the system in this experiment have been provided in Fig. 5.4 and Fig. 5.5.

### **5.5.2 Performance evaluation for the SRCKF and ASRCKF based approach**

In the performance evaluation and comparison experiments, the markers are attached on the UAV to help the reference system to get the sub-millimeter accuracy position information for the UAV to serve as the ground truth. The planned path for the UAV in the experiments is the same as it in the simulations. All the algorithms including the MLE based localisation algorithm, EKF, SRCKF, ASRCKF with constant weighting factors ( $\alpha$  and  $\beta$  equal to 0.1 and 0.2), AEKF with adaptive weighting factors and the ASRCKF with adaptive weighting fac-

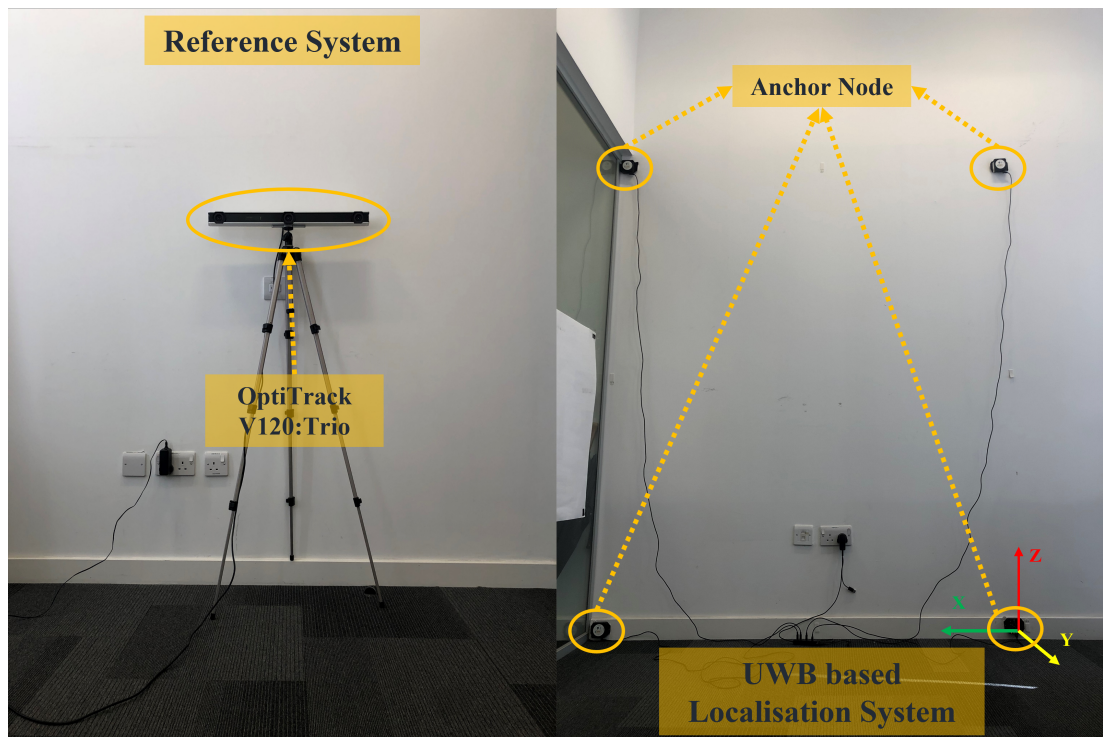


Figure 5.4: Laboratory experiment environment.

tors have been tested and evaluated. The trajectories, RMSE results and the detailed localisation error for each algorithm have been provided in Fig. 5.6 and Table 5.3.

When focused on the RMSE results in Fig. 5.6, it can be observed that the largest performance oscillation can be found for the MLE based algorithm, which is caused by the unreasonable value and the measurement noise within the ranging information from the UWB sensor nodes. This phenomenon can also be proved by the detailed localisation results in Table 5.3, where the worst localisation performance with 0.163m median error, 0.342m 95<sup>th</sup> percentile error and 0.083m average STD was recorded for the MLE based localisation algorithm. With the introduction of the additional IMU, this performance degradation led by the unreasonable value and the measurement noise can be limited. Clearly,

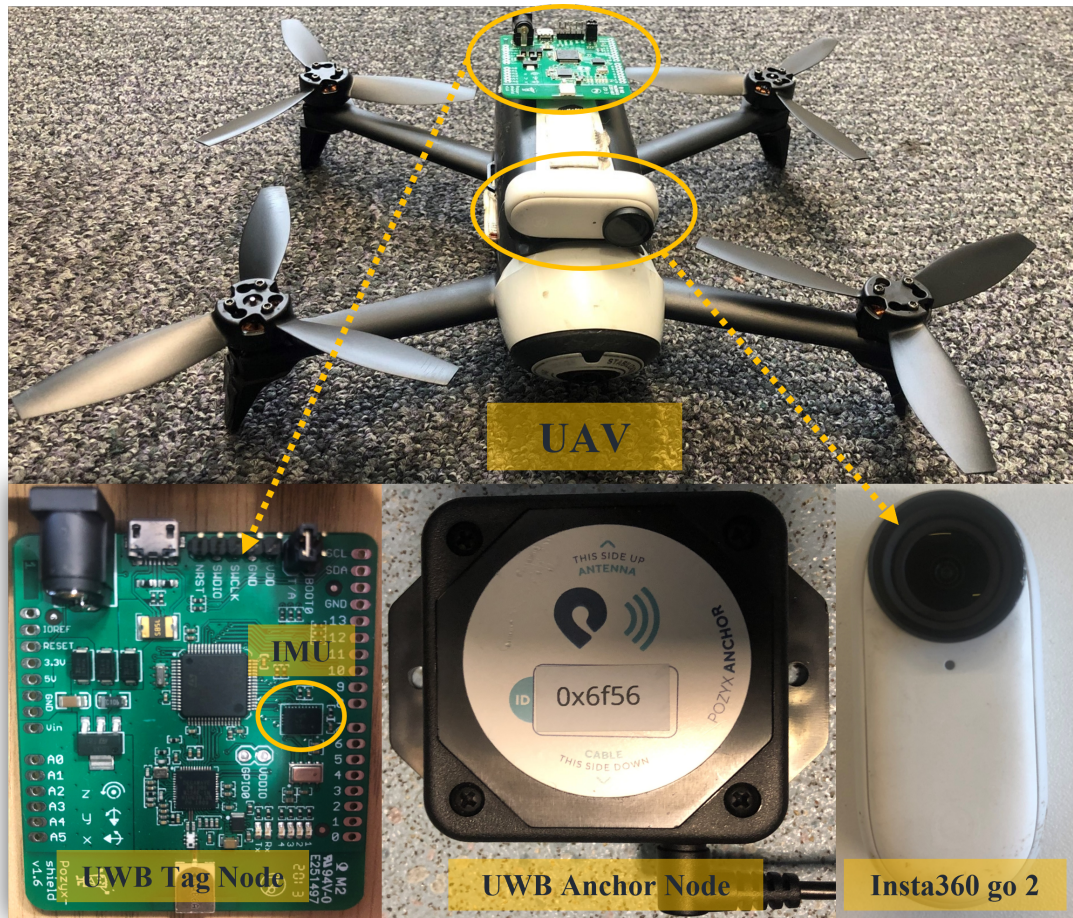


Figure 5.5: The UAV positioning system components.

for all the IMU and UWB based sensor fusion approaches, the median error, 95<sup>th</sup> percentile error and average STD are all limited within 0.15m, 0.29m and 0.08m, respectively. However, same as the simulations, the performance influence still exists for the EKF based sensor fusion approach due to the linearisation of the observation matrix and the unsuitable noise covariance matrices. Even, this influence can be successfully eliminated by the SRCKF with the cubature rule which attained the 0.121m median error, 0.223m 95<sup>th</sup> percentile error and 0.06m average STD. Yet, the influence from the unsuitable noise covariance matrices exists as before.

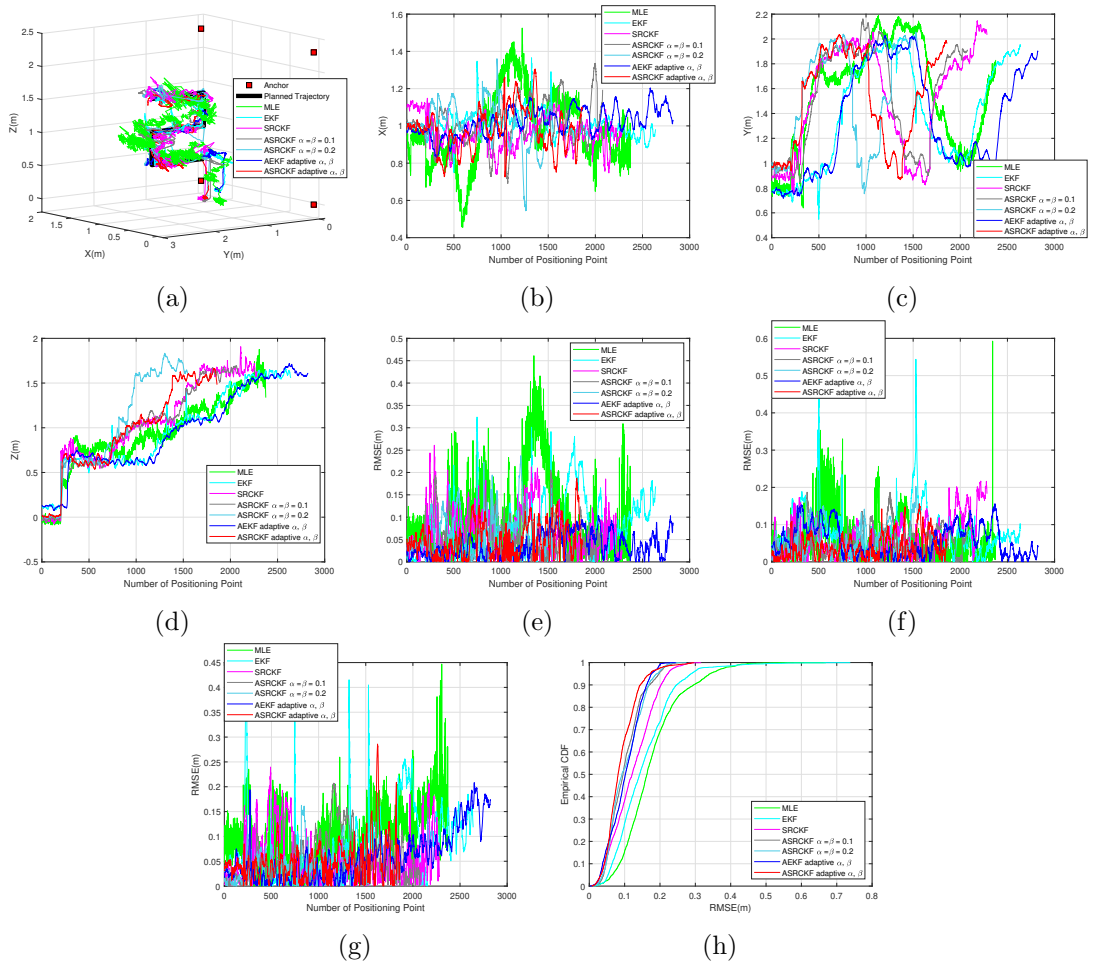


Figure 5.6: Experiment localisation results for the SRCKF based approaches. (a) 3D trajectories. (b) X direction trajectories. (c) Y direction trajectories. (d) Z direction trajectories. (e) X direction RMSE (m). (f) Y direction RMSE (m). (g) Z direction RMSE (m). (h) eCDF.

To further improve the localisation performance of the system under such circumstance, the adaptive Kalman filter (AKF) based methods can be an ideal candidate. Leveraging the adaptively estimated noise covariance matrices for the AEKF, ASRCKF with constant weighting factors and the proposed ASRCKF algorithm with adaptive weighting factors, the noise covariance matrices can be adaptively estimated to catch up the changes for the process and measurement noise within the system. According to the experiment results, the localisation

Table 5.3: Detailed experiment localisation results for the SRCKF based approaches

Algorithm	Median Error	Improved	95 <sup>th</sup> Error	Improved	Average STD	Improved
MLE	0.163m	N/A	0.342m	N/A	0.083m	N/A
EKF	0.143m	12.3%	0.287m	16.1%	0.080m	3.6%
SRCKF	0.121m	25.8%	0.223m	34.8%	0.060m	27.7%
ASRCKF ( $\alpha = \beta = 0.1$ )	0.095m	41.7%	0.198m	42.1%	0.048m	42.2%
ASRCKF ( $\alpha = \beta = 0.2$ )	0.092m	43.6%	0.194m	43.3%	0.049m	41.0%
AEKF (adaptive weighting factors)	0.102m	37.4%	0.176m	48.5%	0.046m	44.6%
<b>ASRCKF (adaptive weighting factors)</b>	<b>0.081m</b>	<b>50.3%</b>	<b>0.172m</b>	<b>49.7%</b>	<b>0.045m</b>	<b>45.8%</b>

performance for the system can be significantly improved with the median error, 95<sup>th</sup> percentile error and average STD around 0.1m, 0.18m and 0.047m, when compared with the EKF and SRCKF with constant and manually adjusted noise covariance matrices. When focused on the comparison within the adaptive approaches, with the ability to deal with the influence from the linearisation of the observation matrix, and the adaptively estimated weighting factors to limit the estimation of the noise covariance matrices to get rid of any potential filtering divergence and eliminate the performance oscillation, the best performance can be obtained by the proposed ASRCKF algorithm, which attained 50Hz position update rate, 0.081m median error, 0.172m 95<sup>th</sup> percentile error and 0.045m average STD.

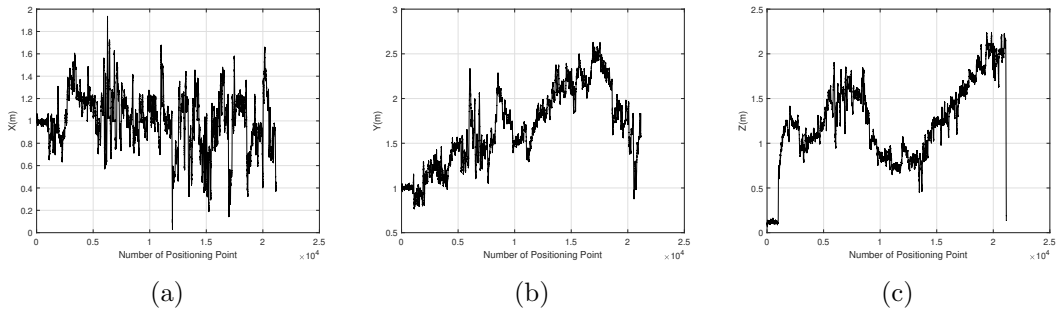


Figure 5.7: Flight trajectory for the ASRCKF based autonomous inspection. (a) Trajectory in X(m) direction in the autonomous inspection flight test. (b) Trajectory in Y(m) direction in the autonomous inspection flight test. (c) Trajectory in Z(m) direction in the autonomous inspection flight test.

### 5.5.3 Autonomous inspection flight test

Considering the focused applications are the autonomous inspection in the extremely confined environments. Thus, in order to comprehensively verify the practicality of the proposed UAV positioning system and the proposed ASRCKF based algorithm for the focused applications, the autonomous inspection flight test has been carried out. Different from the previous experiments, the path of the UAV for this test is from the path planning algorithm, which is to cover the entire localisation area for detailed inspection. The video for this flight test can be found in Appendix B. The UAV trajectories for the test have been given and depicted in Fig. 5.7. It needs to declare that, due to the complexity of the calculated path, the measured position information from the current reference system may be significantly influenced, considering only three cameras exist for the current utilised reference system. Therefore, the ground truth for this test is not provided.

## 5.6 Summary

In this chapter, an ASRCKF based UAV positioning algorithm has been proposed focused on the autonomous inspection in GPS-denied and extremely confined environments. Firstly, introduction and discussion about the EKF, AEKF and TC-AEKF based algorithms in the previous chapter have been provided to illustrate the existing issues such as the performance influence led by the unreasonable value within the ranging information, the linearisation of the observation matrix and the unknown and hard-to-adjust noise covariance matrices. Followed by, in order to remedy the performance influence from the linearisation of the observation matrix, the SRCKF based sensor fusion approach has been introduced. The detailed description about the state prediction and observation correction process for the SRCKF have been provided. Leveraging the cubature rule, the approximation for the state posterior mean and covariance can be obtained to substitute the linearisation process for performance improvement. However, the unknown and hard-to-adjust noise covariance matrices still needs to be taken into account. Therefore, the ASRCKF based sensor fusion algorithm has been presented. Leveraging the integration with IMU, the cubature rule, the adaptively estimated noise covariance matrices and the added estimation weighting factors, all the aforementioned issues can be solved for reliable, high precision and high accuracy positioning of the UAV in focused environments. Finally, numerical simulations and experiments have been carried out to prove the effectiveness of the proposed algorithm. Judging from the results, the proposed ASRCKF algorithm is able to remedy the existing issues and attain the high accuracy and precision performance with 0.081m median error, 0.172m 95<sup>th</sup> percentile error and 0.045m

Chapter 5. UWB and IMU based SRCKF sensor fusion UAV positioning technology

average STD, which is capable for the autonomous inspection in the extremely confined environments. For further confirmation, the autonomous inspection experiment has also been conducted in the mocked extremely confined environment in the laboratory. In summary, the proposed algorithm and system are feasible for the low cost autonomous inspection in the focused environments.

## Chapter 6

# Conclusion and future work

### 6.1 Conclusions of the research

In this thesis, in order to achieve the high accuracy, high precision, high update rate, reliable, low computational complexity and low cost UAV positioning for the autonomous inspection in GPS-denied and extremely confined environments, the investigation on the UWB based UAV localisation technologies and approaches has been made.

Firstly, the comprehensive overview for the existing RF based localisation technologies and the classical localisation mechanisms has been provided help to identify the research questions, the potential solutions and establish the evaluation framework to validate the performance of the RF based UAV positioning system. The overview for the existing UAV platforms has also been provided to find the suitable one for the focused applications.

Afterwards, the investigation on the pure UWB based UAV localisation tech-

nology has been made, which including the research on the MLE based positioning algorithm for the accurate UAV localisation with the pure UWB based technology, and the anchor distribution strategy help to find the suitable geometry configurations of the anchor nodes in different environments. However, due to the existing unreasonable value within the ranging information from the UWB sensor nodes, the localisation performance of the pure UWB based approach is greatly limited. Considering the performance influence from these unreasonable values is not a long lasting influence, thus, for traditional applications such as the positioning of the human or unmanned ground vehicle (UGV), this performance oscillation can be ignored directly. Nevertheless, according to the comprehensive overview and the established evaluation framework in Chapter 2, for UAV applications, even the short time performance oscillation can still lead to the unstable flight of the UAV, and may even cause the crash.

Therefore, in order to limit the influence from the unreasonable value and increase the position update rate, in the following two chapters, the investigation on the IMU and UWB based sensor fusion approach has been conducted. Owing to the characteristics of the EKF based algorithm, including the implementation simplicity, low computational complexity and acceptable accuracy, lots of researches have already been carried out. Yet, the performance limitation leads by the manually adjusted and constant covariance matrices and the drift from the IMU measurements still exists. In order to remedy these issues, in Chapter 4, the AEKF and the TC-AEKF based sensor fusion algorithms were proposed. With the ability to adaptively estimate the noise covariance matrices and the additional weighting factors, the proposed methods significantly improved the UAV positioning performance. The performance influence caused by the drift

from the IMU measurements has also been successfully limited by the additional angular rate considered in the state prediction process. Nevertheless, since the nonlinearity of the transfer matrix for these three EKF based approaches, the first order Taylor expansion is applied. This may lead to the performance degradation caused by the neglected high order terms.

Hence, the researches on the SRCKF and ASRCKF based sensor fusion algorithms have been carried out in Chapter 5. With the utilisation of the cubature rule, the adaptively estimated noise covariance matrices and the added estimation weighting factors, the performance degradation and oscillation led by the unreasonable value within the ranging information from UWB sensor nodes, the linearisation of the observation matrix and the unknown and hard to adjust noise covariance matrices can be resolved by the proposed ASRCKF algorithm. According to the simulation and experiment results, the proposed approach can significantly improve the UAV positioning performance in focused environments.

In summary, the proposed algorithms and developed system are feasible for the low cost UAV based autonomous inspection in GPS-denied and extremely confined environments.

## 6.2 Contributions to knowledge

In this thesis, a number of developments have been made to advance the state-of-the-art UAV positioning approaches for the autonomous inspection in GPS-denied and extremely confined environments. In the following, the summary for the major contributions to knowledge in this area are provided:

- **Comprehensive overview and discussion for the RF based UAV positioning technologies.** In this thesis, a comprehensive overview for the existing RF based UAV localisation systems with different radio communication protocols has been provided. The pros and cons of each has been discussed to highlight the suitability and challenges on UAV positioning. Meanwhile, a detailed survey and discussion for the classical localisation mechanisms with the existing RF based UAV localisation technologies have been provided to analyse the possibility and suitability on precise UAV positioning in GPS-denied environments. In addition, an evaluation framework has been established to provide an overall consideration and rational estimation on KPIs of UAV positioning with RF based localisation technologies in GPS-denied environments. Finally, in order to provide a clear guidance for further research, an in-depth discussion and generalisation have been given for the research challenges and potential issues on UAV localisation with RF based technologies in GPS-denied environments.
- **Pure UWB based localisation system.** In order to deal with the existing issues for the existing localisation technologies, such as the performance influence from the different illumination conditions, the extremely high system cost, the error accumulation, the high energy consumption and the size and weight of the components, the pure UWB based localisation system has been designed and implemented. Within it, the MLE based localisation algorithm and the anchor distribution strategy have been presented to achieve the high accuracy and precision UAV positioning in GPS-denied and extremely confined environments, and to find the most suitable geometry configuration of fixed anchor nodes to keep the high level performance.

- **Adaptive EKF based sensor fusion algorithm.** In order to remedy the performance oscillation leads by the unreasonable value within the UWB measurements and the manually adjusted and constant noise covariance matrices, an AEKF based UAV positioning algorithm has been presented, focusing on the robust and high precision localisation. With the adaptively estimated noise covariance matrices and the additional weighting factors, the proposed approach can significantly improve the UAV localisation performance and the stability in extremely confined environments. Compared with the presented MLE based localisation algorithm in Section 3.2 and the state-of-the-art sensor fusion based approaches, the proposed AEKF algorithm outperforms all these approaches and is feasible for the robust and high precision UAV positioning in focused environments.
- **Tightly Coupled Adaptive EKF based sensor fusion algorithm.** For the purpose of dealing with the performance degradation and oscillation caused by the magnetometer on the IMU and the variation of the operational environment, a TC-AEKF based sensor fusion algorithm has been proposed for high accuracy, precision and robust localisation of UAV in GPS-denied and extremely confined environments. Compared with the traditional loosely coupled sensor fusion approaches, the performance degradation and oscillation can be limited with the additional angular rate considered in the state prediction process and the adaptively estimated noise covariance matrices. Finally, from the evaluation results, it can be proved that the proposed approach significantly elevate the UAV localisation performance in focused environments and outperforms the presented MLE based localisation algorithm in Section 3.2, the traditional loosely coupled sen-

sensor fusion approaches and the proposed loosely coupled AEKF approach in Section 4.5.

- **Adaptive SRCKF based sensor fusion algorithm.** To get rid of the performance influence from the linearisation of the observation matrix, in this thesis, an ASRCKF based sensor fusion algorithm has been proposed for the reliable, high accuracy and high precision UAV positioning in focused environments. Compared with the traditional KF based approaches, the performance degradation, oscillation and potential positioning failure caused by the linearisation of the observation matrix and the unsuitable noise covariance matrices can be significantly improved and eliminated. Furthermore, the estimation of the noise covariance matrices is limited by the additional adaptively estimated weighting factors to prevent the potential filtering divergence for more reliable UAV positioning. Finally, comprehensive simulations, experiments and actual flight tests in the laboratory environment have been conducted to validate the performance of the proposed algorithm and system. According to the results, the presented system and algorithm are able to attain a high level localisation performance of the UAV with the 0.081m median error, 0.172m 95<sup>th</sup> percentile error and 0.045m average STD and achieve the autonomous inspection in focused environments.

### 6.3 Recommendation of future work

Even the high accuracy, precision and reliable UAV positioning in GPS-denied and extremely confined environments can be obtained by the proposed algorithms plus with the developed UAV positioning system. However, the limitations still

exists for the proposed algorithms which may restrict the localisation performance and limit the application scenarios.

Firstly, for all the proposed algorithms, the fixed anchor nodes are the basic requirements for the UAV positioning which may restrict the application scenarios of the system. Even the analysis for the geometry configurations of the anchor nodes has been made, however, enough number of the anchor nodes is still needed. This restriction refers to the second research challenge of the RF based UAV positioning system in Section 2.6.2. Therefore, in order to deal with this issue, the relative UAV positioning with the UAV swarm and the self-localisation of the anchor node can be the ideal candidates. For the future research, the investigation on the UAV swarm based relative positioning will be carried out. With the relative distance information between the UWB tag node on each UAV, the formation control of the swarm and the relative positioning is able to be achieved. Furthermore, for the other potential solution, the anchor self-localisation. For this approach, the localisation process can be divided into two parts, including the offline phase and online phase. During the offline phase, the localisation of the anchor node can be conducted. With the participation of the other localisation technologies such as the vision based approach, or the additional communication between each anchor node, the self-localisation can be achieved, which will also be the future research direction.

Secondly, the increased computational complexity still has the great influence on the position update rate of the system. For the proposed ASRCKF algorithm, even the performance influence from the linearisation of the observation matrix and the unsuitable noise covariance matrices can be significantly eliminated.

However, this is at the expense of the computational complexity. According to the experiment results, the position update rate for the ASRCKF based algorithm is around 50Hz, which is decreased 43%. If the tightly coupled ASRCKF based algorithm is utilised, the position update rate is further decreased below 20Hz. As declared in the evaluation framework, the position update rate is one of the KPIs to evaluate the performance of the RF based UAV positioning system. Thus, the research on how to increase the position update rate or reduce the computational complexity will be conducted in the future. This restriction still belongs to the first research challenge in Section 2.6.1 which known as the performance influence from the unreasonable value.

Finally, rule out of the accurate and precise positioning of the UAV, for the autonomous inspection in GPS-denied and extremely confined environments, the smart path planning is also required for the collision avoidance and the efficient inspection. Hence, the research on the smart path planning algorithm will be carried out in the future.

## Appendix A

# TC-AEKF based autonomous inspection

The video associated with the autonomous inspection flight test for the TC-AEKF algorithm, as detailed in Section 4.5 and Section 4.7, is available in the following URL:

<https://youtu.be/6HjTTZuNQhE>

## Appendix B

# ASRCKF based autonomous inspection

The video associated with the autonomous inspection flight test for the ASRCKF algorithm, as detailed in Section 5.3 and Section 5.5.3, is available in the following URL:

<https://youtu.be/KNKibl3Lqog>

# Bibliography

- [1] L. Yu, E. Yang, P. Ren, C. Luo, G. Dobie, D. Gu, and X. Yan, “Inspection robots in oil and gas industry: a review of current solutions and future trends,” in *2019 25th International Conference on Automation and Computing (ICAC)*. IEEE, 2019, pp. 1–6.
- [2] A. Ranjan, H. Sahu, P. Misra, and B. Panigrahi, “Leveraging unmanned aerial vehicles in mining industry: Research opportunities and challenges,” in *Unmanned Aerial Vehicles in Smart Cities*. Springer, 2020, pp. 107–132.
- [3] G. Ma, Z. Tong, M. Tong, and S. Tang, “Coordinated control of uavs for mine searching,” in *2018 Eighth International Conference on Instrumentation & Measurement, Computer, Communication and Control (IMCCC)*. IEEE, 2018, pp. 259–263.
- [4] L. Piercy, “Could drones save cows? why uk research team thinks so,” <https://news.ca.uky.edu/article/could-drones-save-cows-why-uk-research-team-thinks-so>, accessed October 01, 2022.
- [5] T. M. Fernández-Caramés, O. Blanco-Novoa, I. Froiz-Míguez, and P. Fraga-Lamas, “Towards an autonomous industry 4.0 warehouse: A uav and blockchain-based system for inventory and traceability applications in big

## Bibliography

- data-driven supply chain management,” *Sensors*, vol. 19, no. 10, p. 2394, 2019.
- [6] J. Tiemann and C. Wietfeld, “Scalable and precise multi-uav indoor navigation using tdoa-based uwb localization,” in *2017 International Conference on Indoor Positioning and Indoor Navigation (IPIN)*. IEEE, 2017, pp. 1–7.
- [7] Flyability. Elios 2—Indoor Drone for Confined Space Inspections. [Online]. Available: <https://www.flyability.com/elios-2>
- [8] J. Nikolic, M. Burri, J. Rehder, S. Leutenegger, C. Huerzeler, and R. Siegwart, “A uav system for inspection of industrial facilities,” in *2013 IEEE Aerospace Conference*. IEEE, 2013, pp. 1–8.
- [9] S. S. Mansouri, C. Kanellakis, G. Georgoulas, and G. Nikolakopoulos, “Towards mav navigation in underground mine using deep learning,” in *2018 IEEE International Conference on Robotics and Biomimetics (ROBIO)*. IEEE, 2018, pp. 880–885.
- [10] C. Kanellakis, P. S. Karvelis, S. S. Mansouri, A.-A. Agha-Mohammadi, and G. Nikolakopoulos, “Towards autonomous aerial scouting using multi-rotors in subterranean tunnel navigation,” *IEEE Access*, vol. 9, pp. 66 477–66 485, 2021.
- [11] Y. Li, Z. He, Z. Gao, Y. Zhuang, C. Shi, and N. El-Sheimy, “Toward robust crowdsourcing-based localization: A fingerprinting accuracy indicator enhanced wireless/magnetic/inertial integration approach,” *IEEE Internet of Things Journal*, vol. 6, no. 2, pp. 3585–3600, 2018.

## Bibliography

- [12] N. Ahmad, R. A. R. Ghazilla, N. M. Khairi, and V. Kasi, “Reviews on various inertial measurement unit (imu) sensor applications,” *International Journal of Signal Processing Systems*, vol. 1, no. 2, pp. 256–262, 2013.
- [13] C. Ren, Q. Liu, and T. Fu, “A novel self-calibration method for mimu,” *IEEE Sensors Journal*, vol. 15, no. 10, pp. 5416–5422, 2015.
- [14] N. Bai, Y. Tian, Y. Liu, Z. Yuan, Z. Xiao, and J. Zhou, “A high-precision and low-cost imu-based indoor pedestrian positioning technique,” *IEEE Sensors Journal*, vol. 20, no. 12, pp. 6716–6726, 2020.
- [15] Y. You and C. Wu, “Hybrid indoor positioning system for pedestrians with swinging arms based on smartphone imu and rssi of ble,” *IEEE Transactions on Instrumentation and Measurement*, vol. 70, pp. 1–15, 2021.
- [16] R. Ali, R. Liu, A. Nayyar, B. Qureshi, and Z. Cao, “Tightly coupling fusion of uwb ranging and imu pedestrian dead reckoning for indoor localization,” *IEEE Access*, vol. 9, pp. 164 206–164 222, 2021.
- [17] M. Robotics, “Marvelmind indoor navigation system operating manual,” 2017.
- [18] D. Kang and Y.-J. Cha, “Autonomous uavs for structural health monitoring using deep learning and an ultrasonic beacon system with geo-tagging,” *Computer-Aided Civil and Infrastructure Engineering*, vol. 33, no. 10, pp. 885–902, 2018.
- [19] M. Arifin, Y. Nazaruddin, T. Tamba, R. Santosa, and A. Widyotriatmo, “Experimental modeling of a quadrotor uav using an indoor local position-

## Bibliography

- ing system,” in *2018 5th International Conference on Electric Vehicular Technology (ICEVT)*. IEEE, 2018, pp. 25–30.
- [20] S. Zahran, A. M. Moussa, A. B. Sesay, and N. El-Sheimy, “A new velocity meter based on hall effect sensors for uav indoor navigation,” *IEEE Sensors Journal*, vol. 19, no. 8, pp. 3067–3076, 2018.
- [21] Y. Gu, A. Lo, and I. Niemegeers, “A survey of indoor positioning systems for wireless personal networks,” *IEEE Communications Surveys & Tutorials*, vol. 11, no. 1, pp. 13–32, 2009.
- [22] S. Kuutti, S. Fallah, K. Katsaros, M. Dianati, F. Mccullough, and A. Mouzakitis, “A survey of the state-of-the-art localization techniques and their potentials for autonomous vehicle applications,” *IEEE Internet of Things Journal*, vol. 5, no. 2, pp. 829–846, 2018.
- [23] P. Petráček, V. Krátký, and M. Saska, “Dronument: System for reliable deployment of micro aerial vehicles in dark areas of large historical monuments,” *IEEE Robotics and Automation Letters*, vol. 5, no. 2, pp. 2078–2085, 2020.
- [24] T. Özaslan, G. Loianno, J. Keller, C. J. Taylor, V. Kumar, J. M. Wozencraft, and T. Hood, “Autonomous navigation and mapping for inspection of penstocks and tunnels with mavs,” *IEEE Robotics and Automation Letters*, vol. 2, no. 3, pp. 1740–1747, 2017.
- [25] T. Özaslan, G. Loianno, J. Keller, C. J. Taylor, and V. Kumar, “Spatio-temporally smooth local mapping and state estimation inside generalized

## Bibliography

- cylinders with micro aerial vehicles,” *IEEE Robotics and Automation Letters*, vol. 3, no. 4, pp. 4209–4216, 2018.
- [26] S. S. Mansouri, C. Kanellakis, D. Kominiak, and G. Nikolakopoulos, “Deploying mavs for autonomous navigation in dark underground mine environments,” *Robotics and Autonomous Systems*, vol. 126, p. 103472, 2020.
- [27] C. Luo, S. I. McClean, G. Parr, L. Teacy, and R. De Nardi, “Uav position estimation and collision avoidance using the extended kalman filter,” *IEEE Transactions on Vehicular Technology*, vol. 62, no. 6, pp. 2749–2762, 2013.
- [28] A. Masiero, F. Fissore, A. Guarnieri, F. Pirotti, and A. Vettore, “Uav positioning and collision avoidance based on rss measurements,” *The International Archives of Photogrammetry, Remote Sensing and Spatial Information Sciences*, vol. 40, no. 1, p. 219, 2015.
- [29] S. Goel, J. Gabela, A. Kealy, and G. Retscher, “An indoor-outdoor cooperative localization framework for uavs,” in *Proceedings of the International Global Navigation Satellite Systems (IGNSS) Conference*, 2018.
- [30] B. R. Stojkoska, J. Palikrushev, K. Trivodaliev, and S. Kalajdziski, “Indoor localization of unmanned aerial vehicles based on rssi,” in *IEEE EUROCON 2017-17th International Conference on Smart Technologies*. IEEE, 2017, pp. 120–125.
- [31] D. Vasisht, S. Kumar, and D. Katabi, “Decimeter-level localization with a single wifi access point,” in *13th USENIX Symposium on Networked Systems Design and Implementation (NSDI 16)*, 2016, pp. 165–178.

## Bibliography

- [32] M. Kotaru, K. Joshi, D. Bharadia, and S. Katti, “Spotfi: Decimeter level localization using wifi,” in *Proceedings of the 2015 ACM Conference on Special Interest Group on Data Communication*, 2015, pp. 269–282.
- [33] S. Li, M. Hedley, K. Bengston, M. Johnson, D. Humphrey, A. Kajan, and N. Bhaskar, “Tdoa-based passive localization of standard wifi devices,” in *2018 Ubiquitous Positioning, Indoor Navigation and Location-Based Services (UPINLBS)*. IEEE, 2018, pp. 1–5.
- [34] C. Xiang, S. Zhang, S. Xu, X. Chen, S. Cao, G. C. Alexandropoulos, and V. K. Lau, “Robust sub-meter level indoor localization with a single wifi access point—regression versus classification,” *IEEE Access*, vol. 7, pp. 146 309–146 321, 2019.
- [35] C. Chen, Y. Chen, Y. Han, H.-Q. Lai, and K. R. Liu, “Achieving centimeter-accuracy indoor localization on wifi platforms: A frequency hopping approach,” *IEEE Internet of Things Journal*, vol. 4, no. 1, pp. 111–121, 2016.
- [36] F. Zhao, T. Huang, and D. Wang, “A probabilistic approach for wifi fingerprint localization in severely dynamic indoor environments,” *IEEE Access*, vol. 7, pp. 116 348–116 357, 2019.
- [37] W. Sun, M. Xue, H. Yu, H. Tang, and A. Lin, “Augmentation of fingerprints for indoor wifi localization based on gaussian process regression,” *IEEE Transactions on Vehicular Technology*, vol. 67, no. 11, pp. 10 896–10 905, 2018.
- [38] X. Guo, N. R. Elikplim, N. Ansari, L. Li, and L. Wang, “Robust wifi localization by fusing derivative fingerprints of rss and multiple classifiers,”

## Bibliography

- IEEE Transactions on Industrial Informatics*, vol. 16, no. 5, pp. 3177–3186, 2019.
- [39] Y. Shu, Y. Huang, J. Zhang, P. Coué, P. Cheng, J. Chen, and K. G. Shin, “Gradient-based fingerprinting for indoor localization and tracking,” *IEEE Transactions on Industrial Electronics*, vol. 63, no. 4, pp. 2424–2433, 2015.
- [40] L. Li, X. Guo, N. Ansari, and H. Li, “A hybrid fingerprint quality evaluation model for wifi localization,” *IEEE Internet of Things Journal*, vol. 6, no. 6, pp. 9829–9840, 2019.
- [41] Wikipedia, “Bluetooth low energy,” [https://en.wikipedia.org/wiki/Bluetooth\\_Low\\_Energy](https://en.wikipedia.org/wiki/Bluetooth_Low_Energy), [Online; accessed October 04, 2022].
- [42] M. Zhou, J. Lin, S. Liang, W. Du, and L. Cheng, “A uav patrol system based on bluetooth localization,” in *2017 2nd Asia-Pacific Conference on Intelligent Robot Systems (ACIRS)*. IEEE, 2017, pp. 205–209.
- [43] P. R. Soria, A. F. Palomino, B. Arrue, and A. Ollero, “Bluetooth network for micro-uavs for communication network and embedded range only localization,” in *2017 International Conference on Unmanned Aircraft Systems (ICUAS)*. IEEE, 2017, pp. 747–752.
- [44] M. Coppola, K. McGuire, K. Scheper, and G. de Croon, “On-board bluetooth-based relative localization for collision avoidance in micro air vehicle swarms,” *arXiv preprint arXiv*, vol. 1609, 2016.
- [45] F. Schwiegelshohn, P. Wehner, F. Werner, D. Gohringer, and M. Hubner, “Enabling indoor object localization through bluetooth beacons on the radio robot platform,” in *2016 International Conference on Embedded Com-*

## Bibliography

- puter Systems: Architectures, Modeling and Simulation (SAMOS)*. IEEE, 2016, pp. 328–333.
- [46] A. N. Raghavan, H. Ananthapadmanaban, M. S. Sivamurugan, and B. Ravindran, “Accurate mobile robot localization in indoor environments using bluetooth,” in *2010 IEEE International Conference on Robotics and Automation (ICRA)*. IEEE, 2010, pp. 4391–4396.
- [47] A. Inc, “ios: Understanding ibeacon,” <http://support.apple.com/kb/HT6048>, retrieved August 17, 2022.
- [48] M. S. Aman, H. Jiang, C. Quint, K. Yelamathi, and A. Abdelgawad, “Reliability evaluation of ibeacon for micro-localization,” in *2016 IEEE 7th Annual Ubiquitous Computing, Electronics & Mobile Communication Conference (UEMCON)*. IEEE, 2016, pp. 1–5.
- [49] F. Zafari, I. Papapanagiotou, M. Devetsikiotis, and T. Hacker, “An ibeacon based proximity and indoor localization system,” *arXiv preprint arXiv:1703.07876*, 2017.
- [50] Nokia, “High accuracy positioning,” <https://www.dac.nokia.com/applications/high-accuracy-positioning/>, retrieved August 17, 2022.
- [51] Qualcomm, “Gimbal webpage,” <https://gimbal.com/beacons/>, retrieved August 17, 2022.
- [52] P. Baronti, P. Pillai, V. W. Chook, S. Chessa, A. Gotta, and Y. F. Hu, “Wireless sensor networks: A survey on the state of the art and the 802.15.4 and zigbee standards,” *Computer Communications*, vol. 30, no. 7, pp. 1655–1695, 2007.

## Bibliography

- [53] S. C. Ergen, “Zigbee/ieee 802.15. 4 summary,” *UC Berkeley, September*, vol. 10, no. 17, p. 11, 2004.
- [54] L. Yu, Q. Fei, and Q. Geng, “Combining zigbee and inertial sensors for quadrotor uav indoor localization,” in *2013 10th IEEE International Conference on Control and Automation (ICCA)*. IEEE, 2013, pp. 1912–1916.
- [55] K. Chawla, C. McFarland, G. Robins, and W. Thomason, “An accurate real-time rfid-based location system,” *International Journal of Radio Frequency Identification Technology and Applications*, vol. 5, no. 1, pp. 48–76, 2018.
- [56] RFID4u, “How to select a correct rfid tag – passive vs. active,” <https://rfid4u.com/rfid-basics-resources/how-to-select-a-correct-rfid-tag-passive-vs-active/>, retrieved August 17, 2022.
- [57] J. Zhang, X. Wang, Z. Yu, Y. Lyu, S. Mao, S. C. Periaswamy, J. Patton, and X. Wang, “Robust rfid based 6-dof localization for unmanned aerial vehicles,” *IEEE Access*, vol. 7, pp. 77 348–77 361, 2019.
- [58] J. Zhang, Z. Yu, X. Wang, Y. Lyu, S. Mao, S. C. Periaswamy, J. Patton, and X. Wang, “Rfhui: An rfid based human-unmanned aerial vehicle interaction system in an indoor environment,” *Digital Communications and Networks*, vol. 6, no. 1, pp. 14–22, 2020.
- [59] J. S. Choi, B. R. Son, H. K. Kang, and D. H. Lee, “Indoor localization of unmanned aerial vehicle based on passive uhf rfid systems,” in *2012 9th international conference on ubiquitous robots and ambient intelligence (URAI)*. IEEE, 2012, pp. 188–189.

## Bibliography

- [60] M. Longhi, Z. Taylor, M. Popović, J. Nieto, G. Marrocco, and R. Siegwart, “Rfid-based localization for greenhouses monitoring using mavs,” in *2018 IEEE-APS Topical Conference on Antennas and Propagation in Wireless Communications (APWC)*. IEEE, 2018, pp. 905–908.
- [61] M.-G. Di Benedetto, *UWB communication systems: a comprehensive overview*. Hindawi Publishing Corporation, 2006, vol. 5.
- [62] H. Lücken, “Communication and localization in uwb sensor networks,” Ph.D. dissertation, Department of Information Technology and Electrical Engineering, Eidgenössische Technische Hochschule Zürich, 2013.
- [63] K. Guo, Z. Qiu, C. Miao, A. H. Zaini, C.-L. Chen, W. Meng, and L. Xie, “Ultra-wideband-based localization for quadcopter navigation,” *Unmanned Systems*, vol. 4, no. 01, pp. 23–34, 2016.
- [64] J. Li, Y. Bi, K. Li, K. Wang, F. Lin, and B. M. Chen, “Accurate 3d localization for mav swarms by uwb and imu fusion,” in *2018 IEEE 14th International Conference on Control and Automation (ICCA)*. IEEE, 2018, pp. 100–105.
- [65] T. M. Nguyen, A. H. Zaini, K. Guo, and L. Xie, “An ultra-wideband-based multi-uav localization system in gps-denied environments,” in *2016 International Micro Air Vehicles Conference*, 2016.
- [66] M. Strohmeier, T. Walter, J. Rothe, and S. Montenegro, “Ultra-wideband based pose estimation for small unmanned aerial vehicles,” *IEEE Access*, vol. 6, pp. 57 526–57 535, 2018.

## Bibliography

- [67] J. Tiemann, F. Schweikowski, and C. Wietfeld, “Design of an uwb indoor-positioning system for uav navigation in gnss-denied environments,” in *2015 International Conference on Indoor Positioning and Indoor Navigation (IPIN)*. IEEE, 2015, pp. 1–7.
- [68] N. Macoir, J. Bauwens, B. Jooris, B. Van Herbruggen, J. Rossey, J. Hoebeke, and E. De Poorter, “Uwb localization with battery-powered wireless backbone for drone-based inventory management,” *Sensors*, vol. 19, no. 3, p. 467, 2019.
- [69] W. You, F. Li, L. Liao, and M. Huang, “Data fusion of uwb and imu based on unscented kalman filter for indoor localization of quadrotor uav,” *IEEE Access*, vol. 8, pp. 64 971–64 981, 2020.
- [70] Z. Shi, H. Li, H. Lin, and L. Huang, “A nano-quadcopter formation flight system based on uwb indoor positioning technology,” in *2018 13th International Conference on Computer Science & Education (ICCSE)*. IEEE, 2018, pp. 1–4.
- [71] K. Guo, Z. Qiu, W. Meng, L. Xie, and R. Teo, “Ultra-wideband based cooperative relative localization algorithm and experiments for multiple unmanned aerial vehicles in gps denied environments,” *International Journal of Micro Air Vehicles*, vol. 9, no. 3, pp. 169–186, 2017.
- [72] K. Guo, Z. Qiu, W. Meng, T. M. Nguyen, and L. Xie, “Relative localization for quadcopters using ultrawideband sensors,” in *Proceedings of International Micro Air Vehicle Competition and Conference (IMAV), 2016*, 2016, pp. 243–248.

## Bibliography

- [73] Z. Han, K. Guo, L. Xie, and Z. Lin, “Integrated relative localization and leader–follower formation control,” *IEEE Transactions on Automatic Control*, vol. 64, no. 1, pp. 20–34, 2018.
- [74] K. Guo, X. Li, and L. Xie, “Ultra-wideband and odometry-based cooperative relative localization with application to multi-uav formation control,” *IEEE Transactions on Cybernetics*, vol. 50, no. 6, pp. 2590–2603, 2019.
- [75] —, “Simultaneous cooperative relative localization and distributed formation control for multiple uavs,” *Science China Information Sciences*, vol. 63, no. 1, pp. 1–3, 2020.
- [76] K. Guo, D. Han, and L. Xie, “Range-based cooperative localization with single landmark,” in *2017 13th IEEE International Conference on Control & Automation (ICCA)*. IEEE, 2017, pp. 588–593.
- [77] S. Cao, Y. Zhou, D. Yin, and J. Lai, “Uwb based integrated communication and positioning system for multi-uavs close formation,” in *2018 International Conference on Mechanical, Electronic, Control and Automation Engineering (MECAE 2018)*. Atlantis Press, 2018.
- [78] F. Lazzari, A. Buffi, P. Nepa, and S. Lazzari, “Numerical investigation of an uwb localization technique for unmanned aerial vehicles in outdoor scenarios,” *IEEE Sensors Journal*, vol. 17, no. 9, pp. 2896–2903, 2017.
- [79] F. J. Perez-Grau, F. Caballero, L. Merino, and A. Viguria, “Multi-modal mapping and localization of unmanned aerial robots based on ultra-wideband and rgb-d sensing,” in *2017 IEEE/RSJ International Conference on Intelligent Robots and Systems (IROS)*. IEEE, 2017, pp. 3495–3502.

## Bibliography

- [80] T.-M. Nguyen, T. H. Nguyen, M. Cao, Z. Qiu, and L. Xie, “Integrated uwb-vision approach for autonomous docking of uavs in gps-denied environments,” in *2019 International Conference on Robotics and Automation (ICRA)*. IEEE, 2019, pp. 9603–9609.
- [81] J. Tiemann, A. Ramsey, and C. Wietfeld, “Enhanced uav indoor navigation through slam-augmented uwb localization,” in *2018 IEEE International Conference on Communications Workshops (ICC Workshops)*. IEEE, 2018, pp. 1–6.
- [82] R. De Maesschalck, D. Jouan-Rimbaud, and D. L. Massart, “The mahalanobis distance,” *Chemometrics and Intelligent Laboratory Systems*, vol. 50, no. 1, pp. 1–18, 2000.
- [83] R. Mur-Artal, J. M. M. Montiel, and J. D. Tardos, “Orb-slam: a versatile and accurate monocular slam system,” *IEEE Transactions on Robotics*, vol. 31, no. 5, pp. 1147–1163, 2015.
- [84] R. Mur-Artal and J. D. Tardós, “Orb-slam2: An open-source slam system for monocular, stereo, and rgb-d cameras,” *IEEE Transactions on Robotics*, vol. 33, no. 5, pp. 1255–1262, 2017.
- [85] R. F. Brena, J. P. García-Vázquez, C. E. Galván-Tejada, D. Muñoz-Rodríguez, C. Vargas-Rosales, and J. Fangmeyer, “Evolution of indoor positioning technologies: A survey,” *Journal of Sensors*, vol. 2017, 2017.
- [86] A. Goldsmith, *Wireless Communications*. Cambridge University Press, 2005.

## Bibliography

- [87] L. Cheng, C.-d. Wu, Y.-z. Zhang, and Y. Wang, “An indoor localization strategy for a mini-uav in the presence of obstacles,” *International Journal of Advanced Robotic Systems*, vol. 9, no. 4, p. 153, 2012.
- [88] I. O. Tovkach, O. S. Neuimin, and S. Y. Zhuk, “Filtration of parameters of the uav movement based on the rss-measurement at the unknown power of the transmitter,” in *2018 14th International Conference on Advanced Trends in Radioelectronics, Telecommunications and Computer Engineering (TCSET)*. IEEE, 2018, pp. 57–60.
- [89] T. Pavlenko, M. Schütz, Y. Dobrev, and M. Vossiek, “Design of sparse dome antenna array for angle of arrival localization systems,” in *2019 13th European Conference on Antennas and Propagation (EuCAP)*. IEEE, 2019, pp. 1–4.
- [90] T. Pavlenko, M. Schütz, M. Vossiek, T. Walter, and S. Montenegro, “Wireless local positioning system for controlled uav landing in gnss-denied environment,” in *2019 IEEE 5th International Workshop on Metrology for AeroSpace (MetroAeroSpace)*. IEEE, 2019, pp. 171–175.
- [91] P. Nguyen, T. Kim, J. Miao, D. Hesselius, E. Kenneally, D. Massey, E. Frew, R. Han, and T. Vu, “Towards rf-based localization of a drone and its controller,” in *Proceedings of the 5th Workshop on Micro Aerial Vehicle Networks, Systems, and Applications*, 2019, pp. 21–26.
- [92] L. Zhang and H. Wang, “3d-wifi: 3d localization with commodity wifi,” *IEEE Sensors Journal*, vol. 19, no. 13, pp. 5141–5152, 2019.

## Bibliography

- [93] E. Soltanaghaei, A. Kalyanaraman, and K. Whitehouse, “Multipath triangulation: Decimeter-level wifi localization and orientation with a single unaided receiver,” in *Proceedings of the 16th annual international conference on mobile systems, applications, and services*, 2018, pp. 376–388.
- [94] G. Rebel, J. González, P. Glösekötter, F. Estevez, and A. Romero, “A novel indoor localization scheme for autonomous nodes in ieee 802.15.4a networks,” *I Jornadas de Computación Empotrada y Reconfigurable (JCER2016)*, 2016.
- [95] “Approved ieee draft amendment to ieee standard for information technology-telecommunications and information exchange between systems-part 15.4:wireless medium access control (mac) and physical layer (phy) specifications for low-rate wireless personal area networks (lr-wpans): Amendment to add alternate phy (amendment of ieee std 802.15.4),” *IEEE Approved Std P802.15.4a/D7, Jan 2007*, 2007.
- [96] J. Tiemann, F. Eckermann, and C. Wietfeld, “Multi-user interference and wireless clock synchronization in tdoa-based uwb localization,” in *2016 International Conference on Indoor Positioning and Indoor Navigation (IPIN)*. IEEE, 2016, pp. 1–6.
- [97] —, “Atlas-an open-source tdoa-based ultra-wideband localization system,” in *2016 International Conference on Indoor Positioning and Indoor Navigation (IPIN)*. IEEE, 2016, pp. 1–6.
- [98] J.-L. Rullán-Lara, S. Salazar, and R. Lozano, “Real-time localization of an uav using kalman filter and a wireless sensor network,” *Journal of Intelligent & Robotic Systems*, vol. 65, no. 1-4, pp. 283–293, 2012.

## Bibliography

- [99] P. Sinha, Y. Yapici, and I. Guvenc, “Impact of 3d antenna radiation patterns on tdoa-based wireless localization of uavs,” in *IEEE INFOCOM 2019-IEEE Conference on Computer Communications Workshops (INFOCOM WKSHPS)*. IEEE, 2019, pp. 614–619.
- [100] M. N. de Sousa and R. S. Thomä, “Localization of uav in urban scenario using multipath exploiting tdoa fingerprints,” in *2018 IEEE 29th Annual International Symposium on Personal, Indoor and Mobile Radio Communications (PIMRC)*. IEEE, 2018, pp. 1394–1399.
- [101] X. Tian, Z. Song, B. Jiang, Y. Zhang, T. Yu, and X. Wang, “Hiquadloc: A rssi fingerprinting based indoor localization system for quadrotors,” *IEEE Transactions on Mobile Computing*, vol. 16, no. 9, pp. 2545–2559, 2016.
- [102] C. Kan, G. Ding, F. Song, and J. Qiu, “Efficient relative fingerprinting based uav localization via tensor completion,” in *2018 IEEE 10th Sensor Array and Multichannel Signal Processing Workshop (SAM)*. IEEE, 2018, pp. 592–596.
- [103] N. Bloise, S. Primatesta, R. Antonini, G. P. Fici, M. Gaspardone, G. Guglieri, and A. Rizzo, “A survey of unmanned aircraft system technologies to enable safe operations in urban areas,” in *2019 International Conference on Unmanned Aircraft Systems (ICUAS)*. IEEE, 2019, pp. 433–442.
- [104] V. Chamola, P. Kotesh, A. Agarwal, N. Gupta, M. Guizani *et al.*, “A comprehensive review of unmanned aerial vehicle attacks and neutralization techniques,” *Ad hoc networks*, vol. 111, p. 102324, 2021.

## Bibliography

- [105] O. I. D. Bashi, W. Hasan, N. Azis, S. Shafie, and H. Wagatsuma, “Unmanned aerial vehicle quadcopter: A review,” *Journal of Computational and Theoretical Nanoscience*, vol. 14, no. 12, pp. 5663–5675, 2017.
- [106] V. V. Klemas, “Coastal and environmental remote sensing from unmanned aerial vehicles: An overview,” *Journal of coastal research*, vol. 31, no. 5, pp. 1260–1267, 2015.
- [107] A. Intwala and Y. Parikh, “A review on vertical take off and landing (vtol) vehicles,” *International Journal of Innovative Research in Advanced Engineering (IJIRAE)*, vol. 2, no. 2, pp. 187–191, 2015.
- [108] S. Gupte, P. I. T. Mohandas, and J. M. Conrad, “A survey of quadrotor unmanned aerial vehicles,” *2012 Proceedings of IEEE Southeastcon*, pp. 1–6, 2012.
- [109] Z. Dukowitz, “What are gps-denied drones and why are they important?” <https://uavcoach.com/gps-denied-drones/>, retrieved August 17, 2022.
- [110] P. Doherty and P. Rudol, “A uav search and rescue scenario with human body detection and geolocalization,” in *Australasian Joint Conference on Artificial Intelligence*. Springer, 2007, pp. 1–13.
- [111] Decawave, “Dwm1001 development board product brief,” <https://www.decawave.com/dwm1001dev/productbrief/>, [Online; accessed October 04, 2022].
- [112] POZYX, “Pozyx uwb sensor node product brief,” <https://www.pozyx.io/s-hop/product/developer-tag-68>, [Online; accessed October 04, 2022].

## Bibliography

- [113] E. Karapistoli, F.-N. Pavlidou, I. Gragopoulos, and I. Tsetsinas, “An overview of the iee 802.15. 4a standard,” *IEEE Communications Magazine*, vol. 48, no. 1, pp. 47–53, 2010.
- [114] M. Angjelichinoski, D. Denkovski, V. Atanasovski, and L. Gavrilovska, “Spear: Source position estimation for anchor position uncertainty reduction,” *IEEE communications Letters*, vol. 18, no. 4, pp. 560–563, 2014.
- [115] —, “Cramér–rao lower bounds of rss-based localization with anchor position uncertainty,” *IEEE Transactions on Information Theory*, vol. 61, no. 5, pp. 2807–2834, 2015.
- [116] B. Großwindhager, M. Rath, J. Kulmer, M. S. Bakr, C. A. Boano, K. Witrisal, and K. Römer, “Salma: Uwb-based single-anchor localization system using multipath assistance,” in *Proceedings of the 16th ACM Conference on Embedded Networked Sensor Systems*, 2018, pp. 132–144.
- [117] K. Batstone, M. Oskarsson, and K. Åström, “Towards real-time time-of-arrival self-calibration using ultra-wideband anchors,” in *2017 International Conference on Indoor Positioning and Indoor Navigation (IPIN)*. IEEE, 2017, pp. 1–8.
- [118] F. Zafari, A. Gkelias, and K. K. Leung, “A survey of indoor localization systems and technologies,” *IEEE Communications Surveys & Tutorials*, vol. 21, no. 3, pp. 2568–2599, 2019.
- [119] Y.-T. Chan, W.-Y. Tsui, H.-C. So, and P.-c. Ching, “Time-of-arrival based localization under nlos conditions,” *IEEE Transactions on Vehicular Technology*, vol. 55, no. 1, pp. 17–24, 2006.

## Bibliography

- [120] Z. Wang and S. A. Zekavat, "Omnidirectional mobile nlos identification and localization via multiple cooperative nodes," *IEEE Transactions on Mobile Computing*, vol. 11, no. 12, pp. 2047–2059, 2011.
- [121] V. Y. Zhang and A. K.-s. Wong, "Combined aoa and toa nlos localization with nonlinear programming in severe multipath environments," in *2009 IEEE Wireless Communications and Networking Conference*. IEEE, 2009, pp. 1–6.
- [122] S. Marano, W. M. Gifford, H. Wymeersch, and M. Z. Win, "Nlos identification and mitigation for localization based on uwb experimental data," *IEEE Journal on Selected Areas in Communications*, vol. 28, no. 7, pp. 1026–1035, 2010.
- [123] T. Van Nguyen, Y. Jeong, H. Shin, and M. Z. Win, "Machine learning for wideband localization," *IEEE Journal on Selected Areas in Communications*, vol. 33, no. 7, pp. 1357–1380, 2015.
- [124] X. Yang, F. Zhao, and T. Chen, "Nlos identification for uwb localization based on import vector machine," *AEU-International Journal of Electronics and Communications*, vol. 87, pp. 128–133, 2018.
- [125] K. Bregar and M. Mohorčič, "Improving indoor localization using convolutional neural networks on computationally restricted devices," *IEEE Access*, vol. 6, pp. 17 429–17 441, 2018.
- [126] J.-S. Choi, W.-H. Lee, J.-H. Lee, J.-H. Lee, and S.-C. Kim, "Deep learning based nlos identification with commodity wlan devices," *IEEE Transactions on Vehicular Technology*, vol. 67, no. 4, pp. 3295–3303, 2017.

## Bibliography

- [127] G. Wang, H. Chen, Y. Li, and N. Ansari, “Nlos error mitigation for toa-based localization via convex relaxation,” *IEEE Transactions on Wireless Communications*, vol. 13, no. 8, pp. 4119–4131, 2014.
- [128] G. Wang, A. M.-C. So, and Y. Li, “Robust convex approximation methods for tdoa-based localization under nlos conditions,” *IEEE Transactions on Signal processing*, vol. 64, no. 13, pp. 3281–3296, 2016.
- [129] S. Ganeriwal, R. Kumar, and M. B. Srivastava, “Timing-sync protocol for sensor networks,” in *Proceedings of the 1st International Conference on Embedded Networked Sensor Systems*, 2003, pp. 138–149.
- [130] M. Maróti, B. Kusy, G. Simon, and Á. Lédeczi, “The flooding time synchronization protocol,” in *Proceedings of the 2nd International Conference on Embedded Networked Sensor Systems*, 2004, pp. 39–49.
- [131] J. Elson, L. Girod, and D. Estrin, “Fine-grained network time synchronization using reference broadcasts,” *ACM SIGOPS Operating Systems Review*, vol. 36, no. SI, pp. 147–163, 2002.
- [132] B. Sundararaman, U. Buy, and A. D. Kshemkalyani, “Clock synchronization for wireless sensor networks: a survey,” *Ad Hoc Networks*, vol. 3, no. 3, pp. 281–323, 2005.
- [133] F. Sivrikaya and B. Yener, “Time synchronization in sensor networks: a survey,” *IEEE Network*, vol. 18, no. 4, pp. 45–50, 2004.
- [134] D. Geetha and N. Tabassum, “A survey on clock synchronization protocols in wireless sensor networks,” in *2017 International Conference On Smart*

## Bibliography

- Technologies For Smart Nation (SmartTechCon)*. IEEE, 2017, pp. 504–509.
- [135] L.-A. Phan, T. Kim, T. Kim, J. Lee, and J.-H. Ham, “Performance analysis of time synchronization protocols in wireless sensor networks,” *Sensors*, vol. 19, no. 13, p. 3020, 2019.
- [136] K.-L. Noh, Q. M. Chaudhari, E. Serpedin, and B. W. Suter, “Novel clock phase offset and skew estimation using two-way timing message exchanges for wireless sensor networks,” *IEEE Transactions on Communications*, vol. 55, no. 4, pp. 766–777, 2007.
- [137] S. P. Chepuri, R. T. Rajan, G. Leus, and A.-J. van der Veen, “Joint clock synchronization and ranging: Asymmetrical time-stamping and passive listening,” *IEEE Signal Processing Letters*, vol. 20, no. 1, pp. 51–54, 2012.
- [138] H. Wang, H. Zeng, M. Li, B. Wang, and P. Wang, “Maximum likelihood estimation of clock skew in wireless sensor networks with periodical clock correction under exponential delays,” *IEEE Transactions on Signal Processing*, vol. 65, no. 10, pp. 2714–2724, 2017.
- [139] H. Xiong, Z. Chen, W. An, and B. Yang, “Robust tdoa localization algorithm for asynchronous wireless sensor networks,” *International Journal of Distributed Sensor Networks*, vol. 11, no. 5, p. 598747, 2015.
- [140] H. Xiong, Z. Chen, B. Yang, and R. Ni, “Tdoa localization algorithm with compensation of clock offset for wireless sensor networks,” *China Communications*, vol. 12, no. 10, pp. 193–201, 2015.

## Bibliography

- [141] T. Wang, H. Xiong, H. Ding, and L. Zheng, “Tdoa-based joint synchronization and localization algorithm for asynchronous wireless sensor networks,” *IEEE Transactions on Communications*, vol. 68, no. 5, pp. 3107–3124, 2020.
- [142] S. M. Kay, *Fundamentals of statistical signal processing: estimation theory*. Prentice-Hall, Inc., 1993.
- [143] T. Li, A. Ekpenyong, and Y.-F. Huang, “Source localization and tracking using distributed asynchronous sensors,” *IEEE Transactions on Signal Processing*, vol. 54, no. 10, pp. 3991–4003, 2006.
- [144] T. Wang, H. Ding, H. Xiong, and L. Zheng, “A compensated multi-anchors tof-based localization algorithm for asynchronous wireless sensor networks,” *IEEE Access*, vol. 7, pp. 64 162–64 176, 2019.
- [145] J. Smith and J. Abel, “Closed-form least-squares source location estimation from range-difference measurements,” *IEEE Transactions on Acoustics, Speech, and Signal Processing*, vol. 35, no. 12, pp. 1661–1669, 1987.
- [146] S. Li, G. Li, L. Wang, Y. Zhou, Y. Peng, and J. Fu, “A three-dimensional robust ridge estimation positioning method for uwb in a complex environment,” *Advances in Space Research*, vol. 60, no. 12, pp. 2763–2775, 2017.
- [147] H. V. Poor, *An introduction to signal detection and estimation*. Springer Science & Business Media, 2013.
- [148] H. Soganci, S. Gezici, and H. V. Poor, “Accurate positioning in ultra-wideband systems,” *IEEE Wireless Communications*, vol. 18, no. 2, pp. 19–27, 2011.

## Bibliography

- [149] M. W. Mueller, M. Hamer, and R. D’Andrea, “Fusing ultra-wideband range measurements with accelerometers and rate gyroscopes for quadcopter state estimation,” in *2015 IEEE International Conference on Robotics and Automation (ICRA)*. IEEE, 2015, pp. 1730–1736.
- [150] A. N. Bishop, B. Fidan, B. D. Anderson, K. Doğançay, and P. N. Pathirana, “Optimality analysis of sensor-target localization geometries,” *Automatica*, vol. 46, no. 3, pp. 479–492, 2010.
- [151] I. S. for Low-Rate Wireless Networks, “Ieee std 802.15. 4-2015 (revision of ieee std 802.15. 4-2011),” 2016.
- [152] B. Gao, G. Hu, Y. Zhong, and X. Zhu, “Cubature kalman filter with both adaptability and robustness for tightly-coupled gnss/ins integration,” *IEEE Sensors Journal*, vol. 21, no. 13, pp. 14 997–15 011, 2021.
- [153] G. G. Rigatos, “Nonlinear kalman filters and particle filters for integrated navigation of unmanned aerial vehicles,” *Robotics and Autonomous Systems*, vol. 60, no. 7, pp. 978–995, 2012.
- [154] G. Raja, S. Suresh, S. Anbalagan, A. Ganapathisubramaniyan, and N. Kumar, “Pfin: An efficient particle filter-based indoor navigation framework for uavs,” *IEEE Transactions on Vehicular Technology*, vol. 70, no. 5, pp. 4984–4992, 2021.
- [155] M. Khalaf-Allah, “Particle filtering for three-dimensional tdoa-based positioning using four anchor nodes,” *Sensors*, vol. 20, no. 16, p. 4516, 2020.

## Bibliography

- [156] S. Konatowski, P. Kaniewski, and J. Matuszewski, “Comparison of estimation accuracy of ekf, ukf and pf filters,” *Annual of Navigation*, no. 23, pp. 69–87, 2016.
- [157] A. Benini, A. Mancini, and S. Longhi, “An imu/uwb/vision-based extended kalman filter for mini-uav localization in indoor environment using 802.15. 4a wireless sensor network,” *Journal of Intelligent & Robotic Systems*, vol. 70, no. 1, pp. 461–476, 2013.
- [158] J. Kelly and G. S. Sukhatme, “Visual-inertial sensor fusion: Localization, mapping and sensor-to-sensor self-calibration,” *The International Journal of Robotics Research*, vol. 30, no. 1, pp. 56–79, 2011.
- [159] M.-G. Li, H. Zhu, S.-Z. You, and C.-Q. Tang, “Uwb-based localization system aided with inertial sensor for underground coal mine applications,” *IEEE Sensors Journal*, vol. 20, no. 12, pp. 6652–6669, 2020.
- [160] F. Jiancheng and Y. Sheng, “Study on innovation adaptive ekf for in-flight alignment of airborne pos,” *IEEE Transactions on Instrumentation and Measurement*, vol. 60, no. 4, pp. 1378–1388, 2011.
- [161] S. Akhlaghi, N. Zhou, and Z. Huang, “Adaptive adjustment of noise covariance in kalman filter for dynamic state estimation,” in *2017 IEEE Power & Energy Society general meeting*. IEEE, 2017, pp. 1–5.
- [162] A. Mohamed and K. Schwarz, “Adaptive kalman filtering for ins/gps,” *Journal of Geodesy*, vol. 73, no. 4, pp. 193–203, 1999.
- [163] I. Arasaratnam and S. Haykin, “Cubature kalman filters,” *IEEE Transactions on Automatic Control*, vol. 54, no. 6, pp. 1254–1269, 2009.

## Bibliography

- [164] C. Shen, Y. Zhang, X. Guo, X. Chen, H. Cao, J. Tang, J. Li, and J. Liu, “Seamless gps/inertial navigation system based on self-learning square-root cubature kalman filter,” *IEEE Transactions on Industrial Electronics*, vol. 68, no. 1, pp. 499–508, 2020.
- [165] Y. Huang, Y. Zhang, B. Xu, Z. Wu, and J. A. Chambers, “A new adaptive extended kalman filter for cooperative localization,” *IEEE Transactions on Aerospace and Electronic Systems*, vol. 54, no. 1, pp. 353–368, 2017.
- [166] M. Narasimhappa, A. D. Mahindrakar, V. C. Guizilini, M. H. Terra, and S. L. Sabat, “Mems-based imu drift minimization: Sage husa adaptive robust kalman filtering,” *IEEE Sensors Journal*, vol. 20, no. 1, pp. 250–260, 2019.